International Journal of Extreme Manufacturing

TOPICAL REVIEW • OPEN ACCESS

Multi-physical field coupling polishing of diamond for atomic-scale damage-free surface

To cite this article: Song Yuan *et al* 2026 *Int. J. Extrem. Manuf.* **8** 032004

View the article online for updates and enhancements.

You may also like

- Research on simulation of abrasive belt polishing process for blade finishing
Q W He, S Sun, X Wang et al.
- Study on the influence of polishing pad characteristics on the surface quality and material removal rate of FV520B steel in chemical mechanical polishing
Chengbin Zhao, Longxing Liao, Fuli Cai et al.
- Polishing of Tungsten Carbide by Combination of Anodizing and Silica Slurry Polishing
Hui Deng, Xinquan Zhang, Kui Liu et al.

This content was downloaded from IP address 158.132.161.180 on 10/04/2026 at 07:01

OPEN ACCESS
IMMT | IOP Publishing

International Journal of Extreme Manufacturing

Int. J. Extrem. Manuf. 8 (2026) 032004 (40pp)

https://doi.org/10.1088/2631-7990/ae34fb

Topical Review

Multi-physical field coupling polishing of diamond for atomic-scale damage-free surface

Song Yuan[1], **Chi Fai Cheung**[1,*], **Fengzhou Fang**[2], **Han Huang**[3] and **Chunjin Wang**[1,*]

[1] State Key Laboratory of Ultra-precision Machining Technology, Department of Industrial and Systems Engineering, The Hong Kong Polytechnic University, Hong Kong Special Administrative Region of China, People's Republic of China
[2] State Key Laboratory of Precision Measuring Technology and Instruments, Laboratory of Micro/Nano Manufacturing Technology (MNMT), Tianjin University, Tianjin, People's Republic of China
[3] School of Advanced Manufacturing, Sun Yat-sen University, Shenzhen, People's Republic of China

E-mail: benny.cheung@polyu.edu.hk, chunjin.wang@polyu.edu.hk, song.yuan@polyu.edu.hk, fzfang@tju.edu.cn and hanhuang@mail.sysu.edu.cn

Received 13 July 2025, revised 23 September 2025
Accepted for publication 6 January 2026
Published 28 January 2026

Abstract

Diamond is renowned for its high stability in extreme environments, such as high temperatures, high pressures, and strong corrosive conditions, which makes it demonstrate irreplaceable superior performance in quantum devices, high-power optical systems, and ultra-high-frequency electronic devices. Nevertheless, its intrinsic brittleness, difficulty in material removal, and vulnerability to damage caused by processing severely limit its practical application. The inherently rough surface of as-grown diamond necessitates precision polishing to obtain ultra-smooth, damage-free surface with nanometer-scale roughness, sub-micrometer form accuracy, and minimal subsurface damage. This paper provides a systematic review of state-of-the-art diamond polishing technologies, addressing the challenge of achieving sub-nanometer roughness and damage-free surface, with particular emphasis on the need for atomic-level surface integrity. The discussion covers laser polishing (LP), mechanical polishing (MP), ion beam polishing (IBP), gas cluster ion beam polishing (GCIBP), plasma polishing, dynamic friction polishing (DFP), chemical mechanical polishing (CMP), ultraviolet-assisted polishing (UVAP), plasma-assisted polishing (PAP), laser-assisted polishing (LAP), ultrasonic-assisted polishing (UAP), and other major techniques. By deconstructing these technological approaches, four fundamental material removal mechanisms, i.e., microfracture, graphitization, oxidation, physical sputtering and chemical etching, are identified. This highlights that hybrid, multi-physics polishing strategies can effectively balance the material removal rate (up to several $\mu m \cdot h^{-1}$) and surface quality (down to sub-nanometer scale), outperforming conventional single-field techniques. Finally, the review outlines future

* Authors to whom any correspondence should be addressed.

Original content from this work may be used under the terms of the Creative Commons Attribution 4.0 licence. Any further distribution of this work must maintain attribution to the author(s) and the title of the work, journal citation and DOI.

© 2026 The Author(s). Published by IOP Publishing Ltd on behalf of the IMMT

directions, emphasizing innovations in multi-physics coupling mechanisms and intelligent control of atomic-scale manufacturing processes, thereby providing theoretical guidance and technical pathways to overcome the coupled challenges of atomic precision, efficiency, and extreme service conditions.

Keywords: polishing, diamond, multi-physical field,
atomic and close-to-atomic scale manufacturing (ACSM), ultra-precision machining,
damage-free surface

1. Introduction

Diamond, renowned for its exceptional physical and chemical properties—including extreme hardness, exceptionally high thermal conductivity, broad spectral transparency, and chemical inertness—plays a critical role in extreme environments characterized by high temperatures, high pressures, ultra-high precision, and strong corrosive conditions. Compared with other wide bandgap semiconductors (e.g., SiC or GaN), diamond has multiple advantages in device fabrication, including its high hole and electron mobility (>2 000 $cm^2 \cdot V^{-1} \cdot s^{-1}$), high critical electric field (>10 $MV \cdot cm^{-1}$), extremely high thermal conductivity (∼22 $W \cdot cm^{-1} \cdot K^{-1}$), and very wide bandgap (5.47 eV)[1,2]. In the semiconductor field, diamond can be used to fabricate high-frequency, high-power electronic devices. For instance, diamond-based high electron mobility transistors (HEMT) and field-effect transistors (FET) offer benefits, including high breakdown voltages, low on-resistance, and rapid switching speeds, rendering them well-suited for high-frequency applications such as 5G communications and radar systems[2,3]. In the optical field, diamond windows can withstand high-power laser impacts and can be used to fabricate windows and lenses for high-power lasers as well as infrared optical windows and lenses, applied in missile guidance, infrared imaging, and other fields[4–6]. In the heat sink field, diamond can be used for efficient heat dissipation. For instance, diamond heat sinks can effectively reduce the operating temperature of devices in power electronic devices, improving their reliability and lifespan[7–10]. The main applications of diamond, which are derived from its intrinsic properties, are illustrated in Figure 1.

However, natural diamond, particularly those of larger size, crystal form, and orientation that meet application requirements, is extremely rare and expensive. Recent advances in synthetic diamond production, particularly via microwave plasma chemical vapor deposition (MPCVD), have enabled broader applications of diamond materials[12,13]. Diamond surfaces produced by MPCVD typically have issues such as high roughness and numerous defects, severely limiting their application, as shown in Figure 2[14,15]. For example, surface roughness can cause light scattering, reducing the performance of optical devices, and surface defects can affect the electrical performance of devices[16]. Excessive surface roughness can also impact the success rate of bonding[17].

Moreover, human manufacturing technology is advancing into the new paradigm known as Manufacturing III, where atomic and close-to-atomic scale manufacturing (ACSM), as the fundamental technology, is rapidly evolving[19–26]. In ACSM, achieving an atomically smooth surface and preserving a defect-free surface lattice structure are critical prerequisites for the fundamental investigation of material behaviors at the atomic scale[27–29]. These conditions are also essential for the reliable fabrication of atomic-scale structures and devices[30]. Diamond has emerged as the substrate material of choice for fourth-generation semiconductor technologies. The realization of ultra-smooth, defect-free surfaces mandates the development of atomic-precision polishing techniques capable of achieving atomically smooth surface finishes[31–33]. These advanced fabrication methodologies are critical for maintaining lattice integrity while attaining sub-nanometer surface roughness, which is essential for optimizing device performance in next-generation power electronics and optoelectronic applications.

To provide a comprehensive overview of the state-of-the-art in diamond polishing, this review is structured as follows. Section 2 surveys the state-of-the-art polishing methods, Section 3 consolidates the polishing mechanisms that govern material removal, i.e., microfracture, graphitization, oxidation, physical sputtering, and chemical etching. Section 4 provides conclusions and prospects, highlighting opportunities in multi-physical field coupling and intelligent control aimed at ACSM of diamond. The schematic of the fundamental material removal mechanisms, state-of-the-art diamond polishing technologies, and prospects is shown in Figure 3.

2. State-of-the-art of polishing techniques for diamond

Diamond, the hardest known natural material, exhibits exceptional chemical stability, with negligible reactivity to acidic or alkaline reagents under ambient conditions. However, its inherent brittleness, challenges in material removal, and susceptibility to processing-induced damage significantly limit its practical application. Diamond polishing technology serves as a critical approach for achieving ultra-smooth, high-quality diamond surfaces[43,44]. This paper aims to review the advances in diamond polishing techniques, including laser polishing (LP), mechanical polishing (MP), ion beam polishing (IBP), plasma polishing, gas cluster ion beam

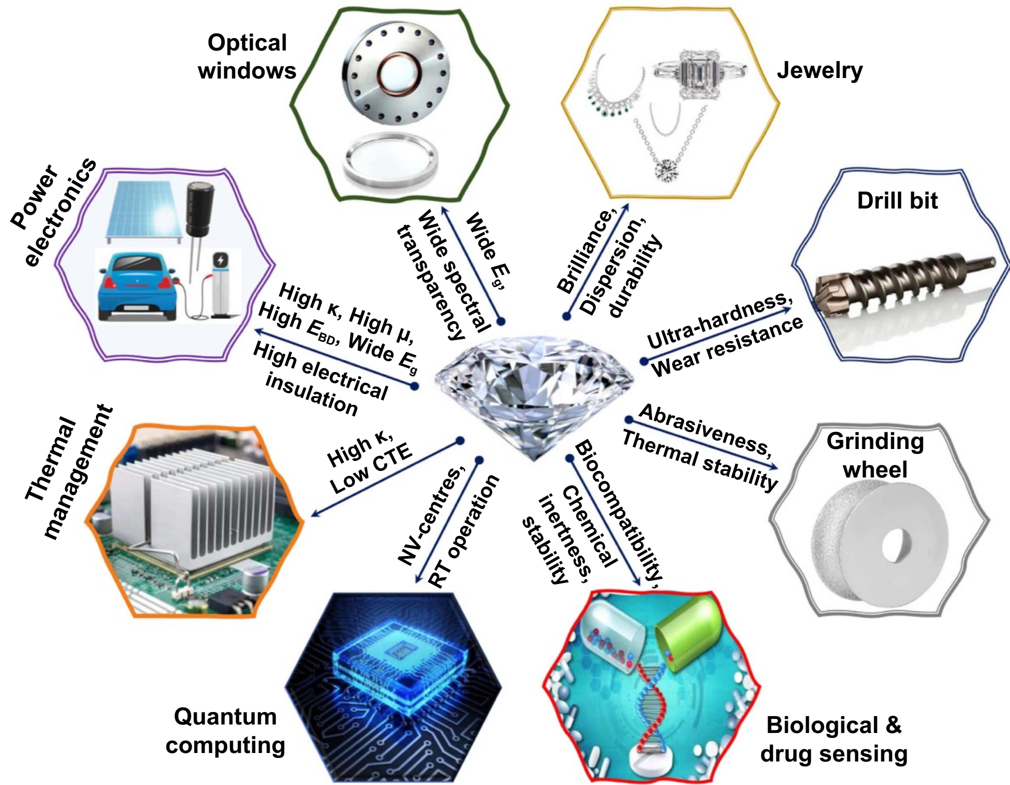

Figure 1. Applications of diamond derived from its intrinsic properties. Reproduced from[11]. CC BY 4.0.

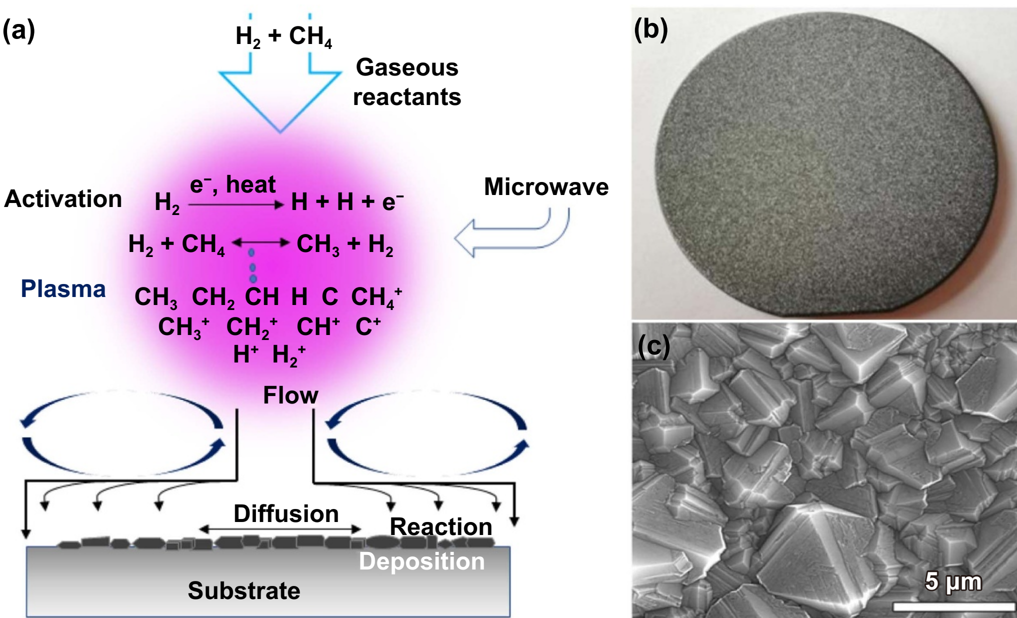

Figure 2. Principle and initial morphology of diamond growth by MPCVD. (a) Schematic diagram of diamond growth. Reproduced from[11]. CC BY 4.0. (b) Photo of as-grown diamond surface. Reproduced from[18]. CC BY 4.0. (c) SEM morphology of as-grown surface. Reproduced from[14]. CC BY 4.0.

polishing (GCIBP), dynamic friction polishing (DFP), chemical mechanical polishing (CMP), ultraviolet-assisted polishing (UVAP), plasma-assisted polishing (PAP), laser-assisted polishing (LAP), ultrasonic-assisted polishing (UAP), and other major techniques. This study evaluates the merits and limitations of each technique, assesses polishing efficiency and surface quality, identifies persistent challenges, and outlines prospects for future advancements in the field.

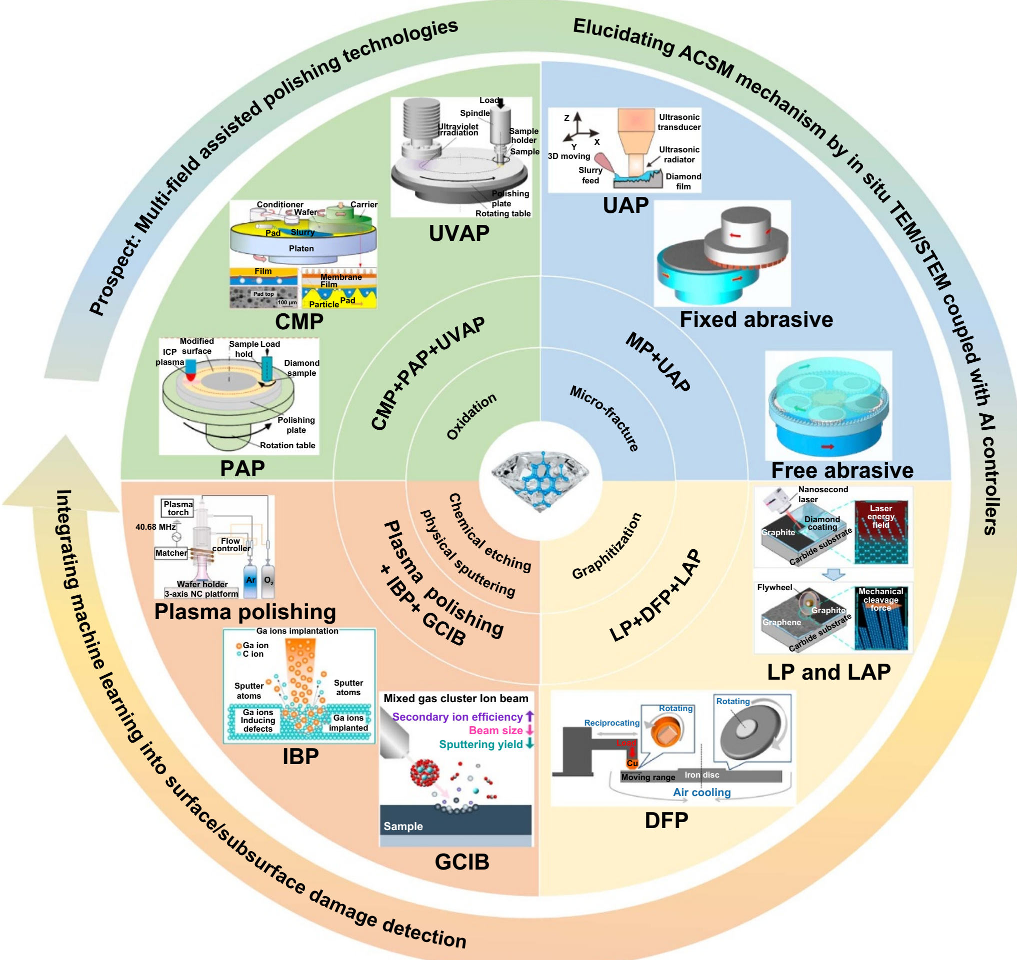

Figure 3. Schematic of the fundamental material removal mechanisms, state-of-the-art diamond polishing technologies, and prospects. Reproduced from[34]. CC BY 2.0. Reprinted from[35], Copyright (2021), with permission from Elsevier. Reprinted from[36], Copyright (2018), with permission from Elsevier. Reprinted from[37], Copyright (2016), with permission from Elsevier. Reprinted from[38], Copyright (2021), with permission from Elsevier. Reprinted from[39], Copyright (2021), with permission from Elsevier. Reprinted from[40], Copyright (2024), with permission from Elsevier. Reprinted from[41], Copyright (2023), with permission from Elsevier. Reprinted from[42], Copyright (2022), with permission from Elsevier.

2.1. Laser polishing (LP)

Laser polishing (LP) is a noncontact processing method that can polish both flat and curved diamond surfaces under room temperature conditions and is unaffected by the hardness or chemical properties of the material. Based on the pulse width, laser processing can be classified into nanosecond, picosecond, and femtosecond lasers. The schematic diagram of laser polishing for diamond is shown in Figure 4.

2.1.1. Nanosecond lasers. The pulse width of nanosecond lasers is on the order of nanoseconds (10^{-9} seconds). The processing principle primarily involves the generation of thermal effects on the surface through laser energy[45], causing local melting, evaporation, or thermal decomposition of the material, thereby achieving material removal.

Under nanosecond laser irradiation, a micrometer-scale graphite recast layer forms on the diamond surface, indicating transformation into softer graphite at high temperatures. The surface roughness strongly depends on the laser incidence angle; reducing the angle decreases the roughness, while the polishing rate increases logarithmically with laser flux[46]. The main surface damage features include grooves, cracks, ripple patterns, and debris deposition[47]. Cracks result from rapid thermal stresses, ripples from groove-wall reflections, and groove deformation from enhanced plasma absorption. The ablation debris consists of spherical graphite particles and irregular diamond fragments[48].

Given the confined interaction zone of the laser, full surface coverage requires synchronized motion between the laser spot and the substrate. Pulse frequency, peak power, spot diameter, and scanning speed are the key parameters controlling polishing efficiency, surface quality, and MRR. High-power nanosecond lasers with low scanning speeds and frequencies are effective for fabricating deep, wide microchannels (up to 62.82 μm wide and 31.56 μm deep), although they yield moderate surface roughness (Ra ≈ 41.38 nm)[49]. Defects in the diamond lattice enhance local energy absorption, generating

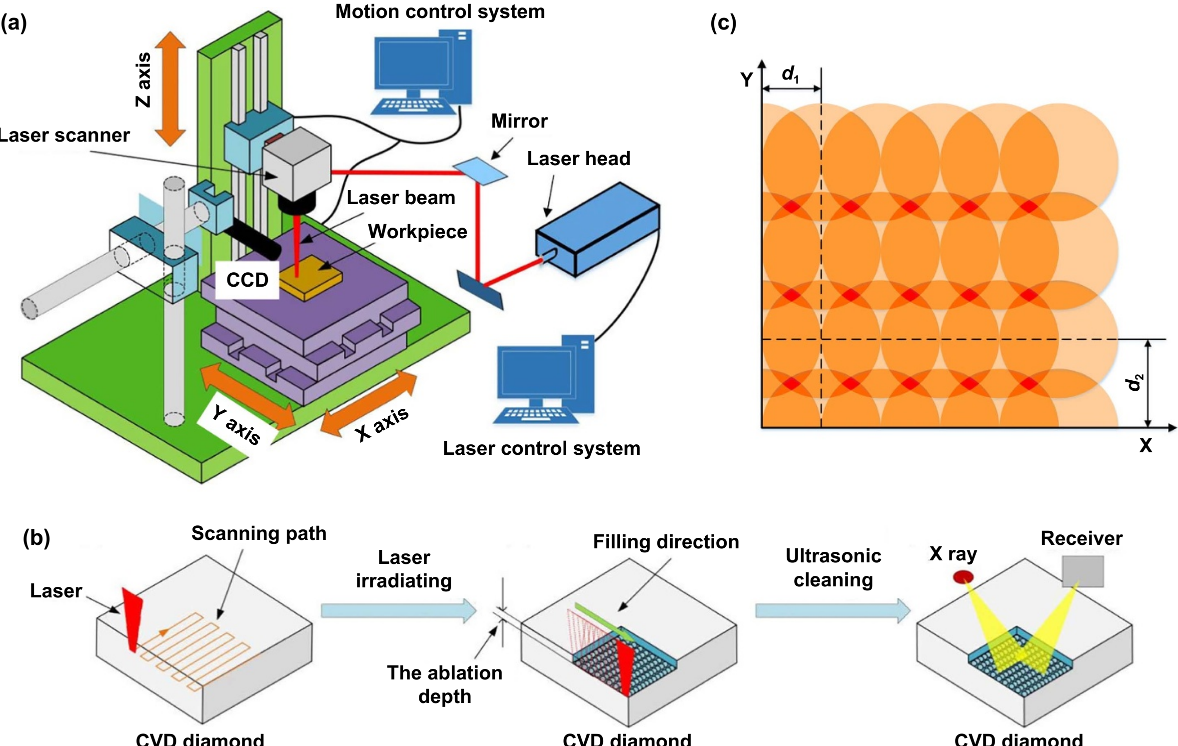

Figure 4. Schematic diagram of laser polishing for diamond. (a) Schematic diagram of the laser equipment. (b) Schematic illustration of the laser machining outline. (c) Schematic illustration of pulse spot overlap on the machined surface. Reprinted from[38], Copyright (2021), with permission from Elsevier.

thermal spikes, heterogeneous temperature distributions, and residual stress. Part of the energy propagates into the bulk, causing subsurface defect formation, microcracks, or fractures due to stress concentration[50]. Wei et al. used UV nanosecond lasers ($\lambda = 335$ nm) to fabricate microgrooves on uncoated and gold-coated diamonds, observing a 24% reduction in the ablation threshold for coated substrates[51]. Titanium coatings further reduce post-processing roughness by up to 53%, enhancing surface integrity[52]. Liu et al. proposed a metal film-induced self-sustaining graphitization (MISG) method, depositing ~100 nm metallic films on diamond to mediate graphitization kinetics. Using nanosecond UV–IR lasers, they achieved precise removal with minimal subsurface damage, as illustrated in Figure 5[53,54].

2.1.2. Picosecond lasers. Picosecond lasers generate pulses with durations on the order of 10^{-12} seconds, facilitating ultrafast energy deposition that limits heat accumulation. Material removal is dominated by non-thermal mechanisms such as multiphoton absorption and nonlinear ionization processes, thereby suppressing thermal diffusion and collateral damage.

Compared with nanosecond lasers, picosecond systems combine ultrashort pulse widths ($<10^{-12}$ s) and high peak power densities, allowing precise micromachining with reduced heat-affected zones and improved surface integrity. Beam expansion further lowers roughness and enhances throughput, enabling faster achievement of target geometries[55]. This facilitates the fabrication of high-integrity microgrooves with submicron-dimensional accuracy and negligible peripheral cracking[56]. Grooves machined with picosecond lasers exhibit significantly higher thermal stress compared to those produced by nanosecond lasers. The MRR of picosecond lasers is less than one-tenth that achieves with nanosecond lasers, rendering the latter more effective for cutting and fabricating high-aspect-ratio microstructures in diamond substrates. Conversely, picosecond lasers are superior for high-precision applications requiring minimal thermal damage and refined surface quality[57].

Based on Gaussian beam theory and ultrafast ablation mechanisms, Yan et al.[38] proposed a physics-based model that predicts diamond surface roughness and removal depth with average errors of 9.6% and 16.6%, respectively. Picosecond pulsed ablation significantly reduces PCD surface roughness (Sa from 1.85 μm to 0.51 μm), and pulses below 10 ps effectively suppress graphite formation[58]. Damage evolution scales with pulse count, while crystal orientation strongly influences groove morphology, cracking, and phase transformation due to variations in cleavage energy and atomic rearrangement energy[59]. However, the local crystalline anisotropy inherent to PCD leads to non-uniform material removal rates, producing irregular groove topography. Picosecond laser ablation is dominated by vaporization, resulting in negligible byproduct deposition and minimal graphitic residue[60]. After picosecond laser processing, structural changes induced by the laser occur on the (111) plane, which is known for having the lowest cleavage energy and strength

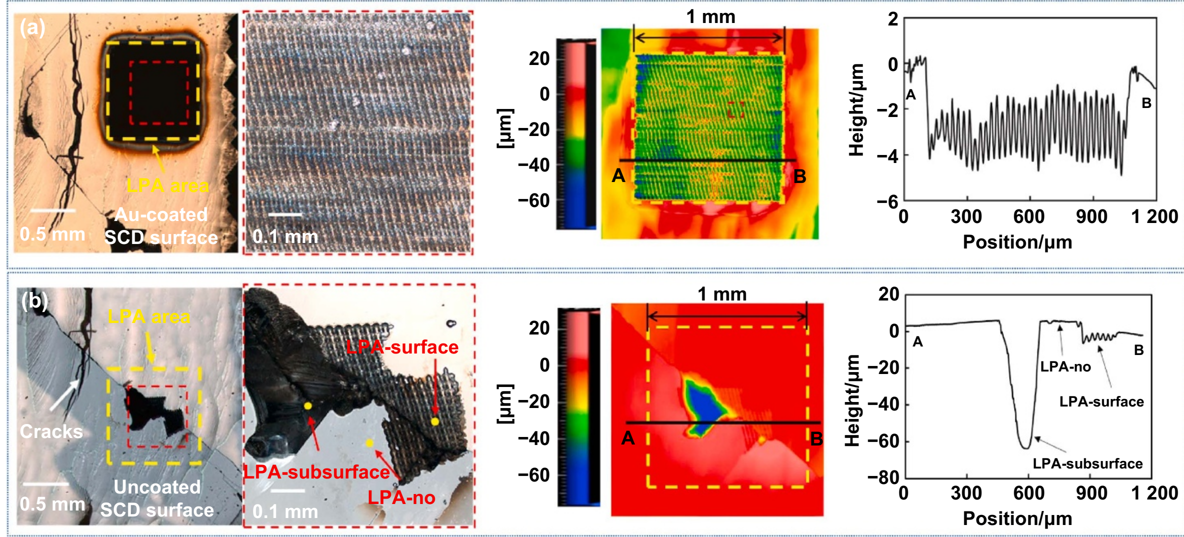

Figure 5. Comparison of coated and uncoated SCD (100) substrates processed by LPA. (a) Coated SCD substrate, (b) uncoated SCD substrate. Reprinted from[53], Copyright (2023), with permission from Elsevier.

in diamond[61]. Cleavage is observed along the (111) planes parallel to the crystal orientation, and smooth surfaces can be achieved through layer-by-layer removal. While some graphite formation may occur, the diamond crystal structure remains largely intact[62].

2.1.3. Femtosecond lasers. Femtosecond lasers generate ultrashort pulses (10^{-12} s), enabling energy delivery to materials at timescales insufficient for significant thermal diffusion. Material removal is dominated by non-thermal mechanisms such as multiphoton absorption and nonlinear ionization, effectively suppressing heat-affected zones and collateral damage.

Femtosecond lasers achieve material removal via sublimation, localizing energy deposition at the surface to minimize thermal energy transfer to subsurface regions. These lasers uniquely enable the fabrication of micro/nanoscale features on surfaces due to their ultrafast ablation regime[63,64]. This capability facilitates precision micromachining, where ultrashort pulse durations ($<10^{-15}$ s) suppress thermal diffusion, thereby mitigating heat-affected zones and residual stresses in adjacent materials[65]. Figure 6 shows the surface topography of femtosecond-laser-ablated diamond microgrooves, highlighting morphology variations under differing energy density parameters[66].

Femtosecond lasers heat electrons on the diamond surface to peak temperatures within hundreds of femtoseconds, with electron−lattice thermal equilibrium achieved within tens of picoseconds[67]. This distinctive feature of femtosecond lasers enables the formation of intricate surface morphologies and miniaturized structures on device surfaces[65], including laser-induced periodic surface structures (LIPSS) on diamond. LIPSS can interact with natural light to generate structural colors[40], a phenomenon unattainable by traditional machining methods[68]. Following femtosecond laser treatment, the graphite layer beneath the microgroove becomes nanometer-thin, and periodic nanostructures emerge on the processed surface[38]. At higher scanning speeds or lower single-pulse energies, the diamond coating surface undergoes melting and re-solidification. However, with decreased scanning speed or increased pulse energy, the ablation process progresses through three stages: melting, graphitization, and sublimation. The surface roughness and material removal rate (MRR) are strongly influenced by variations in scanning speed and pulse energy[69]. At high energy densities, repeated treatments progressively degrade the edge morphology, leading to irregular and uncontrolled shapes. In contrast, at lower energy densities, even after multiple treatments, the mesh edge morphology remains consistent with distinct boundaries[70].

Femtosecond, picosecond, and nanosecond lasers are the main technologies for diamond processing, each with distinct features. Femtosecond lasers minimize thermal effects, prevent damage, and yield smooth finishes, but they are costly and less efficient. Picosecond lasers also limit thermal effects but have lower precision than femtosecond lasers do, require high power for diamond machining, and depend on beam quality, with equipment still expensive. Nanosecond lasers are faster and cheaper but cause greater thermal effects, leading to poorer surface quality, thicker graphite layers, and more subsurface damage, whereas femtosecond and picosecond lasers produce thinner nanometer-scale graphite layers.

2.2. Ion beam polishing (IBP)

Ion beam polishing (IBP) is a noncontact technique that employs energetic ions to bombard material surfaces, removing atoms and inducing surface modification through kinetic energy transfer. The fundamental principle lies in the acceleration of charged ions under an external electric field, followed by their impact on the target surface, which triggers sputtering, etching, amorphization, and even chemical reactions.

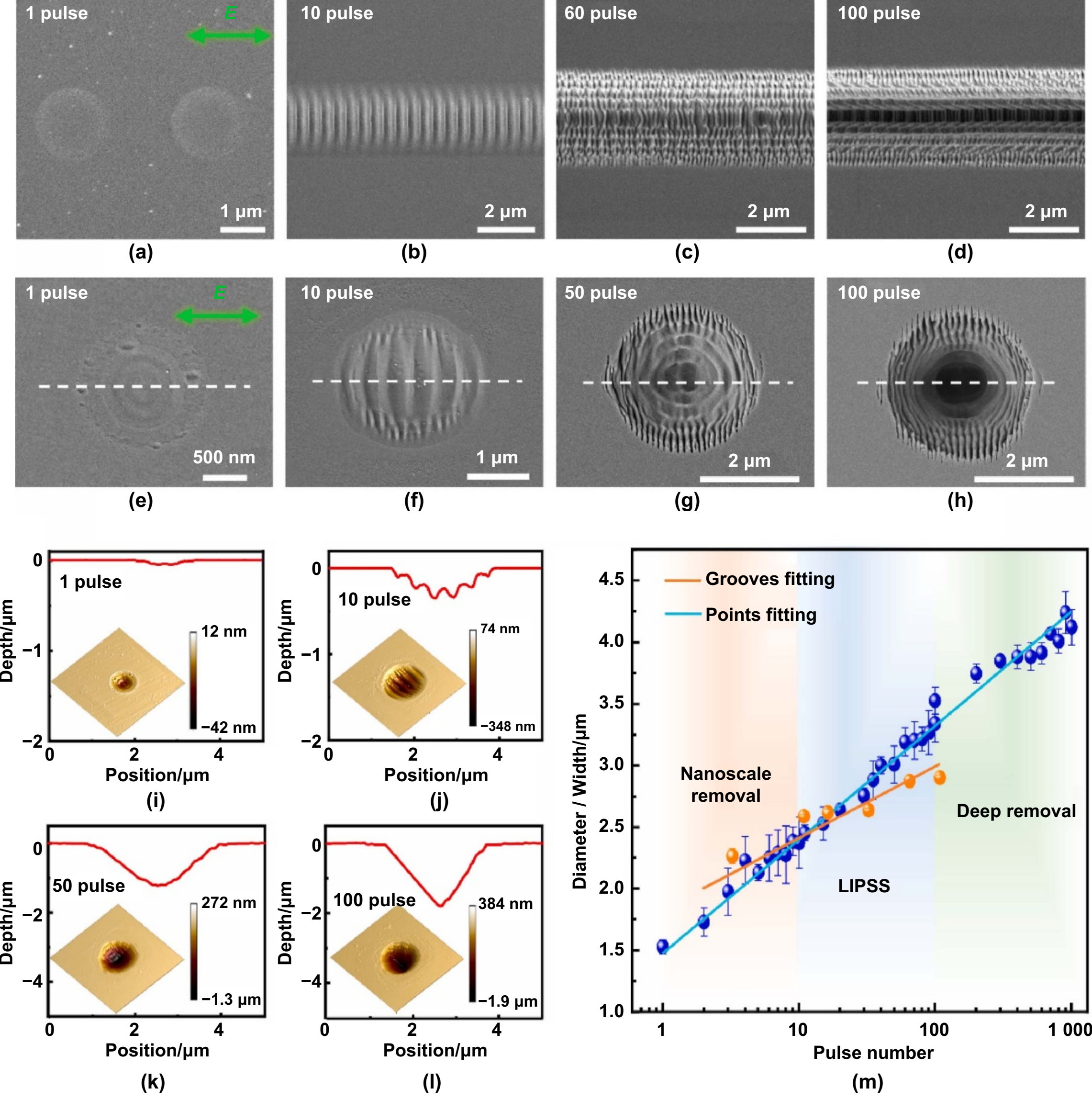

Figure 6. Surface ablation morphologies under femtosecond laser irradiation: (a)–(h) SEM images from line scanning and point processing with varying pulse numbers. (i)–(l) AFM structures and profiles. (m) Ablation diameter/width versus pulse number. Reprinted from[66], Copyright (2025), with permission from Elsevier.

Compared with conventional mechanical polishing, IBP offers remarkable advantages, such as the absence of mechanical damage, high precision, and strong controllability, making it particularly suitable for nanometer-scale processing of hard and brittle materials like diamond. In addition, the surface structure and properties can be flexibly tuned by adjusting the incident angle, ion energy, and ion species[71,72]. Nevertheless, IBP also has certain limitations, such as surface amorphization or graphitization induced by ion implantation, and generally has a lower efficiency than traditional mechanical methods. Against this background, extensive studies have focused on different ion species (e.g., Ar^+, Ga^+), energy ranges, and irradiation strategies to elucidate the removal mechanisms, damage characteristics, and surface morphology evolution of diamond during IBP. The experimental setup and schematic of IBP are shown in Figure 7.

Early investigations demonstrated that argon ion beams exhibit significant advantages in drilling and milling diamond. Truncated conical microholes and larger through-holes with polished-like sidewalls and negligible collateral damage were successfully fabricated, confirming the high processing precision and surface quality of Ar^+ beam machining[73]. To further clarify the sputtering mechanism, the sputter yield, surface damage, and morphology evolution of diamond were systematically analyzed, and predictive models for sputter-processed surface profiles were established, providing theoretical support for diamond polishing and sharpening of tip tools[74].

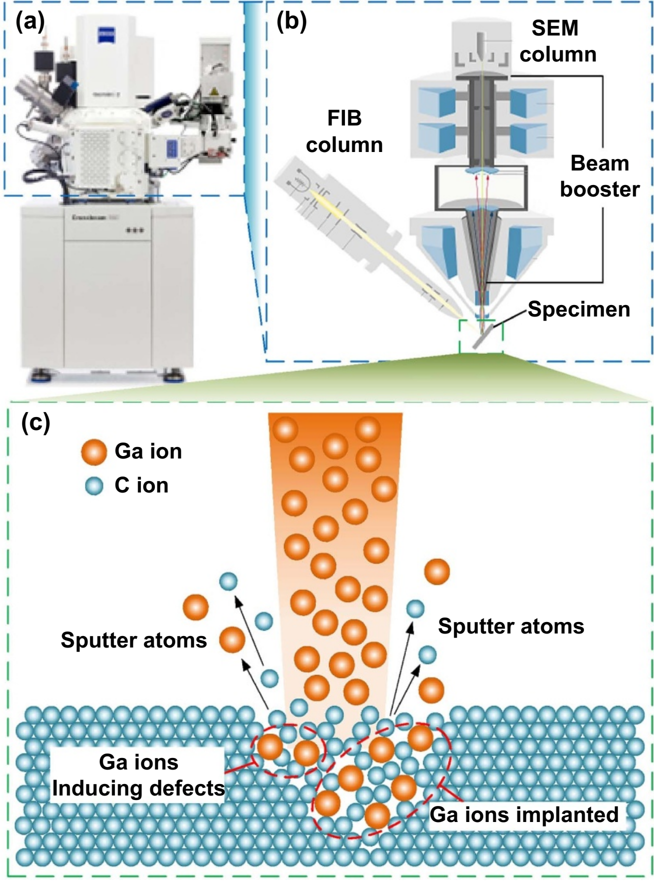

Figure 7. The experimental setup and schematic of IBP. (a) Dual-beam workstation, (b) schematic of the SEM and FIB system, (c) schematic of ion implantation. Reprinted from[41], Copyright (2023), with permission from Elsevier.

Under low-energy ion irradiation, diamond surfaces undergo complex structural transformations. For instance, Ar^+ or H^+ ions at 1.5 keV can induce amorphous layers or graphitic regions at sufficiently high fluences[75]. Low-energy Ar^+ bombardment at grazing incidence shows a pronounced dependence on initial surface states: ultra-smooth surfaces remain nearly unaffected, while nanopillar structures on nanostructured surfaces are effectively removed, reducing surface roughness to ultra-smooth levels. In contrast, plasma-treated rough surfaces show limited improvement[76]. Moreover, Ar^+ irradiation significantly modifies the surface wettability of diamond. With increasing ion dose, surfaces gradually transition from hydrophilic to hydrophobic states, while subsequent high-temperature oxidation restores their inherent hydrophilicity[77]. Zong et al. systematically investigated the effects of the Ga^+ dose and injection conditions on diamond. With increasing ion dose, the diamond structure sequentially experienced ion implantation, local damage, partial amorphization, and eventually complete amorphization. The injection angle was also found to strongly influence the extent of damage: perpendicular implantation along the crystal axis led to a pronounced channeling effect, whereas a 7 inclination effectively suppressed this phenomenon[78]. Furthermore, surface modification of diamond cutting tools using Ga^+ demonstrated improved wear resistance and wettability compared with unmodified tools, and was shown to facilitate surface smoothness by reducing roughness[79].

For diamond thin films, flattening strategies have been proposed by introducing intermediate sacrificial planarization layers. For example, photoresist or Ti-Si mixtures have been used to match the etching rates of the coating and diamond films, effectively reducing surface roughness from the micrometer scale to the sub-micrometer scale, thereby expanding the application potential of diamond films in infrared optics[80]. Further studies revealed that varying the incidence angle of Ar^+ irradiation enables the controlled adjustment of surface roughness from sub-nanometer to ultra-smooth levels, while also elucidating the competitive interplay between smoothing and roughening mechanisms[81]. The IBP relies on the physical bombardment of inert gas ions on the substrate surface to polish the local scratches and spots after MP. Within 20 minutes, the depth of the scratches decreases from 108 nm to 8 nm[82].

In addition to Ar^+, IBP with Ga^+ ions has also been extensively investigated for precision machining of diamond. However, Ga^+ irradiation inevitably introduces damage to the layers. At an accelerating voltage of 30 kV, the damage layer thickness reaches approximately 43 nm and exhibits a bilayer structure consisting of a sp^2-rich a-C I layer and a sp^3-dominated a-C II layer. Notably, the a-C II layer possesses a bandgap of $\sim$4.0 eV, suggesting potential applications in all-carbon heterostructure devices[83]. Further studies combining TEM, EELS, and SRIM simulations revealed the structural evolution of Ga-induced damage layers and their fluence-dependent characteristics, identifying the amorphization threshold and amorphous density features[84,85]. Experimental observations and molecular dynamics simulations were in excellent agreement, showing that the Ga^+-induced damage layer thickness increased from $\sim$11.5 nm to 27.6 nm with increasing beam voltage and exhibited a strong crystallographic orientation dependence. In particular, diamond with (110) orientation demonstrated higher sputtering efficiency and greater damage sensitivity, elucidating orientation-dependent mechanisms of amorphization and graphitization[86,87].

In summary, IBP has demonstrated unique advantages in the micro/nanoscale machining of diamond. Ar^+ beams enable effective surface smoothing, wettability control, and thin-film planarization under different conditions, while Ga^+ FIB achieves high-precision micro/nanomachining at the cost of introducing damage layers. Mechanistic insights into these processes provide critical guidance for optimizing processing conditions and extending application fields. IBP is expected to achieve precise control over diamond surface structures and properties through optimization of processing parameters, careful selection of ion species, and multi-physical coupling strategies, thereby promoting its applications in advanced optics, electronics, and quantum devices.

2.3. Plasma polishing

Plasma polishing is a versatile, noncontact technique that utilizes chemically reactive plasma species—commonly CF_4, O_2, Cl_2, or their mixtures—to etch material surfaces through a combination of chemical reactions and physical sputtering. Compared with conventional mechanical polishing, this approach provides stress-free and damage-free material removal, enabling the achievement of atomically smooth surfaces with sub-nanometer roughness and high MRR reaching several hundred micrometers per minute. The technology has been widely applied to materials such as silicon[88,89], Ga_2O_3[90], GaN[91], and fused silica glass[92].

The application of plasma in diamond polishing dates back to the 1990s, when researchers developed plasma-based polishing techniques to meet the demand for smooth diamond surfaces in studies investigating the structure and reactivity of low-index diamond planes[93,94]. Early studies demonstrated that hydrogen plasma treatment at elevated temperatures (~870 °C, 40 mbar) could produce atomically flat (100) and (111) diamond surfaces with a mean roughness of approximately 1 nm[95]. Buchkremer et al.[96]. employed electron cyclotron resonance (ECR) plasma for the polishing of CVD diamond and reported polishing rates of up to 2.5 $\mu m \cdot h^{-1}$ under conditions of 500 W and 5 Pa. Their study highlighted the critical role of plasma species reactivity in plasma-based polishing. In air plasmas at pressures above 100 Pa, the low reactivity of oxygen species can result in selective etching, leading to non-uniform surface patterns. In contrast, under highly dissociated and ionized low-pressure electron cyclotron resonance (ECR) air plasma, the etching of diamond films exhibited significantly improved uniformity. Early studies on plasma-assisted polishing were predominantly conducted under low-pressure conditions[21,97]. In recent years, with the advancement of atmospheric-pressure plasma processing technologies and their proven success in the ultra-precision polishing of silicon-based materials[22,98], researchers have begun exploring the feasibility of applying atmospheric-pressure plasmas to diamond processing, which has demonstrated significant advantages.

For diamond, mixtures of O_2, CF_4, Ar, and SF_6 are widely used to selectively etch sp^3-bonded carbon[99]. The principal diagram of plasma polishing for diamond is shown in Figure 8. By investigating the influence of different ICP process parameters on the surface roughness of SCD, Zhao et al. found that increasing the etching time and SF_6 flow rate would increase the surface roughness. Although increasing the ICP and power could reduce the roughness to 0.562 nm, they would also form nanostructures[100]. Deng et al. proposed a plasma-based atom-selective etching (PASE) method for diamond, achieving an MRR of up to 56.533 $\mu m \cdot min^{-1}$ and a surface roughness of 0.5 nm, which is several thousand times higher than that of traditional polishing[40]. Furthermore, plasma polishing is equally effective for PCD. Experiments indicate that the apex sites of PCD grains are rapidly removed, significantly reducing the height differences between the grains. The surface roughness Sa decreased from 10.1 μm to 93.7 nm within 30 minutes, with an MRR of 34.4 $\mu m \cdot min^{-1}$, and no amorphous carbon or new stress-induced damage was introduced[101]. Liu et al. further reported that by optimizing plasma parameters, preferential etching of pyramid-like top regions could reach MRRs up to 127 $\mu m \cdot min^{-1}$[102]. However, this method suffers from excessive polishing at the sample edges, making it difficult to maintain surface shape accuracy. Therefore, it is more suitable as a rough polishing technique for PCD and can be combined with other fine polishing processes to significantly improve the overall polishing efficiency of PCD.

The plasma polishing process is governed by the synergistic effects of reactive radical adsorption, ion bombardment, and localized heating. The selectivity toward sp^3 carbon over sp^2 carbon plays a key role in preserving the crystalline quality. Nonetheless, several issues require further investigation. First, plasma sheaths near sample edges enhance ion flux, leading to over-polishing and local curvature changes. Second, achieving uniform reactive species distribution across large-area substrates remains challenging, especially under atmospheric pressure. Third, although generally considered damage-free, energetic ion bombardment may still induce near-surface defects or graphitization if the process parameters are not optimized. Future research directions include the development of hybrid plasma-mechanical processes, adaptive plasma control based on in-situ diagnostics (e.g., optical emission spectroscopy), and integration with AI-driven process parameter optimization to dynamically adjust plasma conditions for uniform, defect-free finishing of large-area diamond substrates.

2.4. Gas cluster ion beam polishing (GCIBP)

Gas cluster ion beam polishing (GCIBP) is an emerging high-precision material processing technology characterized by its simplicity, environmental friendliness, high efficiency, and low damage. GCIB is generated by ionizing gas molecules or their mixtures, typically through a sequence of processes, including gas aggregation, condensation expansion, ionization, acceleration, magnetic filtering, and neutralization. Unlike monatomic ion beams, GCIB consists of clusters containing tens to thousands of atoms, each with very low energy. When bombarding a material surface, GCIB primarily acts on the near-surface region and achieves surface smoothing through lateral sputtering effects, thereby significantly reducing subsurface damage[103,104]. This feature has already been demonstrated in silicon surface polishing[105].

Figure 9 illustrates schematics of the GCIB apparatus and principle[106]. Monatomic ion beams exhibit deeper penetration depths and are more likely to cause extensive subsurface damage, whereas gas clusters typically range from 1 nm to 100 nm in diameter, carry only a few charges, and possess extremely low per-atom energies. As a result, damage

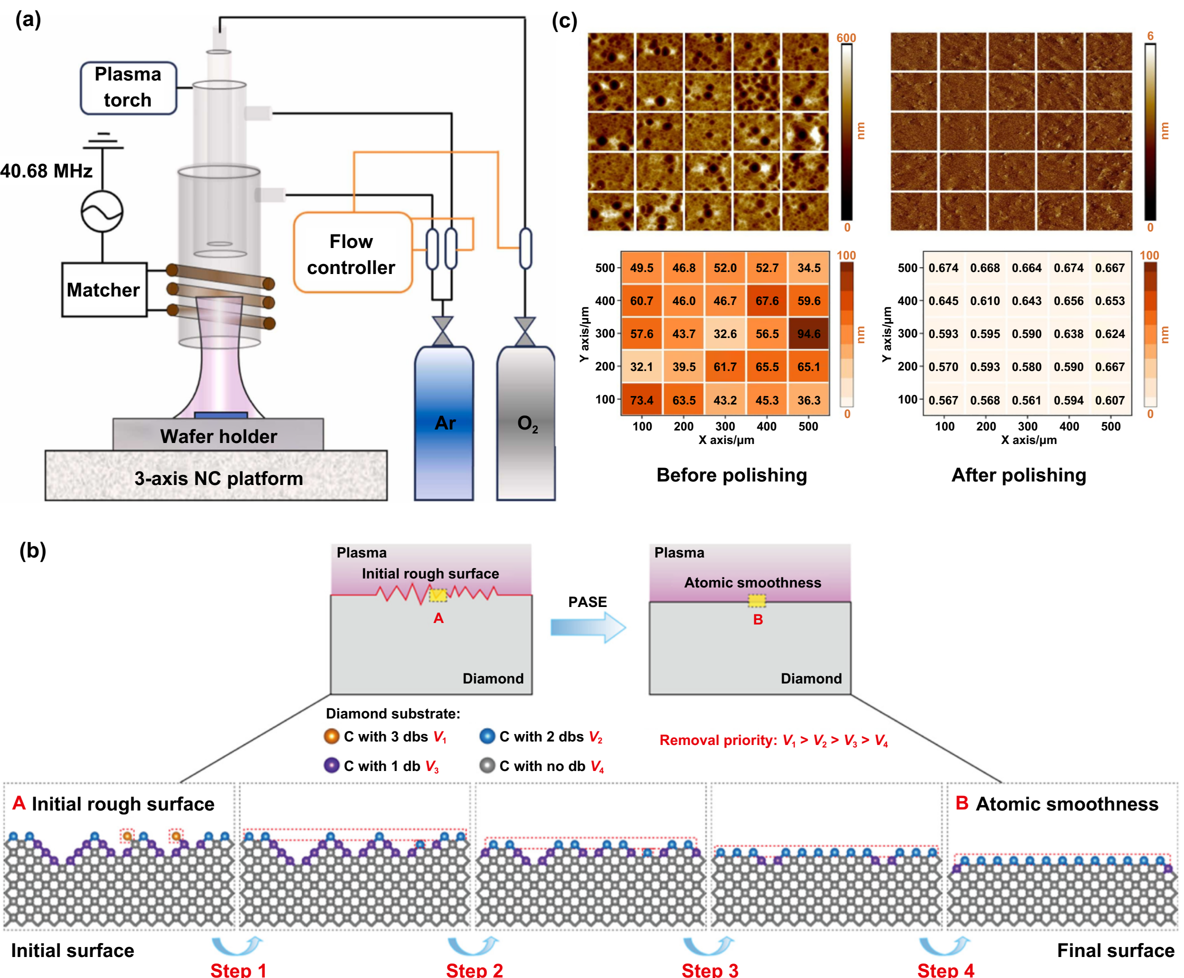

Figure 8. Schematic of plasma polishing. (a) Schematic of the experimental setup of plasma polishing. Reprinted from[102], Copyright (2024), with permission from Elsevier. (b) Principle diagram of plasma polishing. Reprinted from[40], Copyright (2024), with permission from Elsevier. (c) Surface morphology of SCD before and after plasma polishing. Reprinted from[40], Copyright (2024), with permission from Elsevier.

is confined to the near-surface region. These characteristics enable GCIB to simultaneously remove material and achieve effective surface planarization, which is difficult to accomplish with other ion beam techniques.

In diamond processing, studies have shown that Ar-GCIB can effectively reduce the surface roughness of CVD diamond, but it also tends to induce graphitization. In comparison, O_2-GCIB does not cause graphitization but exhibits limited smoothing capability[107]. More recently, mixed-gas GCIB has opened new avenues for diamond polishing. For example, Ar/SF_6-GCIB not only prevents obvious graphitization but also enhances the removal rate through the formation of volatile SF_6 generated by reactions between F and C atoms, achieving nanometer-scale surface roughness (Ra $\sim$ 0.5–0.6 nm)[108,109]. The experimental results further demonstrate that under identical processing conditions, SF_6-GCIB achieves a higher etching rate than Ar-GCIB without degrading the crystallinity of diamond. Through a combination of coarse and fine polishing, the surface roughness of CVD diamond has been significantly reduced from hundreds of nanometers to a Ra of 0.6 nm, thereby meeting the stringent requirements for direct bonding in high-power device applications[110].

In summary, GCIB, with its advantages of low damage, high smoothness, and process flexibility, has emerged as a promising technique for precision polishing of diamond surfaces. Current research primarily focuses on the selection of gas species, optimization of process parameters, and multi-step or mixed-gas irradiation strategies, laying a solid foundation for achieving atomically smooth and damage-free diamond surfaces.

2.5. *Dynamic friction polishing (DFP)*

Dynamic friction polishing (DFP) is a contact-based method that removes diamond material via frictional heating between the sample and a rotating metallic disc. This thermal energy activates solid-phase reactions, converting diamond to graphitic carbon and inducing diffusion, oxidation, and mechanical wear for efficient material removal. The DFP method operates at room temperature, effectively leveraging the frictional

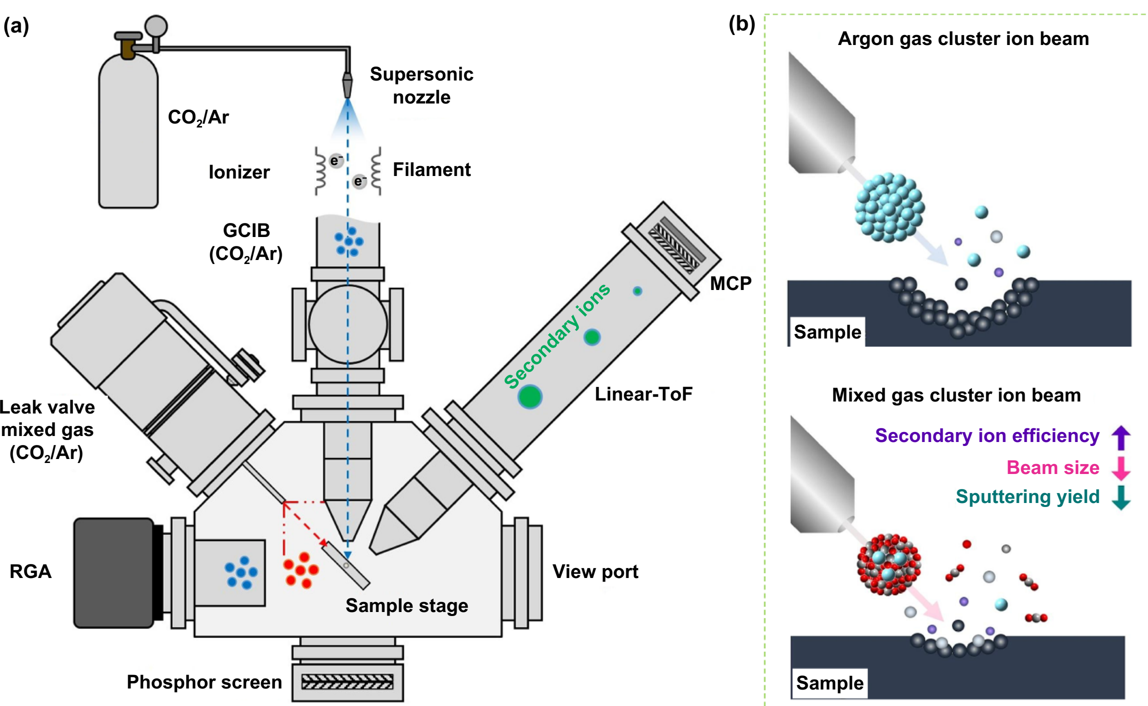

Figure 9. Schematic of a GCIB apparatus (a) and principle (b). (a) and (b) Reprinted from[42], Copyright (2022), with permission from Elsevier.

heat generated during polishing, without requiring specialized equipment to heat the polishing disk or the diamond sample. A schematic of DFP is provided in Figure 10.

When the thermochemical reaction is initiated, the contact temperature between the polishing disk and the diamond surface reaches a critical threshold. The MRR is influenced by various polishing parameters, including the polishing disk material, applied pressure, and disk rotation speed. DFP typically requires high-pressure conditions to generate the elevated temperatures—generally exceeding 700 °C—necessary for effective polishing. Among these parameters, the pressure applied to the diamond and the rotation speed of the polishing disk are particularly critical. If either the speed or pressure is too low, material removal is hindered. Only when the pressure or speed exceeds a certain threshold will further increases in these parameters lead to higher removal rates. At a pressure of 2.2 MPa and a speed of 16 $m \cdot s^{-1}$, material removal is negligible. Below 10 $m \cdot s^{-1}$, higher pressures yield minimal polishing rates. Above a 12 $m \cdot s^{-1}$ threshold, however, the removal rate depends on both parameters, scaling nearly linearly with the sliding speed at fixed pressures. The diamond's initially rough surface (R max = 10 μm) results in a small contact area, causing high contact stress at rough surface points. As a result, under a constant polishing load, the initial MRR peaks at 1 260 $\mu m \cdot h^{-1}$, and the surface roughness decreases from around 1.7 μm to 0.2 μm within two minutes of polishing[111]. Higher loads promote higher MRRs and smoother surfaces; nevertheless, excessively high combinations of speed and pressure result in surface/subsurface cracks[112–114]. Additionally, under high-pressure conditions, the substantial temperature rise induced by interfacial friction promotes both the chemical reaction and diffusion of carbon atoms. Increased frictional forces and shear stresses at the diamond surface further exacerbate crack formation, particularly in the contact regions of surface asperities[39].

Although DFP can achieve ultra-smooth diamond surfaces with a roughness <5 nm (even as low as 1 nm), subsurface damage extends to a depth of approximately 10 μm in (100) SCD, manifesting as micro-cleavage fault zones, transition zones, and compression zones, as shown in Figure 11[115]. The debris layer adhered to the diamond surface after DFP contained metal oxides and non-diamond carbon phases. The layer adhering directly to the diamond grains consists predominantly of amorphous carbon, demonstrating direct phase transformation from diamond to amorphous carbon during DFP[116]. For PCD, individual grains with orientations of (100), (110), and (111) have a roughness <0.5 nm. However, in regions containing multiple grain boundaries, the Ra roughness of PCD can reach 5.7 nm. Mechanical sliding, coupled with frictional heat, causes uneven thermal expansion and contraction in multi-oriented crystals, leading to increased roughness[117].

DFP is highly effective for the initial coarse processing of diamonds. However, preventing the occurrence of surface and subsurface cracks remains a critical challenge. Cracking is primarily caused by excessive pressure and speed. DFP requires high-pressure and high-speed experimental parameters to ensure that the wafer reaches high temperatures (typically above 700 °C) for removal. Therefore, a core issue to resolve is lowering the temperature required for thermal

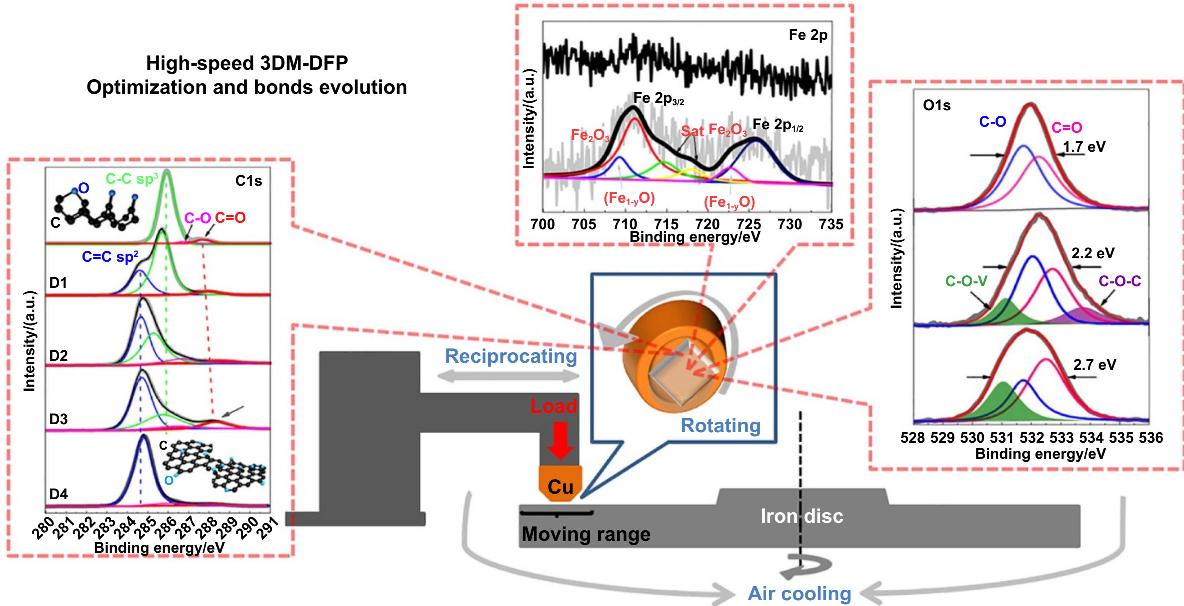

Figure 10. Schematic diagram of DFP. Reprinted from[39], Copyright (2021), with permission from Elsevier.

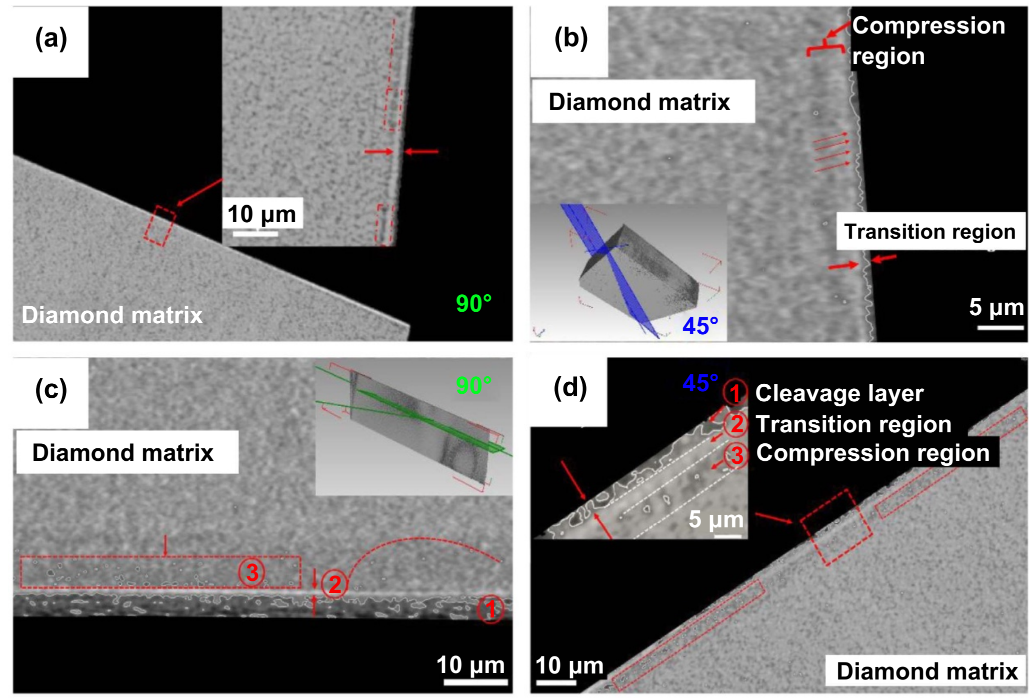

Figure 11. HR X-ray CT micrographs of polished SCD samples. (a) Cross-sectional images of the polished (100) surface of SCD-3, (b) 45° oblique section images of the polished (100) surface of SCD-3, (c) cross-sectional images of the polished (100) surface of SCD-5, and (d) 45° oblique section images of the polished (100) surface of SCD-5. Reprinted from[115], Copyright (2020), with permission from Elsevier.

reactions. Diamond exists as a metastable allotrope and can be converted into more thermodynamically stable form of graphite under certain conditions. A considerable activation energy barrier lies between diamond and graphite, making the reverse transformation—from graphite to diamond—possible only at elevated temperatures above 1 000 °C and under high-pressure environments.

Studies indicate that transition metals can accelerate diamond graphitization and lower the reaction temperature[118,119]. Thus, polishing disks can be developed using transition metals to exploit diamond graphitization, converting diamond into graphite or other amorphous carbon phases. The resulting non-diamond phases can be removed through mechanical, diffusion, and oxidation processes,

enabling effective diamond polishing. The polishing disk is a key component in DFP, requiring excellent catalytic capability as well as superior high-temperature mechanical properties, oxidation resistance, and wear resistance.

When diamond and iron plates are directly rubbed under room-temperature atmospheric conditions, the high temperatures generated during friction promote carbon diffusion and graphitization, effectively removing scratches from the diamond surface[120]. Fe-Ni-Cr alloy polishing disks, prepared using mechanical alloying and hot-press sintering techniques, exhibit increased hardness, oxidation resistance, and a higher MRR (3.7 $\mu m \cdot min^{-1}$) compared to traditional 304 stainless steel and cast iron polishing disks[121]. Additionally, W-Mo-Cr polishing disks further increase the diamond removal rate to 1.5 $\mu m \cdot min^{-1}$ while showing extremely low wear rates and high grinding ratios, demonstrating excellent wear resistance and polishing efficiency[122]. Polishing with a 0Cr18Ni9 stainless steel disk at 100 $m \cdot s^{-1}$ and pressures of 0.17–0.31 MPa yields an MRR of 36–51 $\mu m \cdot h^{-1}$[123]. Furthermore, by adding nickel and iron powders to the polishing pad and performing high-speed polishing (1 800–4 200 rpm), the roughness of the diamond surface can be significantly reduced to Ra 0.25 nm and PV 2.30 nm, further improving the surface quality of the polished diamond[124]. These studies demonstrate that optimizing the polishing disk materials and process parameters can significantly increase the efficiency and surface quality of diamond polishing.

2.6. Mechanical polishing (MP)

Mechanical polishing (MP) can be categorized into fixed abrasive polishing and free abrasive polishing. In fixed abrasive polishing, diamond abrasives are embedded onto a grinding disc or wheel[125], and polishing is achieved through the mechanical action of protruding diamond abrasive grits against the workpiece surface. This approach provides a stable grinding force, but abrasive wear and failure can compromise polishing quality. Under high pressure, deep scratches on the polished surface or damage to the diamond disc may occur. Therefore, it is of great significance for controlling damage and obtaining high-quality surfaces to focus on the brittle−plastic transformation mechanism of hard and brittle materials. For example, Li et al.[126] developed a normal scratch force theoretical model driven by the strain rate effect, and verified the strain rate sensitivity coefficient of brittle and hard materials, such as GaN. The results revealed that the brittle−plastic transition and subsurface damage behavior exhibited a significant strain rate dependence, which not only deepened the understanding of the influence of abrasive coupling effect on the evolution of surface microstructure, material removal, and damage accumulation, but also provided theoretical guidance for parameter optimization in brittle solid grinding. In contrast, free abrasive polishing involves suspending diamond grits in a liquid medium. The abrasives move freely with the liquid, which helps reduce surface damage to the workpiece[127]. However, controlling the distribution and movement of abrasives is challenging, often resulting in inconsistent surface roughness. Therefore, this approach requires more stringent control over the uniformity and dispersibility of the grit distribution. Furthermore, free abrasive polishing typically has a lower efficiency compared to fixed abrasive polishing.

2.6.1. Fixed abrasive polishing.

Precise control of the polishing parameters is critical for achieving satisfactory surface and subsurface quality during diamond mechanical polishing. Inadequate control of these parameters can lead to surface damage, such as scratches and pits, as well as subsurface damage like crystallite defects or even microcracks[128]. Key parameters, such as the polishing pressure and rotational speed, significantly affect the polished surface morphology and damage features. For example, when diamond wheels are used, larger diamond grits may induce irregularly spaced microcracks perpendicular to the polishing direction due to stick-slip motion on the polishing disc, as shown in Figure 12[129]. To minimize such damage, Kubota et al. evenly distributed micron-sized diamond abrasives on the polishing plate and carefully controlled the process parameters, which enabled an average surface roughness of 0.1–0.3 nm on SCD to be achieved[130]. Similarly, Lu et al. reported surface roughness Sa values of 0.548 nm to 4.20 nm when using vitrified bond diamond wheels at rotation speeds of 750 rpm and 1 050 rpm to polish PCD, with no subsurface damage observed[128]. However, at a speed of 1 350 rpm, subsurface defects such as stacking faults, micro-cracks several microns deep, and a 15 nm thick graphite layer were observed[128]. Further studies revealed that during PCD polishing, a new ripple-like structure with a <110> orientation was formed on the diamond surface, attributed to the uneven distribution of defect carbon atoms, resulting in a periodic surface pattern[131]. In contrast, polishing with SiO_2 wheels exhibited isotropic behavior, with minimal difference in the polishing rates along the <110> and <100> directions on the (100) surface. It also led to minimal surface and subsurface damage, and no dark contrasts associated with lattice distortion or crystal defects were observed via SEM[132]. These studies suggest that by optimizing the polishing parameters and selecting appropriate tools, both surface and subsurface damage can be effectively minimized, enabling high-quality surface finishes.

Significant breakthroughs have been made through improving the tooling technology to increase the diamond polishing efficiency. Xin et al.[133] used a high-speed spin polishing device equipped with highly self-sharpening diamond wheels to polish PCD, achieving ultra-low surface roughness of Ra 0.523 nm. Nevertheless, the removal rate was extremely low at only 32.4 $\mu m \cdot h^{-1}$, underscoring the trade-off between surface quality and efficiency. To address this limitation, Xu et al.[134] developed a titanium-containing alumina wheel by incorporating Ti into the wheel matrix, which enabled an MRR of 5.57–56.35 $\mu m \cdot h^{-1}$ in the polishing of diamond. The performance of the new wheels outperformed that of traditional metal wheels. In subsequent work, Xu et al. fabricated a new ceramic wheel by incorporating iron, cerium (Ce)[135], and

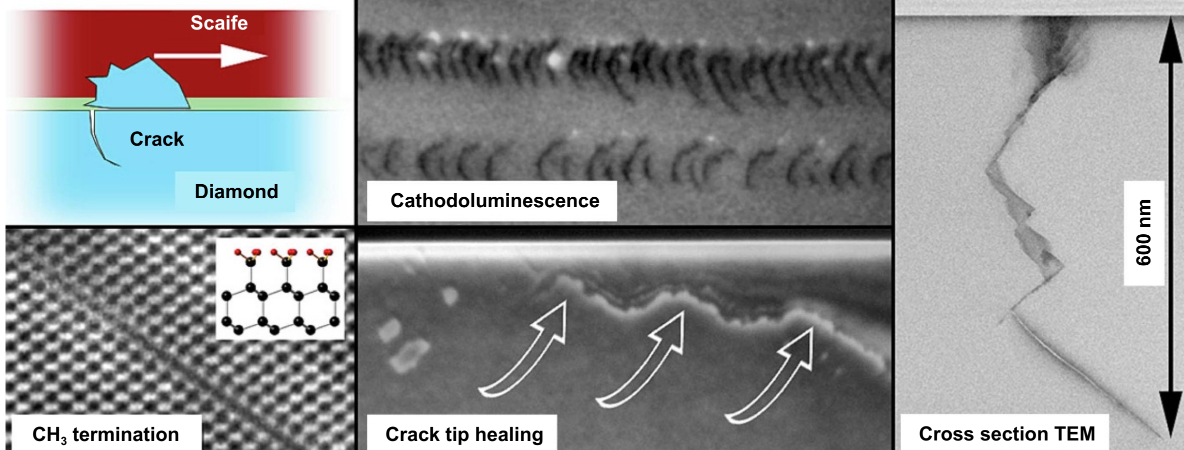

Figure 12. Microcracks on the polished diamond surface and subsurface. Reprinted from[129], Copyright (2024), with permission from Elsevier.

Ti[136] into an aluminum (Al) matrix, which further increased the MRR to 120.2 μm·h^{-1}[136]. Zhou et al.[137] used a vacuum micro-evaporation coating technology to deposit a uniform Ti thin film on diamond grains, producing a novel diamond wheel with an MRR as high as 1 662 nm·min^{-1}, while also improving the surface quality. Nevertheless, high-efficiency processing often comes at the cost of increased surface damage. For example, Li et al.[138] fabricated a CuO-reactive resin matrix diamond wheel for 2-inch PCD, achieving a removal rate of 118.8 μm·h^{-1} but exhibiting severe surface damage, including deep cracks, pits, and a roughness of Ra 4.65 nm. In summary, the "hard grinding hard" processing strategy, while effective in improving efficiency, resulted in significant wear of the grinding tool.

During polishing of diamond, anisotropy plays a critical role in determining both the polishing efficiency and surface quality. Significant differences in Young's modulus, bulk modulus, shear modulus, and Poisson's ratio of different crystallographic faces of diamond led to different threshold values for damage initiation on each crystal face[139,140]. This anisotropy causes substantial differences in MRR in different directions[141], where even minor changes in the polishing angle can lead to distinctly different polishing outcomes[142]. For example, polishing along hard crystallographic directions typically produces higher surface roughness, whereas polishing in softer directions results in smoother surfaces[127]. In the polishing of PCD, anisotropic effects are even more pronounced because of the random orientation of the grain types and their heterogeneous textures[143]. Furthermore, the wheel rotation direction also affects the anisotropy behavior during polishing[144], further complicating the process control. In terms of polishing parameters, higher scratching speeds and pressures can increase the MRR, but they also exacerbate wear on the polishing disc or wheel, leading to severe surface and subsurface damage[145]. The residual stresses generated during polishing can induce micro-cracks or even fractures in the diamond matrix, further compromising the structural integrity and performance of the workpiece. Therefore, while striving for high efficiency, it is crucial to consider the combined effects of anisotropy and process parameters on surface quality to avoid excessive damage.

When combined with optimized processing conditions and proper tool orientation selection, MP enables controllable fabrication of diamond tools with surface roughness down to the sub-nanometer scale and cutting edge sharpness at the nanometer level, providing a reliable pathway for ultra-precision diamond tool manufacturing. Zong et al. proposed a simple and efficient thermomechanical lapping process using a cast iron scaife covered by diamond grits with a size of 0.1 μm, in which material removal is primarily governed by carbon atom diffusion, accompanied by partial graphitization and oxidation. During MP, surface carbon atoms continuously detach from the crystal lattice, sustaining the wear process and enabling tool sharpness in the range of 2–9 nm[146,147]. Further studies revealed that factors such as vibration of the lapping apparatus, surface quality of the lap, spindle precision, grinding pressure, and speed significantly affect the contact accuracy and, consequently, the edge radius. Under optimized conditions, ductile-mode lapping can produce high-quality tools with an edge radius of 30–40 nm and a rake face roughness of Ra 0.7 nm[148].

In summary, the interplay between anisotropy, process parameter, and surface/subsurface damage in diamond polishing is complex. Future research should focus on optimizing the polishing direction, precisely controlling the process parameters, and developing innovative polishing tools to maximize the MRR while minimizing surface and subsurface damage. Such efforts are essential to achieve efficient, high-quality diamond polishing.

2.6.2. Free abrasive polishing. In free abrasive polishing, diamond grits of various sizes are mixed with water to form a polishing slurry, which is used for polishing with a cast iron disk[149,150]. Owing to the low rotational speed of the polishing disk, typically only a few tens of revolutions per minute,

this method effectively minimizes the risk of surface and subsurface cracking, making it particularly suitable for polishing large size diamond wafers. The surface roughness of the diamond wafer can be reduced from several microns to the nanometer range, but the process is time-consuming, often requiring several dozen hours, with a removal rate typically ranging from 4 μm·h^{-1} to 15 μm·h^{-1}[151]. Research indicates that the abrasive concentration and particle size, polishing pressure, and polishing speed are key factors affecting both the MRR and surface quality[18,151–153]. By optimizing the oscillation amplitude of the polishing head, polishing disk, and polishing head speed, for instance, the surface PV value of a 2-inch PCD after polishing was controlled to 2.4 μm, with a surface roughness of Ra 139 nm and an MRR of 10.1 μm·h^{-1}[154]. These studies demonstrate that optimizing abrasive combinations and process parameters can enhance polishing efficiency, while maintaining high surface quality. Future research may further explore the integration of novel abrasives and polishing technologies to achieve higher efficiency and reduce damage in diamond polishing. MP remains a key method for fabricating high-performance diamond tools. Traditional polishing with 0.25 μm diamond abrasives on the (110) crystal plane yields a residual roughness of about 1 nm rms, while dry polishing with a tin lap in air can further reduce the roughness to below 0.1 nm rms, with a lateral resolution of approximately 100 nm[155].

The key advantage of mechanical polishing lies in its ability to obtain nanometer-level surface roughness on large-sized wafers. As a rough polishing method, MP enables global planarization, which is essential for applications such as optical windows where high wafer shape accuracy is required. However, its polishing efficiency is relatively low compared with that of advanced approaches such as laser polishing and dynamic friction polishing.

2.7. Chemical mechanical polishing (CMP)

Chemical mechanical polishing (CMP) synergistically integrates chemical etching and mechanical abrasion. This process relies on slurry-based chemical agents to generate a softened reaction layer on the material surface, enabling controlled material removal[156]. Moreover, the mechanical friction between the slurry's nano-abrasives and the polishing pad removes this reaction layer, achieving efficient and uniform material removal in dynamic equilibrium, ultimately resulting in an atomically smooth surface. CMP is widely used to achieve atomic surface globally[157]. However, in traditional CMP, toxic and corrosive slurries are normally employed, resulting in pollution of the environment[158]. To overcome this challenge, novel green CMP was developed for diamond[159], copper[160], silicon[161], sapphire[162], fused silica[163], alloy[164], and quartz glass[165]. Using the green CMP, an atomic surface is acquired for potential use in the semiconductor, microelectronics, and optoelectronics industries[166]. Nevertheless, the most important thing is that these studies are a great contribution to the conventional CMP and manufacturing, effectively reducing the pollution to the environment[167].

The schematic diagram of CMP is depicted in Figure 13. The three key elements of CMP are the polishing slurry, polishing pad, and polishing parameters. In CMP, the mechanical action not only directly participates in material removal but also promotes the decomposition of oxidizing agents, accelerating the chemical reactions. Jin et al.[168] developed a system to monitor the interface frictional force in real time during polishing. The experiments revealed that when the friction coefficient was between 0.060 and 0.065, the polishing system was in a mixed lubrication state, which provided the optimal polishing conditions. Yuan et al.[169] developed a polishing head integrating real-time friction force measurement, achieving a removal rate of 0.055 mg·h^{-1}. Thermodynamic analysis demonstrated that the composition of the oxidized diamond reaction products critically governs both the surface quality and removal efficiency.

Owing to its high hardness, brittleness, and chemically stable nature at room temperature, diamond is difficult to polish efficiently via traditional "hard-to-hard" methods and is prone to substantial surface and subsurface damage. Thus, improving the oxidation degree of the diamond surface is a core issue in CMP processing. Extensive research has been conducted worldwide on designing and optimizing polishing slurries to overcome this challenge. Temperature is a key factor affecting the activity of chemical agents. Cheng et al.[170] heated the polishing pad to 70 °C and used $KMnO_4$ and diluted H_2SO_4 solution as oxidants, reducing the surface roughness of the diamond to Ra 20 nm, with local roughness Ra < 10 nm. However, heating the polishing pad leads to evaporation of the polishing slurry, reducing oxidation efficiency, which in turn limits the removal rate. Studies have shown that the pH value, composition, and particle size of the abrasives in the slurry significantly affect the polishing rate, with smaller abrasive particles usually achieving higher polishing rates[171,172]. Additionally, the diamond (111) crystal face yields a lower roughness than the (100) crystal face after polishing[173]. Yang et al.[174] controlled the temperature by adding liquid nitrogen to the slurry, finding that low temperatures effectively suppressed the removal rate of diamonds, keeping it within the nanometer range, and thus achieving atomic-scale material removal. Strong oxidants such as potassium ferrate (K_2FeO_4), potassium permanganate ($KMnO_4$), potassium dichromate ($K_2Cr_2O_7$), and hydrogen peroxide (H_2O_2) are widely used in diamond CMP slurries, but these oxidants often struggle to balance the surface quality and removal rate. For example, a K_2FeO_4 slurry achieved an Ra of 0.478 nm surface roughness but with an MRR of only 160 nm·h^{-1}[175]. The root cause of the diamond polishing problem lies in the inability of existing oxidants to fully oxidize their surface. Hydroxyl radicals (•OH), as strong oxidants second only to F_2 in nature, can be generated through the Fenton reaction. The Fenton reaction, using an iron catalyst (Fe) and H_2O_2, generates •OH. The core principle involves Fe^{2+} reacting with H_2O_2 to form Fe^{3+} and •OH, with Fe^{3+} further reacting with H_2O_2 to regenerate Fe^{2+}. Various Fenton reaction

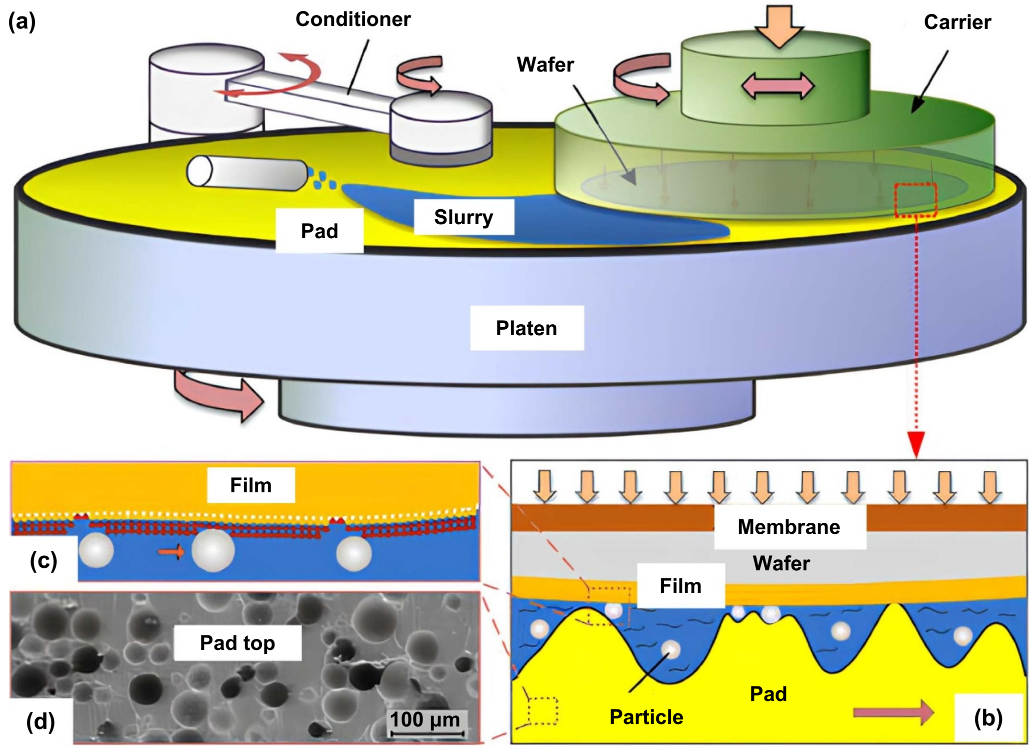

Figure 13. Schematic of CMP equipment and wafer−pad interactions: (a) CMP equipment, (b) wafer−pad interactions, (c) details of particle−film interactions, and (d) SEM image of the top surface of the pad. Reproduced from[34]. CC BY 4.0.

types include classic Fenton reactions[176], photo Fenton reactions (using UV light to enhance the reaction efficiency)[177], electro-Fenton reactions (continuously generating H_2O_2 and Fe^{2+} through electrolysis)[178], and modified Fenton reactions (using other transition metals, iron complexes, or solid catalysts)[179].

With respect to the literature on Fenton polishing slurries for diamond CMP, the type of abrasives (such as silica (SiO_2)[159], boron carbide (B_4C)[180], alumina (Al_2O_3)[171], ceria (CeO_2)[171], and diamond abrasives[181]), abrasive particle size[171], slurry pH value[171], and additives[182] significantly influence the polishing effect. Under the combined influence of Fenton reaction solutions and diamond abrasives, the MRR of SCD can reach 586.43 μm^2, which is 1.56 times higher than that of the Fenton reaction alone[183]. Additionally, the type of Fenton reaction also impacts polishing performance. Kubota et al.[120,184,185] immersed diamond wafers in H_2O_2 solution with cast iron pads under high pressure (1 MPa) and high rotational speed (500 rpm), achieving an Ra of 0.058 nm surface roughness, but with an MRR of only 200 nm·h^{-1}. Yuan et al.[186] developed different types of Fenton polishing slurries, achieving an Sa of 0.076 nm surface roughness and an MRR of 881 nm·h^{-1} in a new homogeneous-type modified Fenton polishing slurry containing diamond abrasives. Additionally, the use of solid-phase catalysts such as Fe_3O_4 ensures continuous and stable Fenton reactions with higher catalytic efficiency[187]. The optimized slurry achieved a removal rate of 742.7 nm·h^{-1} and Ra of 0.292 nm surface roughness[188].

Along with optimizing the polishing slurry, enhancing the polishing pad design is essential for improving the diamond removal rates. For example, sol-gel (SG) technology has been used to prepare semi-fixed abrasive polishing pads[189,190], while increasing the removal rate to 500 nm·h^{-1}, leading to issues like significant pad wear. Kim and Kang[191] deposited diamond on a silicon nitride substrate to create new polishing pads that showed excellent performance in MRR, chemical stability, and durability but still resulted in subsurface damage due to hard abrasive polishing. Moreover, optimizing process parameters[192] or increasing the types and concentrations of oxidants in the slurry can increase the oxidation rate of diamond surfaces, but the improvement in MRR remains limited.

In summary, CMP is applied for the planarization of diamond substrates used in high-power electronic devices and quantum sensing chips, emphasizing its capability to achieve an Ra $<$ 1 nm, but also noting its low MRR and slurry cost, which can be limiting for large-area wafer-scale processing. The core challenge in diamond CMP processing lies in balancing surface quality with MRR. By optimizing slurry composition, improving polishing pad design, and controlling process parameters, the polishing efficiency and quality can be improved. However, further research is needed to explore new oxidants, catalysts, and polishing techniques to achieve efficient, low-damage diamond polishing.

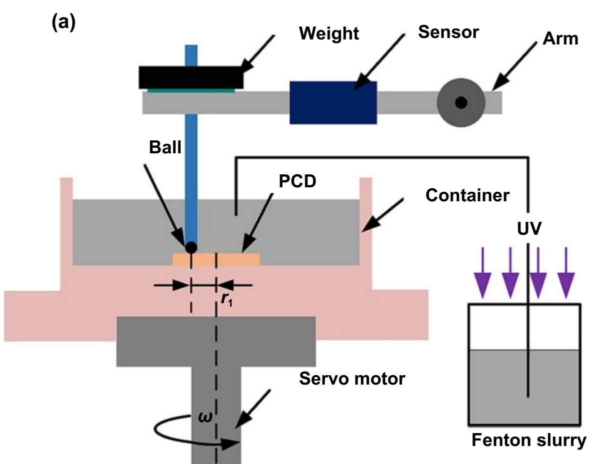

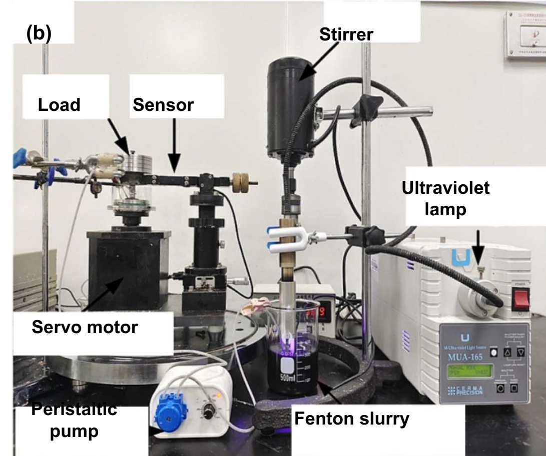

Figure 14. Schematic of (a) the friction and wear experiment and (b) device. Reproduced with permission from Elsevier Copyright (2023). Reprinted from[205], Copyright (2023), with permission from Elsevier.

2.8. Energy field-assisted polishing

Energy field-assisted polishing is a technology that uses external energy fields (such as lasers, ultraviolet light, plasma, and ultrasonic waves) to assist traditional mechanical polishing methods. The objective of energy field-assisted polishing is to improve the material removal efficiency, enhance the surface quality, and minimize subsurface damage. Its underlying principle lies in utilizing an external energy field to alter the physical and chemical properties of the material surface—either by reducing hardness or increasing surface activity—thereby facilitating material removal. This approach significantly enhances the efficiency and surface finish of conventional mechanical polishing, particularly for ultra-hard materials (e.g., diamond) and components with complex geometries. However, these methods generally face issues like high equipment costs and complex processes. Further optimization of the technology, cost reduction, and expanding its application scope is needed in the future.

2.8.1. Ultraviolet-assisted polishing (UVAP).

Ultraviolet-assisted polishing (UVAP) works by exciting catalysts in the polishing slurry[193] or directly irradiating the workpiece surface with UV light to induce surface electronic transitions, weaken chemical bonds, and increase surface reactivity. This makes the material more likely to chemically react with the polishing slurry, and the mechanical action then removes the reaction products.

The UV light-mechanical synergistic mechanism enables efficient and low-damage polishing to achieve nano-level surface precision at room temperature. UVAP has been applied to materials such as SiC[194–196], GaN[197–199], and Si[200], and has since been extended to diamond processing[201]. Research has shown that under UV light, photocatalysts exhibit strong oxidative properties. For example, a polishing slurry containing P25 TiO_2 reduced the diamond surface roughness from Ra 33.6 nm to Ra 2.6 nm within 8 hours[202]. Nanodiamonds (ND) and CuFe layered double hydroxide (LDH) were used as catalysts to increase the removal rate of diamond from 260 $nm{\cdot}h^{-1}$ to 370 $nm{\cdot}h^{-1}$. Additionally, Xiong et al. demonstrated that the combination of UV light and the Fenton reaction further increased the generation efficiency of •OH through friction and wear experiments, as shown in Figure 14[203]. UV light irradiation of H_2O_2 solution promotes the generation of large amounts of •OH, yielding the highest MRR of 4.888 $\mu m^3{\cdot}min^{-1}$[204]. By optimizing the slurry parameters (such as pH = 3, light intensity = 100 $mW{\cdot}cm^{-2}$, Fe_3O_4 concentration = 2 wt%, H_2O_2 concentration = 10 wt%), the removal rate of PCD can be increased to 285.4 $\mu m^3{\cdot}min^{-1}$[205]. Using Al_2O_3 polishing pads, an MRR of 713.5 $nm{\cdot}h^{-1}$ can be achieved, whereas SiO_2 pads yield a super-smooth surface with an Ra of 0.26 nm[206].

The core of UVAP lies in the use of UV light to irradiate the polishing slurry or pad, promoting the generation of strong oxidative products, and thereby enabling MRR. The current polishing devices of UV-irradiated disc are presented in Figure 15. For instance, UV light irradiation of the slurry on the polishing pad[182] or the polishing liquid in a beaker[204,207] yields ultra-smooth surfaces below Ra $\leq$ 0.1 nm, with material removal rates of up to 698.7 $nm{\cdot}h^{-1}$. Yuan et al. developed a novel Fenton slurry and UVAP testing device using JGS glass as a polishing pad. UV light irradiated the workpiece and slurry from beneath the polishing pad, resulting in a surface roughness of Ra 0.071 nm and a removal rate of 1 021 $nm{\cdot}h^{-1}$, with a subsurface damage layer of only 0.6 nm[208]. During PCD polishing, the highest MRR achieved was 666.9 $nm{\cdot}h^{-1}$, with a surface roughness of Ra 2.58 nm[209]. To further improve the polishing efficiency, Yu et al. developed a green photocatalyst, PB/TiO_2, made from nontoxic PB and TiO_2, which broadened the pH range of the Fenton reaction. After CMP experiments, the diamond surface roughness was only 0.079 nm, with a damage layer thickness of only 0.66 nm, and the MRR reached 1 168 $nm{\cdot}h^{-1}$[210].

In addition to directly irradiating the polishing slurry, UV light can also be used to irradiate the polishing pad to enhance the polishing effect. Mutsumi et al.[211,213] used quartz glass

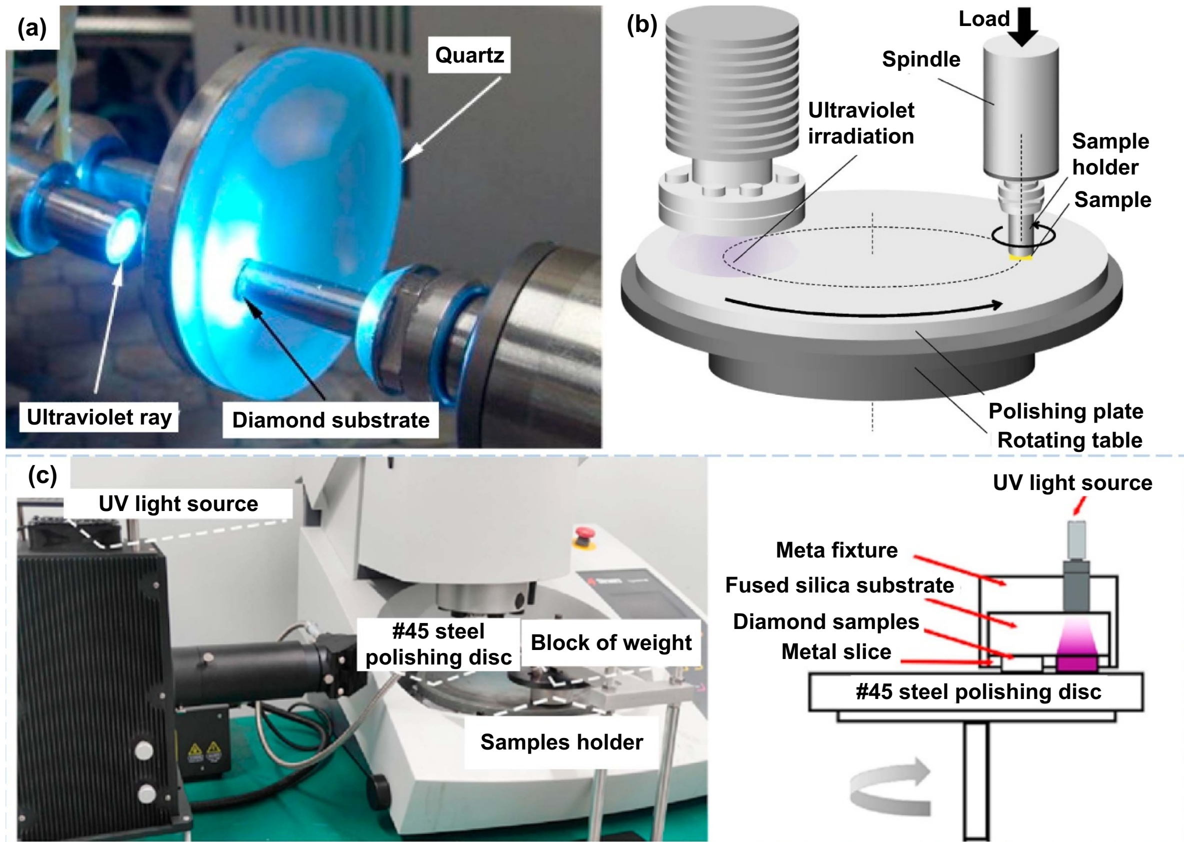

Figure 15. Current polishing devices of UV-irradiated discs. (a) UV irradiating quartz glass disk. Reprinted from[211], Copyright (2013), with permission from Elsevier. (b) UV irradiating sapphire disk. Reprinted from[36], Copyright (2018), with permission from Elsevier. (c) UV irradiating #45 steel disk. Reprinted from[212], Copyright (2023), with permission from Elsevier.

as a polishing pad and irradiated it with UV light, achieving a surface roughness of Ra 0.35 nm and a removal rate of 0.5 $\mu m \cdot h^{-1}$. However, this method relies on high mechanical pressure and rotational speeds (600–2 000 rpm), leading to severe pad wear and no use of polishing slurry, limiting its application. Kubota and Takita[36] used sapphire as a polishing pad and irradiated it with UV light under vacuum, achieving an RMS surface roughness of less than 0.1 nm but with a removal rate of only 238.1 $nm \cdot h^{-1}$.

To address the issues associated with high-speed polishing, Jiang et al.[212] developed a UV-assisted low-speed polishing technique for diamond, employing a #45 steel polishing pad and embedding the diamond specimen in quartz glass. The UV light penetrates the quartz and irradiates the contact interface between the diamond and the pad, thereby promoting phase transformation and oxidation processes on the diamond surface. This method enables efficient material removal at low speeds and yields an ultra-smooth diamond surface with a roughness of Ra = 0.18 nm and Rq = 0.26 nm. In subsequent studies, Wu et al.[214] further optimized the process with sample rotation and lateral oscillation, which significantly improved polishing uniformity, with a surface roughness Sa less than 0.175 nm over a 160 $\mu m \times 140$ μm area. The theory of rupture of C–C bonds initiated by graphitization was proposed, and low-gas-pressure UV-assisted polishing was initially developed for highly efficient atomic-scale smooth diamond polishing. The MRR reached 15.8 $\mu m \cdot h^{-1}$, which was considerably higher than that of previously reported damage-free polishing techniques[215].

UVAP, leveraging the light-mechanical synergistic mechanism, offers unique advantages for efficient, low-damage diamond processing. Recent research has balanced surface quality and removal efficiency by optimizing photocatalysts, slurry formulations, and process parameters. However, challenges such as tool wear from high-speed polishing, complex equipment needs, and the anisotropy of PCD still need to be addressed. Future research may focus on developing more efficient photocatalytic systems, wear-resistant polishing pads, and multi-physical field coupling techniques to further enhance ultra-precision diamond processing.

2.8.2. Plasma-assisted polishing (PAP). Plasma-assisted polishing (PAP) is a composite polishing technology that combines plasma activation with mechanical polishing. It leverages high-energy particles in the plasma, such as ions, electrons, and free radicals, to chemically react with the surface of the material, creating volatile compounds or softening the surface layer. The mechanical action then removes the material efficiently. Compared with traditional mechanical polishing, PAP significantly improves polishing efficiency while reducing subsurface damage. It has been successfully applied in

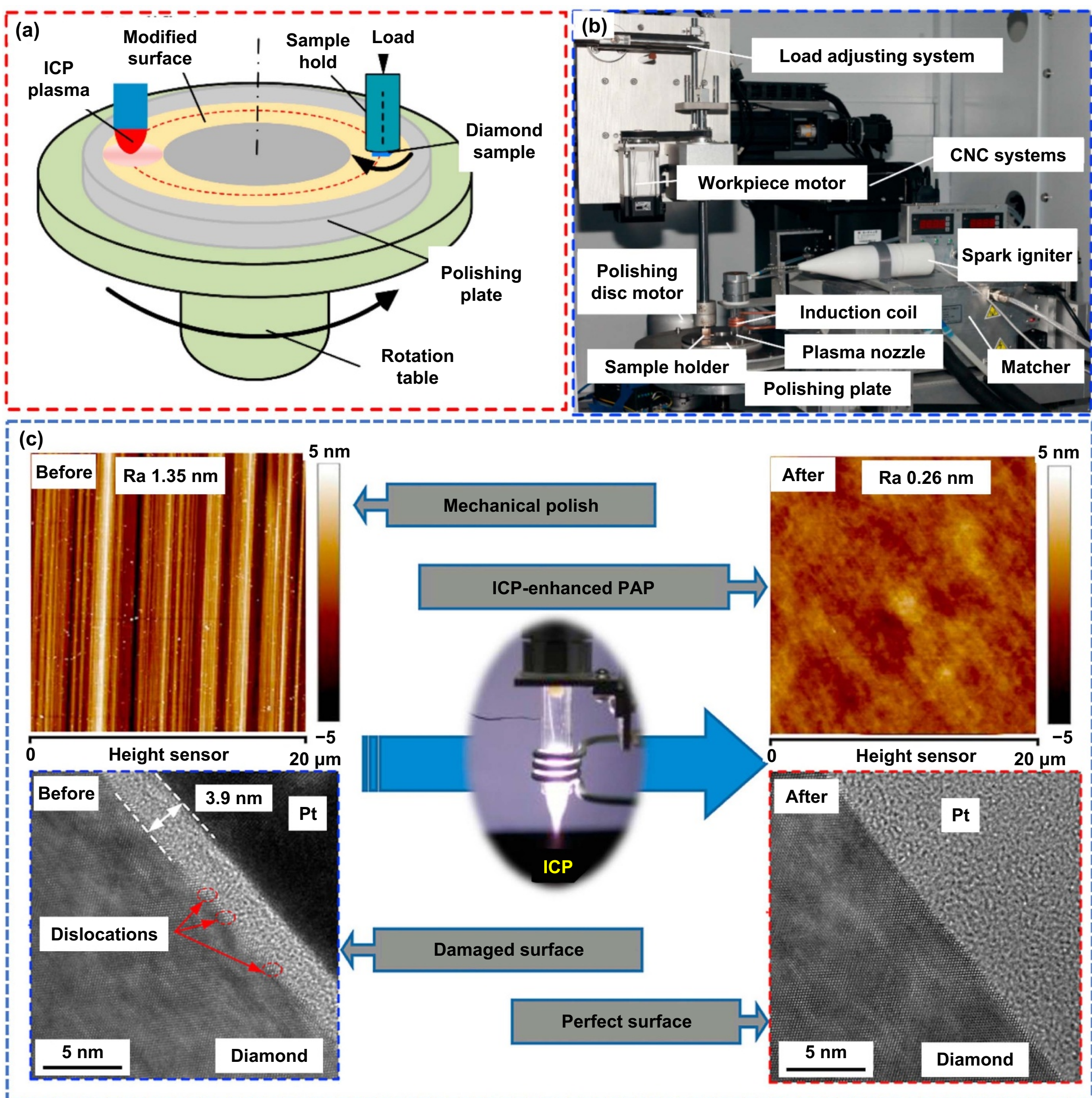

Figure 16. PAP device and its effect. (a) Schematic diagram of the device. (b) Photo of the device. (c) Surface morphology and subsurface damage after polishing. (a)–(c) Reprinted from[35], Copyright (2021), with permission from Elsevier.

the polishing of materials such as SiC[216–218], GaN[219,220], and Lu_2O_3[221,222], and the method has since been extended to diamond polishing.

The key to PAP technology is the use of plasma to activate the polishing pad or diamond surface to promote chemical reactions. For example, Yamamura modified glass polishing pads in a vacuum environment by using water vapor or O_2 as reactive gases, enabling the surface of the pad to adsorb •OH. When SCD interacts with the modified polishing pad, the •OH radicals react with the carbon atoms on the diamond surface, resulting in oxidation and achieving ultra-smooth surfaces with an Ra of 0.46 nm and an MRR of 2.1 $\mu m \cdot h^{-1}$[223]. Building on this, Deng et al. further explored the mechanism of plasma-modified silicon polishing pads and discovered that •OH effectively removed carbon atoms from the diamond surface through dehydration condensation reactions at the interface, reducing the SCD roughness to 0.86 nm[35], while the PCD roughness was 10.7 nm[224]. The related device and results are shown in Figure 16. Furthermore, Yuan et al.[225]. developed an atomic-scale planarization method for PCD that combined •OH-mediated plasma oxidation and CMP. The •OH plasma pretreatment formed a uniform ∼30 nm-thick modified layer comprising carbon−oxygen mixed and oxygen−rich regions. Subsequent CMP removal of this layer resulted in atomic-level flatness with a surface roughness of Sa 0.366 nm.

However, the short lifetime of •OH (on the nanosecond scale) limits its oxidation effect, preventing a significant increase in polishing efficiency. To address issues like pad wear and surface profile accuracy, Liu et al.[226] proposed a strategy of continuously irradiating quartz glass polishing pads with plasma. Under a polishing pad speed of 300 rpm,

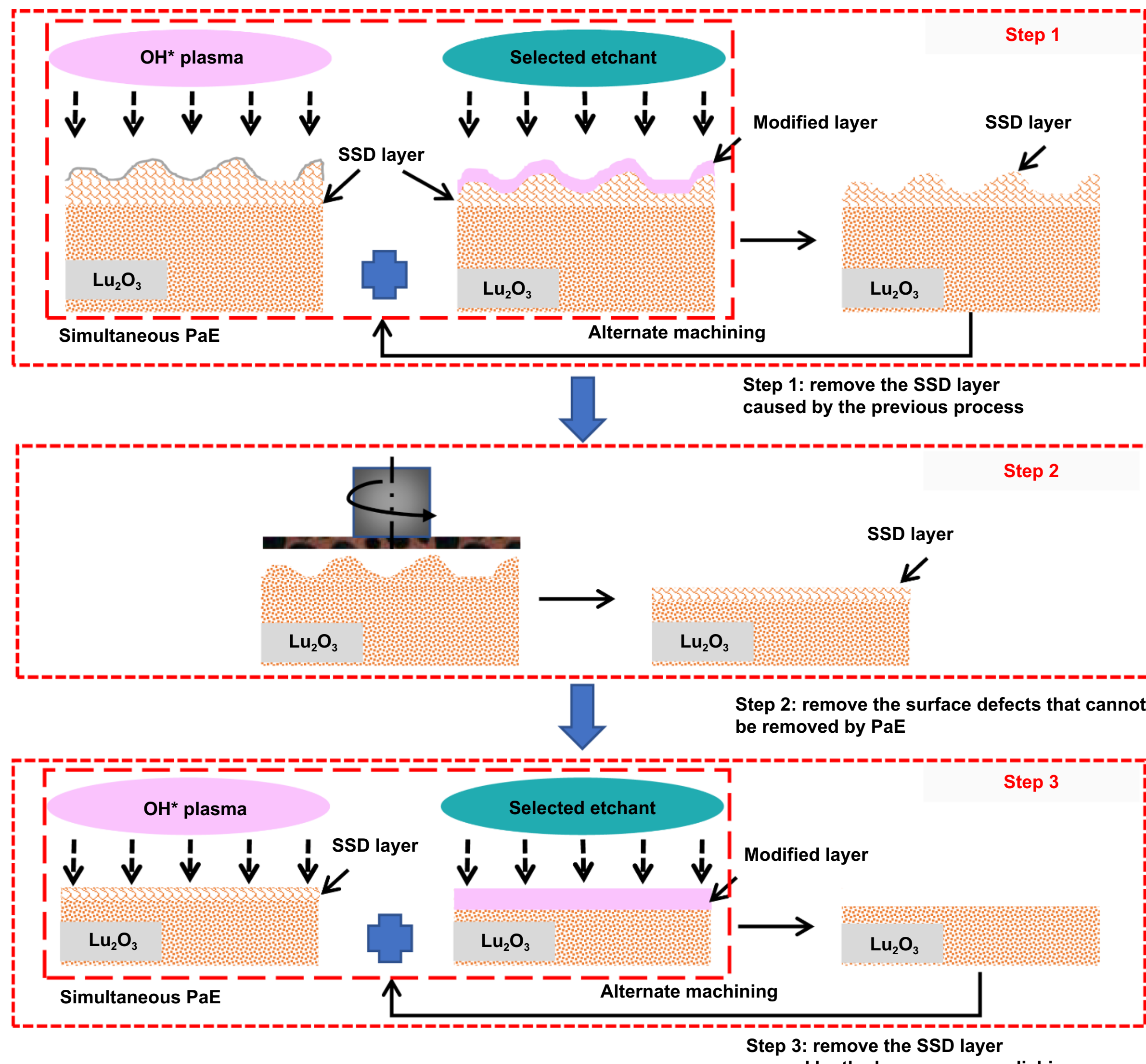

Figure 17. Schematic illustration of the hybrid process combining PaE with low-pressure polishing. Reprinted from[222], Copyright (2023), with permission from Elsevier.

plasma activation simultaneously removed subsurface damage caused by MP, ultimately achieving a diamond surface with an Sq roughness <0.5 nm and an increase in the initial MRR to 13.3 μm·h^{-1}[227]. This result demonstrated that plasma activation could effectively suppress pad wear while maintaining the integrity of the polished surface. To further optimize this process, Yu et al. developed a composite method combining inductively coupled plasma (ICP) etching and DFP. First, O_2 plasma treatment was used to generate a sp^2 amorphous carbon layer on the SCD surface, followed by MP to remove the softened amorphous layer, which achieved ultra-precise surfaces with an Ra of 0.185 nm[228].

To minimize or even entirely eliminate atomic-scale damage to the outermost surface layer caused by direct mechanical contact, a noncontact polishing technique known as plasma-assisted etching (PaE) has been developed[221,222]. This method utilizes the high chemical reactivity of active species in the plasma to generate a modified surface layer on the sample, which is subsequently removed via wet chemical etching, resulting in a completely damage-free surface. The schematic illustration of the hybrid process combining PaE with low-pressure polishing is shown in Figure 17. To further increase processing efficiency, PaE is often employed in combination with low-pressure mechanical polishing in an alternating sequence. In this hybrid process, the duration of low-pressure polishing is significantly shorter than that of conventional CMP, thereby substantially minimizing the thickness of the subsurface damage layer caused by mechanical contact. Moreover, when plasma-assisted etching is used as the final processing step, surfaces with nearly perfect crystalline structures can be achieved. This endows the method with remarkable potential for damage-free processing of chemically inert crystalline materials[229,230].

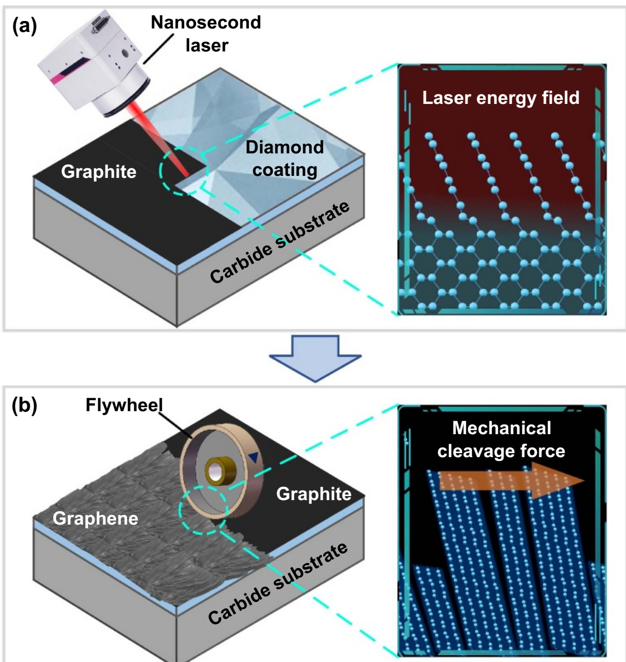

Figure 18. Schematic diagram of LAP. Reproduced from[231]. The Author(s). CC BY 4.0. (a) Laser induction. (b) Mechanical cleavage.

Despite the significant advantages of PAP and PaE in diamond polishing, several challenges remain for their practical application. For instance, when using glass or silicon as the polishing pad, the high hardness of diamond in direct contact with the pad leads to rapid pad wear and difficulty in maintaining profile accuracy. Additionally, the transient and localized nature of plasma activation makes it challenging to control the reaction uniformity. Future research should focus on developing methods to stabilize long-lifetime active particles and innovative designs for wear-resistant polishing pad materials, aiming to scale up PAP technology for ultra-precision processing applications.

2.8.3. Laser-assisted polishing (LAP). Laser-assisted polishing (LAP) represents a hybrid approach that synergistically combines laser-induced surface modification with mechanical material removal, aiming to achieve high-efficiency and high-quality polishing of hard and brittle materials such as diamond. The fundamental principle of LAP relies on the thermal effect of laser irradiation, which induces localized melting, graphitization, phase transformation, or oxidation on the diamond surface. This surface-modified layer is then selectively removed by subsequent mechanical polishing, thereby realizing a significant increase in the material removal rate (MRR) while maintaining acceptable surface integrity. The schematic diagram of LAP is illustrated in Figure 18.

Typically, nanosecond-pulsed lasers are employed in LAP due to their relatively low cost and high energy efficiency. Such lasers can generate a thick graphitized or softened layer on the diamond surface, which is more easily removed mechanically compared with pristine diamond. Consequently, LAP achieves higher removal rates and improved processing efficiency compared with conventional mechanical polishing methods, making it particularly suitable for machining superhard and brittle materials. However, the thermal nature of nanosecond laser irradiation inevitably introduces challenges. Excessive thermal loading may cause undesirable effects, such as heat-affected zones, surface roughening, and severe subsurface damage, all of which can degrade the optical and mechanical performance of the final component. Moreover, achieving a uniform and controlled modification layer remains a key technical bottleneck, as uneven graphitization or oxidation may lead to inconsistent material removal and surface defects.

Recent studies have explored strategies to optimize LAP. For example, Yan et al.[231] proposed thermal stress control at coating interfaces and demonstrated a novel process of precise graphitization on a diamond surface through laser induction and mechanical cleavage, ultimately enabling rapid conversion of the diamond coating surface to graphene while controlling the thickness and roughness. Moreover, Liu et al.[53] proposed an innovative laser processing strategy using thin film coatings, where a 36 nm gold film was first deposited on the SCD surface. The gold film ensures uniform laser energy absorption, preventing uneven processing caused by local energy distribution variations. After treatment with nanosecond laser pulses, a continuous self-maintaining graphite layer formed on the diamond surface. This approach allowed for the uniform removal of several micrometres of material, achieving a surface roughness of Sq $=$ 7.81 µm. The “energy buffering” function of the gold film solved the problem of uneven laser absorption on the bare diamond surface, providing a controlled pre-processing method for rough diamond machining. However, the laser-treated surface still exhibited a serrated appearance and relatively high roughness, requiring subsequent fine polishing (such as CMP) to remove the graphite layer and achieve nanometer-level surface precision.

The efficiency and quality of LAP are highly dependent on the synergistic optimization of process parameters. The laser energy density, scanning speed, and gold film thickness influence the uniformity and thickness of the graphite layer, which in turn affects the efficiency of the subsequent MP. Future research needs to further explore the dynamic mechanisms of laser-mechanical synergy and develop femtosecond or picosecond laser processes that produce low heat-affected zones (HAZ), balancing processing efficiency with subsurface integrity. Moreover, combining laser pre-treatment with other polishing techniques (such as ultraviolet catalytic polishing) could form a “rough-fine” integrated composite processing chain, opening new avenues for high-efficiency ultra-precision processing of superhard materials. By refining the understanding of laser processing dynamics and integrating it with mechanical polishing methods, LAP holds great potential for advancing the ultra-precision machining of hard materials like diamond, reducing damage while improving both the efficiency and surface quality.

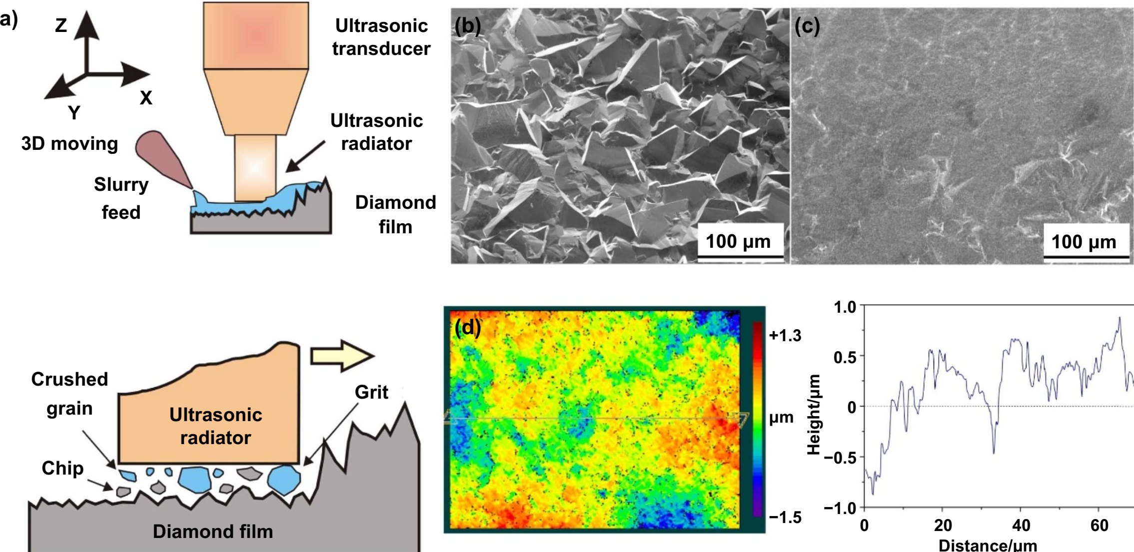

Figure 19. Schematic diagram of UVP. (a) Schematic of ultrasonic-assisted lapping of a diamond surface in a flow of a microdiamond-based slurry; (b) SEM images of diamond surface as received; (c) SEM images of diamond surface after UVP for 5 min; (d) the optical profilometer with a measurement area of 0.90 mm × 0.67 mm after polishing for 5 min. Reprinted from[37], Copyright (2016), with permission from Elsevier.

2.8.4. Ultrasonic-assisted polishing (UAP). Ultrasonic-assisted polishing (UAP) utilizes high-frequency ultrasonic vibrations (typically 20–40 kHz) to induce cavitation effects within the polishing slurry. When the ultrasonic wave propagates through the liquid medium, it generates alternating compression and rarefaction cycles, leading to the formation of cavitation bubbles. The violent collapse of these bubbles produces localized high temperature (up to thousands of Kelvin) and high pressure (several hundred MPa), which can temporarily soften the diamond surface, activate surface atoms, and enhance the chemical reactivity of the slurry. In addition, ultrasonic agitation improves the uniform dispersion of abrasive particles, increasing their kinetic energy and collision frequency with the workpiece surface. Together, these effects significantly enhance the MRR compared with conventional mechanical polishing.

Ralchenko et al.[37] demonstrated the potential of UAP by polishing PCD in an ultrasonic bath with diamond slurry. As shown in Figure 19, under the action of an ultrasonic transducer, the abrasive particles repeatedly impact the surface, leading to a drastic reduction in roughness. The average surface roughness Ra decreased from approximately 5 μm to 0.5 μm within only 5 minutes of processing, demonstrating the remarkable efficiency of the UAP. However, a subsurface damage layer of approximately 6 μm thickness occurs, which necessitates subsequent fine polishing or chemo-mechanical finishing for full removal. Hybrid approaches—such as combining UAP with PAP or CMP are emerging as promising solutions to achieve a balance between high efficiency and atomic-level surface quality.

Despite its advantages, UAP still faces challenges in achieving atomically smooth, damage-free surfaces, particularly for applications requiring sub-nanometer roughness and intact lattice integrity. Future research should emphasize in situ monitoring of cavitation dynamics, numerical modeling of bubble collapse effects, and integration with real-time feedback control systems. These efforts could enable precise tuning of the cavitation energy and process parameters, paving the way for reproducible, damage-free ultrasonic polishing of diamond suitable for extreme manufacturing applications such as high-power optical components and quantum devices.

Energy-field-assisted polishing technologies have demonstrated unique advantages for processing diamond components that must perform reliably under extreme service conditions. Compared with purely mechanical or chemical approaches, these hybrid techniques utilize external energy fields to activate surface reactions, soften the near-surface layer, or enhance slurry transport, thereby achieving a balance between high removal rates and minimal subsurface damage. PAP, in particular, enables damage-free surface finishing by generating chemically reactive species (e.g., O radicals and CF_x species) that selectively etch the sp^3-bonded diamond lattice. When integrated with mechanical action, PAP can reach material removal rates of up to 1 $\mu m \cdot h^{-1}$ while maintaining roughness below 1 nm, making it highly suitable for large-area infrared windows and high-power laser optics, where both surface flatness and optical transparency are critical. LAP leverages localized thermal activation to reduce the hardness of the diamond surface and facilitate ductile-mode removal, offering strong potential for polishing thick heat spreaders or large-area power electronic substrates, where high throughput is essential. UVAP enhances surface oxidation kinetics at relatively low temperatures, while UAP promotes slurry renewal and reduces the polishing force, minimizing the risk of brittle fracture on thin or delicate substrates. These methods are particularly promising for quantum device substrates and precision

optical components, where lattice integrity must be preserved to avoid degrading coherence times or optical performance.

Overall, energy-field-assisted polishing approaches address a crucial challenge of extreme manufacturing: achieving atomic-level surface integrity under conditions that also demand scalability and throughput. The synergistic combination of chemical activation, thermal softening, and mechanical removal of these materials offers a pathway toward ACSM.

3. State-of-the-art polishing mechanism for diamond

Manufacturing technologies evolve through three distinct phases: an initial empirical craftsmanship stage (Manufacturing I), a classical continuum mechanics-governed stage (Manufacturing II), and a quantum-dominated stage where classical theories breakdown (Manufacturing III)[19,23,232]. As processing scales transition from the micro- and nanoscale to the atomic scale, both the objects and mechanisms of manufacturing involve direct interactions at the atomic level. Consequently, a fundamental understanding of the mechanisms governing atomic-scale material removal, migration, and addition becomes essential for enabling ACSM[24,25,233,234]. During the polishing process of diamond, material removal is influenced by the coupling effects of parameters such as the polishing fluid, polishing pad/disc, polishing pressure, and polishing speed, making it difficult to quantitatively express the relationship between each parameter and atomic removal. As a result, researchers mostly use single-point contact models to study the microscopic removal of materials, gradually revealing the influence of each individual factor on atomic-level material removal[235,236]. However, experimental instruments are unable to obtain the dynamic microscopic atomic details or the specifics of chemical reactions and mechanical effects, thus failing to fully explain the atomic removal mechanism. The advent of simulation modeling has provided new insights into the study of atomic-scale mechanisms[237]. The main methods currently include first-principles calculations, molecular dynamics (MD)[238,239], and reactive force field molecular dynamics (ReaxFF MD)[240]. For instance, Li et al.[241] employed an MD model of dual abrasive particles and GaN crystals to understand the complex interactions between the workpiece material and the abrasive particles, which deepened the understanding of the damage accumulation and material removal caused by the interaction between abrasive particles, providing a feasible method for the development of ordered abrasive wheel designs. Additionally, the damage mechanism induced by abrasive particles in SiC was outlined, with a particular emphasis on the crucial role of the mixed energy field in reducing brittle damage and improving removal efficiency, which not only clarified the intrinsic interaction between the workpiece material and the abrasive particles but also provided valuable insights for the optimization of brittle material processing techniques[242]. ReaxFF MD bridges the gap between first-principles and classical MD, enabling the calculation of chemical reactions involving hundreds of thousands of atoms at the nanosecond time scale. It not only handles complex chemical reactions but also studies the mechanical properties and surface reactions of materials. The ReaxFF MD method has been used to study the interactions between chloride ions and copper oxide[243], oxidation of nickel surfaces[244], dissociation of water on TiO_2[245], Al[246], Si[247], and Fe[248] surfaces, and it has successfully simulated the friction processes of Si[249–253], Cu[254,255], glass[256–259], and diamond-like materials[260–262].

Based on the overview of polishing methods, diamond polishing mechanisms can be categorized into four types: micro-fracture removal, graphitization removal, oxidation removal, and chemical etching.

3.1. Micro-fracture removal mechanism

This method uses diamond wheels or microparticles in a "hard-to-hard" approach, relying on the mechanical force of the abrasive particles to induce micro-fracture removal. After polishing, the diamond surface often exhibits numerous pits. Under high-pressure processing conditions, defects such as surface collapse, cracks, and pits are easily formed, even leading to fragments, resulting in poor surface quality after processing. Typical methods include MP and UAP.

The removal mechanisms of diamond during MP have long been a subject of debate, and various explanations have been proposed[263]. Early studies highlighted the influence of crystallographic orientation. Tolkowsky attributed this process to micro-cleavage along the (111) plane, based on the anisotropy of MP rates and the observation of micro-chips on the surface[264]. Bowden suggested that thermal wear, involving carbonization or burning at elevated temperatures, dominated the process[265]. Brezoczky argued that electrostatic attraction generated by triboelectric charging in the nanometer-to-tens-of-nanometers gap between abrasive grains and the diamond surface facilitated the detachment of carbon atoms[266]. Couto reported that in the "hard" orientation, diamond is removed through fracture or micro-chipping, while in the "soft" orientation, the surface is characterized by nanometer-scale grooves[267,268]. Grillo and Field further proposed that the transformation of diamond from sp^3 bonding to sp^2 bonding occurs during grinding along the "soft" direction, producing amorphous carbon[269,270]. While these models provided valuable insights, they were often limited to either the "soft" or "hard" orientation, lacking a unified explanation. To address this, Zong et al.[271] introduced the brittle-to-ductile transition theory to systematically describe the material removal behavior during grinding. According to this model, when the dynamic grinding depth is smaller than the critical cutting depth, plastic deformation dominates surface removal in both "soft" and "hard" orientations, leading to a brittle–ductile transition. Experimental studies combined with AFM measurements confirmed that the nanogroove morphology observed on different planes and orientations agrees well with the predicted critical cutting depths, thereby explaining the anisotropy of the removal rates[148,271].

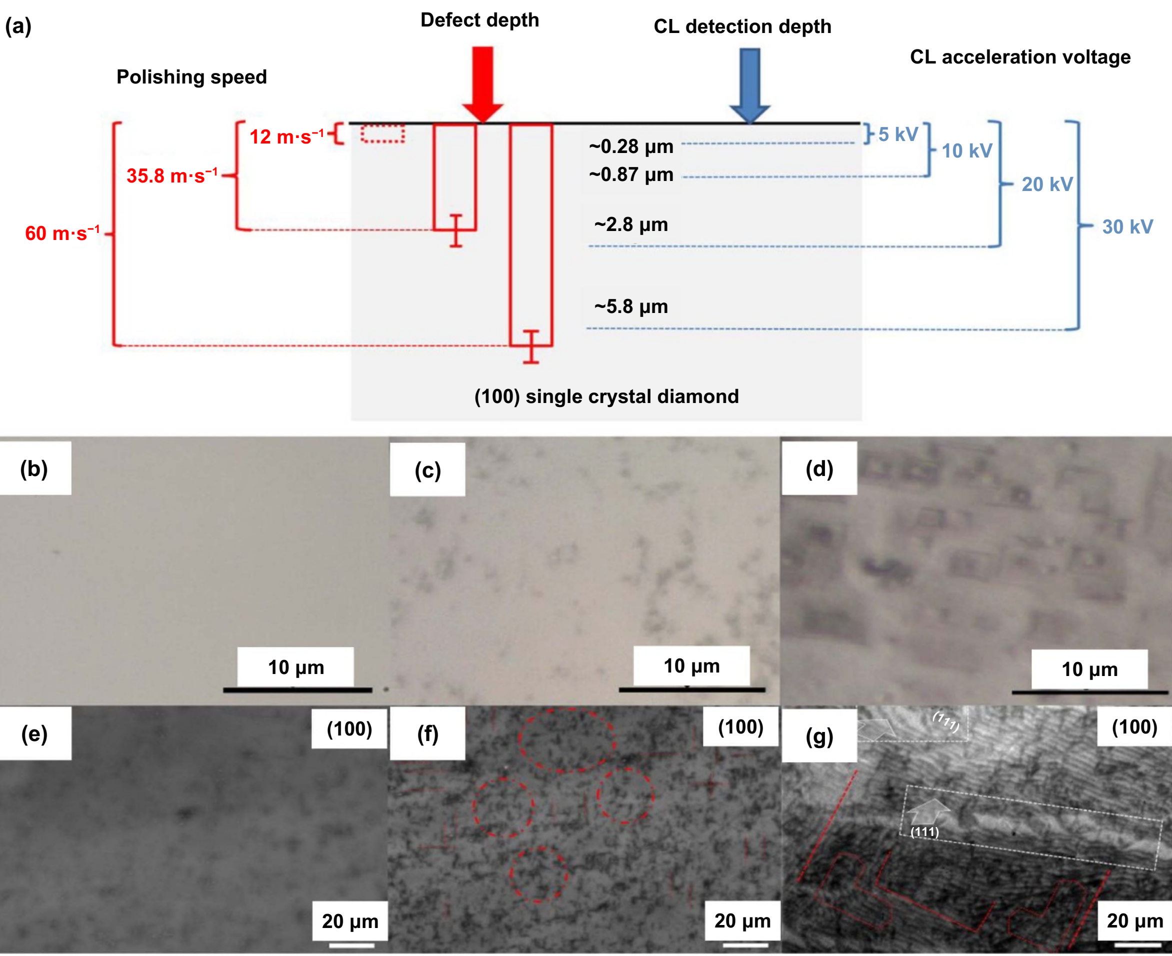

Figure 20. Evolution of subsurface damage at varying depths. (a) Defect depth vs. polishing velocity and penetration depth vs. beam energy. (b)–(d) Transmission mode optical images at 12 $m \cdot s^{-1}$, 35.8 $m \cdot s^{-1}$, and 60 $m \cdot s^{-1}$. (e)–(g) CL images at 10 kV for the same velocities. Reprinted from[115], Copyright (2020), with permission from Elsevier.

Further investigations revealed that intrinsic point defects in natural SCD, such as nitrogen and phosphorus, significantly reduce the external stress required for plastic deformation. For instance, when the (110) plane is used as the rake face, the actual stress during grinding is only about one-ninth of the theoretical strength along the "soft" direction[272]. This suggests that conventional MP cannot directly achieve the theoretical limit of edge sharpness. In addition, factors such as vibrations of the MP apparatus, lap surface quality, spindle balance and accuracy, pressure, and speed critically influence the contact precision and ultimately determine the edge radius[148]. The understanding of diamond grinding mechanisms has evolved from early cleavage, wear, and transformation-based models to the more comprehensive brittle-to-ductile transition framework. Current studies indicate that under appropriate MP conditions, material removal is predominantly governed by plastic deformation, while removal rates and surface morphology exhibit a pronounced crystallographic orientation dependence.

Diamond wheels and abrasives often induce micro-fracture removal. While a nanometer-scale ultra-smooth surface can be achieved, subsurface damage to the diamond matrix is inevitable during processing. Subsurface defects can range from minimal to partial damage, forming micro-fracture zones, transition regions, and compression zones, which can ultimately lead to subsurface fractures, as shown in Figure 20[115]. After polishing diamond with wheels, the differences in performance are observed in different directions. When diamond is polished with a softer silica wheel, the polishing differences across various crystal orientations are reduced, and the polishing rate becomes more isotropic. The wear reaction between diamond and silica wheels is primarily a chemical reaction, where diamond undergoes plastic removal[132].

During the MP of diamond, polishing in a specific direction yields a high-quality surface, while polishing in other directions not only makes material removal more difficult but also leads to a poorer surface. This issue is more pronounced in PCD and is caused by the anisotropy of diamond. First-principles and MD simulations can effectively explain the anisotropy mechanisms at the atomic level. MD simulations show that after MP, the damage layer on the diamond surface consists of amorphous sp^3 and sp^2 carbon[273]. The

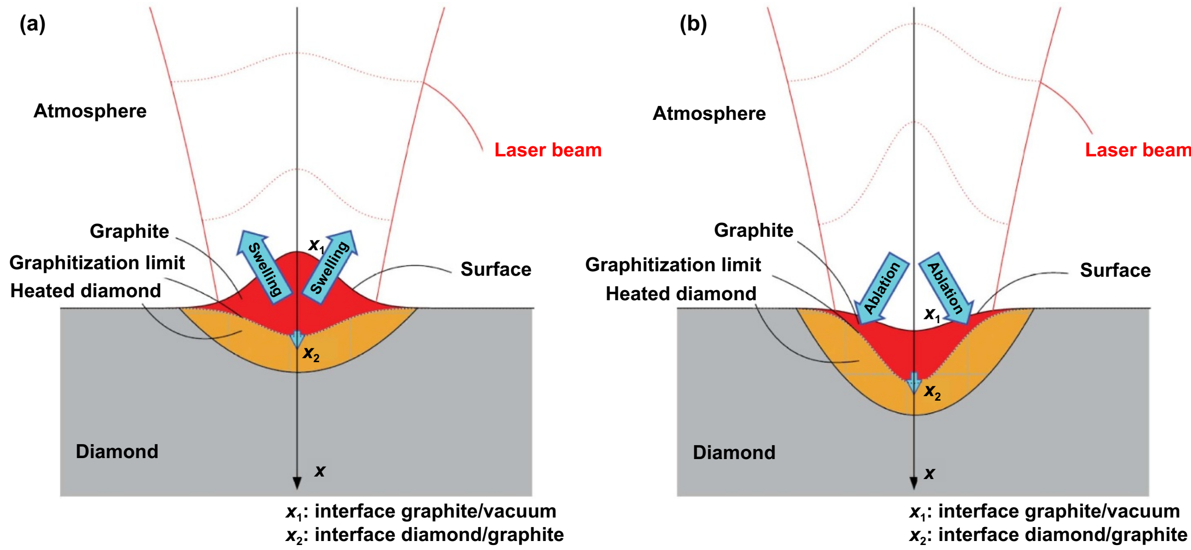

Figure 21. Scheme of diamond ablation. (a) At low fluences and (b) high fluences. Reproduced from[280]. © IOP Publishing Ltd. All rights reserved.

disordered transformation from sp^3 to sp^2 within the diamond is the main reason why the wear rate depends on the surface orientation and sliding direction[274]. The anisotropy in the removal rate is determined by the concentration of sp^2 hybridized carbon in the generated amorphous layers and debris[275,276]. The appearance of amorphous defects, dislocations, and slip in the diamond matrix causes the friction surface to generate von Mises shear strain, which is the reason for the anisotropic friction force[277]. First-principles simulations can model the formation and rupture of interface bridging bonds during abrasive particle scratching and removal from the diamond surface, providing an explanation for the differences in atomic removal from the perspective of bond energy[278,279]. MD simulations, being an empirical computational method, have advantages in studying the mechanical removal process and material anisotropic tool wear, but they can only describe mechanical effects and not chemical reactions. The limitations of first-principles simulations mainly lie in the small spatial scale (dozens of atoms) and temporal scale (picosecond level).

3.2. Graphitization removal mechanism

The graphitization removal mechanism involves the use of high-energy laser beams (such as lasers) to interact with the diamond surface, achieving material removal through photothermal effects (localized high-temperature graphitization or sublimation) or photochemical decomposition (breaking C−C bonds). High-frequency vibrations are applied at the polishing interface, and heat generated by friction triggers localized chemical reactions (such as the formation of a graphite layer through reaction with Fe-based polishing pads), followed by mechanical action to remove the softened material. Representative processing methods include LP, LAP, and DFP.

Single laser experiments are employed to explore the laser ablation of diamond by nanosecond laser pulses. For low-energy-density single-pulse lasers, due to the graphitization effect, the laser causes surface expansion; while for high-energy-density laser pulses, due to the vaporization effect, it leads to surface depression; the schematic of diamond ablation at different fluences is illustrated in Figure 21[280].

Current researches on graphitization removal primarily focus on the use of transition metal elements to develop novel polishing pads or incorporate transition metals into diamond wheels, aiming to explore how the type of polishing pad influences diamond removal. Different alloys are selected to prepare metal polishing pads, including 0Cr18Ni9 stainless steel[123], Mn-Cu and Mn-Ni alloys[281], and W-Mo-Cr alloys[282,283]. On the diamond surface, micro-convex peaks undergo a graphitization transformation, forming a softer, more easily oxidized graphite phase with stronger diffusion ability. The graphite phase is removed under the combined effects of mechanical action, oxidation, and diffusion. After diamond is polished with a Mn-Ni-based alloy polishing pad, a higher removal rate can be achieved[281].

Another approach involves doping transition metals into diamond wheels, which are subsequently used to grind the diamond surface. For instance, when a titanium−alumina wheel is used, a chemical reaction occurs between the diamond and the titanium in the wheel. After grinding, the diamond surface exhibits graphitization. The combination of graphitization and mechanical cracks is the primary reason for the higher MRR during grinding[134]. Adding iron and cerium metals to traditional alumina wheels has been found to produce carbon−iron compounds in the grinding debris. This indicates that a chemical reaction occurs between the diamond and polishing pad under high-speed rotation, and the frictional heat generated by high-speed friction leads to the graphitization removal of the diamond[135]. Guo et al. employed first-principles calculations to develop interaction models between diamond and various metal atoms, including chromium, iron, cobalt, titanium, platinum, aluminum, and copper. These findings suggest that when a metal features empty d-orbitals and

aligns with diamond along specific crystallographic planes, the unpaired electrons in the metal's valence shell can interact with the electrons of diamond atoms, resulting in chemical bond formation. This interaction promotes the gradual conversion of diamond into graphite. Moreover, the metal's catalytic efficiency in inducing diamond graphitization correlates positively with the number of its unpaired electrons. Conversely, transition metals with fully paired valence electrons exhibit no catalytic effect on diamond graphitization[118,119]. The unpaired electrons in the iron surface atoms pair with the electrons in the diamond surface atoms, forming chemical bonds that produce an adsorption effect, causing the carbon atoms to move.

3.3. Oxidation removal mechanism

The oxidation removal mechanism involves the use of methods such as chemical corrosion, photochemical reactions, and plasma activation of the surface to oxidize the diamond surface, forming a softer oxide layer. This oxide layer is then removed through the collaborative action of mechanical polishing (using nanomaterials) and the abrasive mechanical shear force. Representative processing methods include CMP, UVAP, and PAP.

Comprehensive studies of diamond polishing mechanisms depend on the use of multi-scale surface analysis techniques, such as using transmission electron microscopy (TEM) to detect subsurface damage after polishing[189], scanning electron microscopy (SEM) for surface morphology imaging[186], Raman spectroscopy and X-ray diffraction (XRD) for material composition and atomic structure analysis[28], X-ray photoelectron spectroscopy (XPS) for qualitative or quantitative element analysis[208], and atomic force microscopy (AFM) for high-precision surface roughness measurements[284]. The AFM results indicate that after diamond polishing, atomic-level smooth surfaces can be achieved with a P-V of 0.939 nm, Ra of 0.052 nm, and RMS of 0.065 nm. The TEM results show that the lattice structure of the diamond matrix remains intact after polishing, with almost no crystal distortions or other damages[120]. Using an SG polishing pad on diamond, the TEM results indicate a subsurface damage layer ranging from 2.0 nm to 3.3 nm, including amorphization, dislocations, and lattice distortions[189]. XPS reveals that adding reducing agents to a silica polishing slurry accelerates the attachment of Si or O atoms to the diamond surface, thereby promoting material removal[284].

The atomic oxidation of diamond is elucidated using a high-temperature and high-pressure oxygen by a developed scanning electron microscopy, which is important for atomic-level polishing. The crystal geometry of the diamond sample and schematic illustration of the self-developed operando variable pressure scanning electron microscope (VP-SEM) system are shown in Figure 22[285].

One important oxidation mechanism in diamond polishing is •OH, which has received widespread attention. When TiO_2 is used as a catalyst in Fenton polishing slurry, upon exposure to ultraviolet light with wavelengths shorter than 387.5 nm, UV light excites valence band electrons in TiO_2 to the conduction band, generating holes that oxidize surface-adsorbed OH^-/H_2O to yield reactive •OH. The •OH then oxidizes the carbon atoms in the diamond, forming species such as C–O, C=O, and O=C–OH structures. Therefore, during the polishing process, mechanical action enhances the chemical interaction between carbon and •OH[286]. Additionally, plasma excitation generates •OH, and water vapor or O_2 is used as a reactive gas to modify the polishing pad. The modified polishing pad can adsorb •OH, and when the workpiece contacts the pad through rotational friction, material removal occurs, or the material surface is directly modified[223,227,228]. During polishing, •OH and H^+ adsorb onto the diamond surface, forming C–H, C–O, and C=O groups, and the TEM results show that the subsurface damage layer in polished diamonds is less than 1 nm thick with a roughness under 0.1 nm[159,186,208,210]. Since •OH decays in nanoseconds, its short-lived nature makes it a challenge to fully utilize its oxidation potential. To gain a deeper atomic-level understanding of the oxidation mechanism of •OH on diamond, Yuan et al. introduced ReaxFF MD simulations into the CMP process of diamond for the first time. They discovered that •OH oxidation exhibits anisotropy on different crystal faces[287]. Adsorption activates C−C bonds in the diamond lattice. Abrasive particles form interfacial C−C bridge bonds with the lattice, facilitating carbon removal[288,289]. Concurrently, Fe^{2+} ions with unpaired electrons combine with lattice carbon, further activating C–C bonds and promoting bridge bond formation. Under combined chemical−mechanical action, atomic removal occurs[181]. Crucially, abrasive mechanical disruption destabilizes covalent bonds, lowering chemical activation energies[290]. Polishing pressure can catalyze the decomposition of H_2O and H_2O_2, allowing them to adsorb on the diamond surface in the form of C–H, C–O, and C–OH groups, thereby passivating the diamond. Passivating the surface reduces friction and wear by lowering the friction force and coefficient on the diamond surface[291]. The forms of atom removal during polishing include C−C single bridge bond removal and C−C multiple bridge bond removal. After polishing, subsurface damage in diamond workpieces occurs primarily in the form of amorphous carbon damage. In macroscopic terms, the polishing pressure, polishing speed, and other process parameters influence the number of C–C and C–O–C bridge bonds formed at the interface, which in turn affects the interface friction, friction coefficient, removal rate, and surface quality[292,293]. Defects in diamond make atoms more prone to oxidation; if initial defects are too large, significant damage to the matrix can occur, accompanied by abrasive wear[294]. ReaxFF MD simulations revealed that H_2O_2 plasma treatment modifies PCD surfaces via energy-dependent mechanisms. The modified layer comprises carbon−oxygen mixed and oxygen−rich regions, evolving through three distinct stages governed by the •OH incident energy: (i) •OH adsorption on the topmost surface; (ii) •OH adsorption with concurrent C−C bond dissociation; and (iii) •OH penetration and subsurface

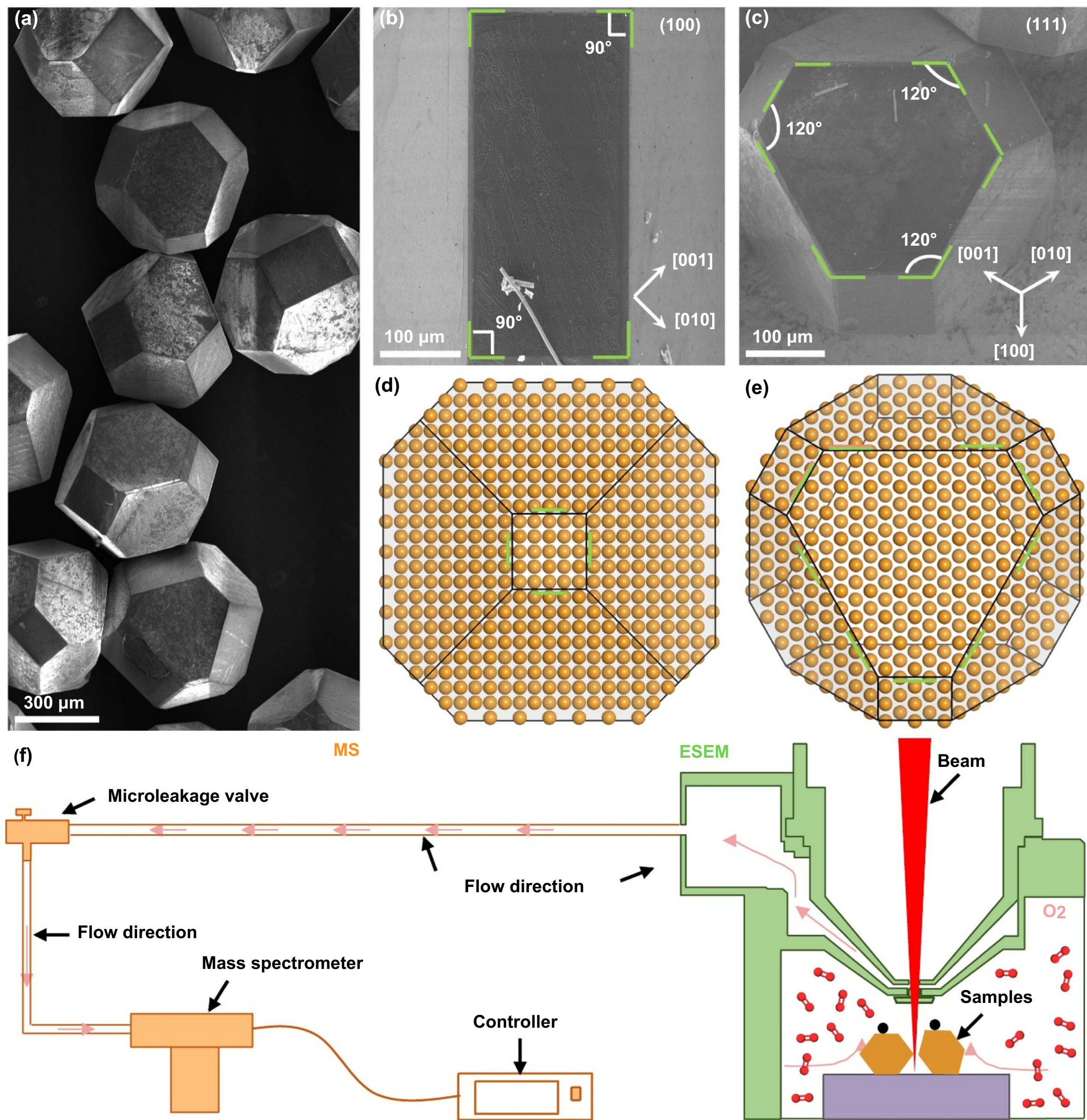

Figure 22. Crystal geometry of diamond and schematic of the operando VP-SEM system. (a) SEM images of diamond crystals. (b)–(e) Enlarged SEM images with atomic models of the (100) and (111) facets. (f) Schematic of the VP-SEM system with online mass spectrometer for real-time gas analysis. Reprinted with permission from[285]. Copyright (2025) American Chemical Society.

C−C bond dissociation. The posttreatment analysis is shown in Figure 23[225].

Under UV irradiation, H_2O_2 and H_2O undergo photodissociation into reactive species (•OH/•OH + H^+), while diamond simultaneously generates electron−hole pairs through valence-to-conduction band excitation. The •OH is more likely to combine with the holes and adsorb on the surface, promoting diamond oxidation and modification. Under mechanical action, the •OH radicals adsorbed on the diamond surface detach, and the carbon atoms connected to •OH form interface bridge bonds with the abrasive. The carbon atoms from the abrasive, affected by ultraviolet light and chemical reactions, weaken the strength of the C−C bonds in the matrix, making the C atoms from the matrix more easily removed by the diamond abrasive[208]. The atomic level surface is garnered with an Sa of 0.079 nm, and material removal rate is 1 168 nm·h^{-1} by UVAP, and the atomical mechanism is illustrated in Figure 24[210]. Liu et al. simulated the PAP process via ReaxFF MD and revealed diamond carbon removal via two pathways: (i) covalent attachment to quartz through C–O–Si bonds, or (ii) transformation into graphitic/gaseous species. This material removal is driven synergistically by oxygen radical oxidation and bond-strain-induced lateral forces from the C–O–Si linkages[295]. During the UVAP process, extensive C−C bond fractures occur, and atomic wear is achieved through the combined effect of O

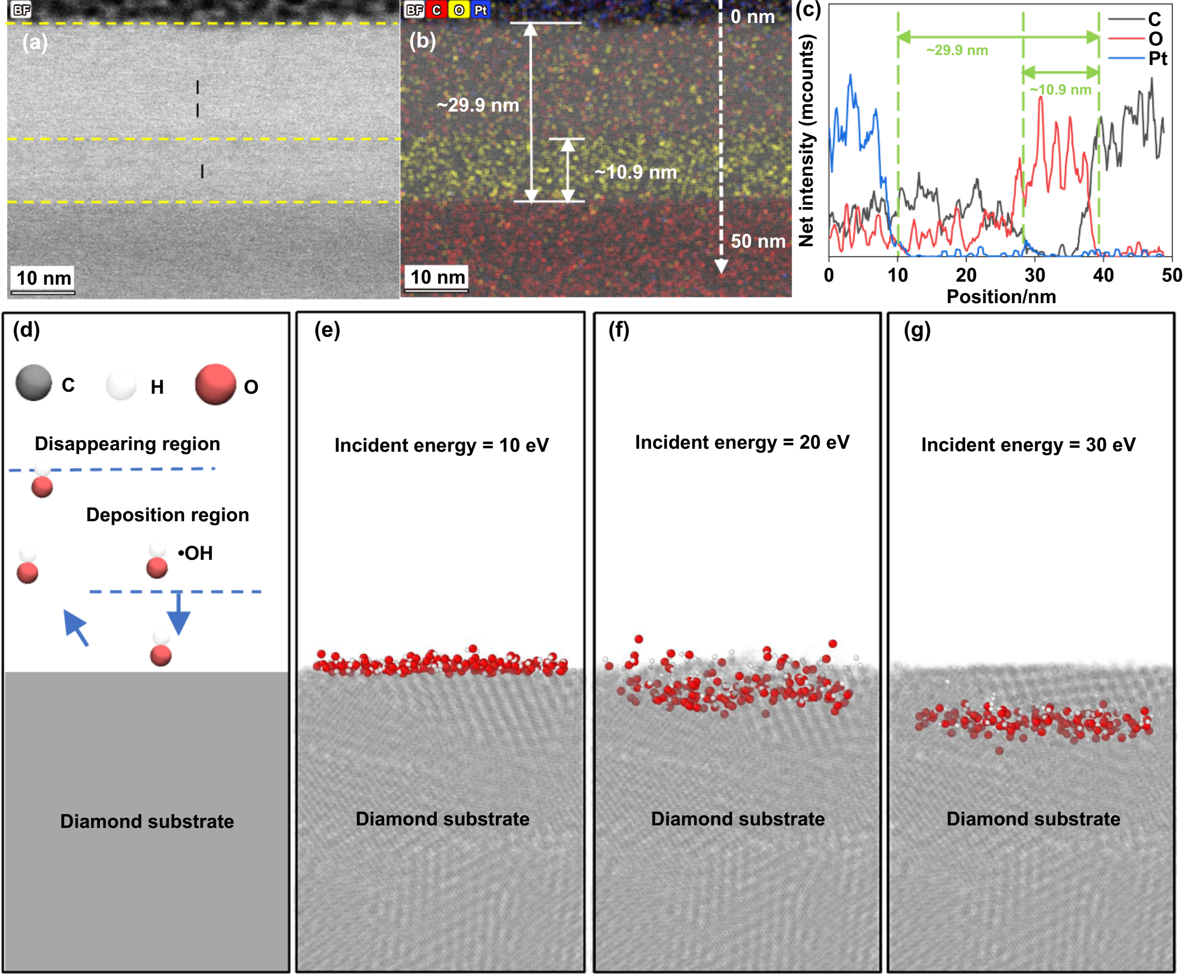

Figure 23. Analysis of PCD after plasma modification. (a) Cross-sectional BF-STEM image. (b) Corresponding bright-field EDS elemental map. (c) C, O, and Pt intensity profiles across the modified layer, as shown in the dashed line of (b). (d) ReaxFF MD model of •OH radicals approaching PCD at varied incident energies. (e)–(g) Atomic configuration snapshots after •OH impact at (e) 10 eV, (f) 20 eV, and (g) 30 eV. Reproduced from[225]. CC BY 4.0.

atoms, ultraviolet energy, and interface chemical bond pulling forces[215].

3.4. Physical sputtering and chemical etching removal mechanism

The physical sputtering and chemical etching removal mechanism involves the use of electrochemical reactions, plasma (e.g., oxygen/argon plasmas), ion beam (e.g., Ar^+, Ga^+) to bombard the surface, and material removal through ion sputtering or chemical reactions. The comparison of (a) monatomic and (b) cluster ion beam characteristics is shown in Figure 25. Owing to the difficulty in controlling these reactions, the sputtering or etching rate on the material's surface can vary significantly. As a result, it is challenging to form a uniform oxide layer, unlike the oxidation removal process.

The modification mechanisms of diamond under IBP are primarily reflected in structural damage, phase transformations, evolution of electrical properties, and doping effects. At the initial stage, energetic ions lose energy mainly through nuclear stopping, producing extensive displacement damage, such as vacancies, interstitial atoms, and collision cascades. With increasing fluence, diamond evolves from a defect-rich crystalline state into an amorphous structure, and eventually undergoes graphitization once the critical fluence is exceeded[296]. The morphology and structure of the damage layer strongly depend on the mass and energy of the incident ions: heavy ions generate denser collision cascades and more severe damage, whereas light ions result in shallower damage distributions. Overall, the modification process is governed by a complex interplay of ion species, energy, fluence, and temperature.

Under 30 kV Ga^+ ion irradiation, a damage layer with a thickness of ~43 nm was observed on the surface of CVD diamond. This layer exhibits a bilayer structure: the a-C I layer, rich in sp^2-bonded carbon, originates mainly from direct Ga implantation, while the a-C II layer, dominated by sp^3 carbon, is largely caused by carbon recoil atoms[83]. The evolution of the modified structure is highly dependent on the fluence: when the dose is below the critical value, carbon atoms in the

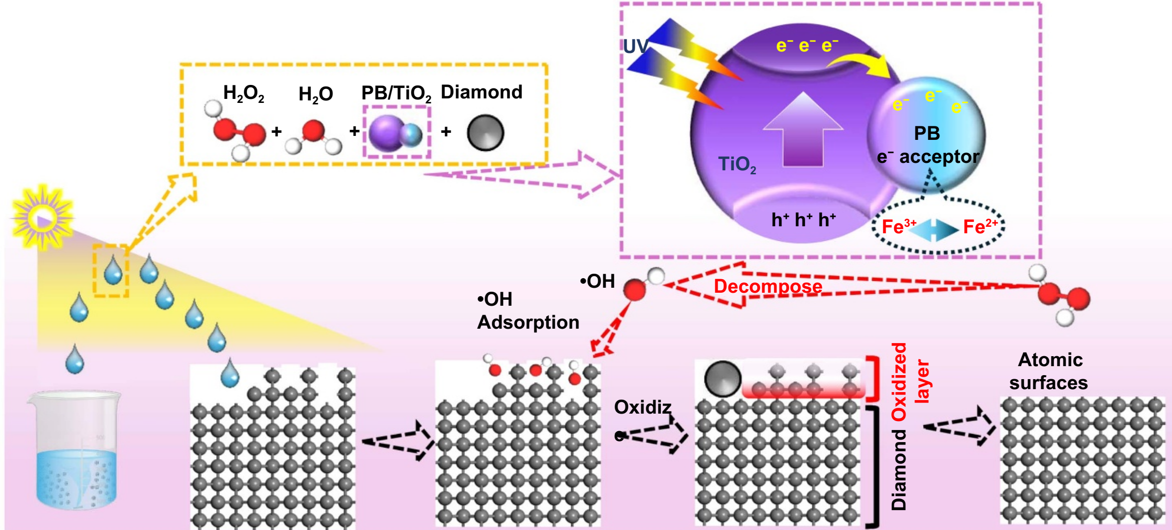

Figure 24. The atomical mechanism of UVAP. Reproduced from[210]. The Author(s). CC BY 4.0.

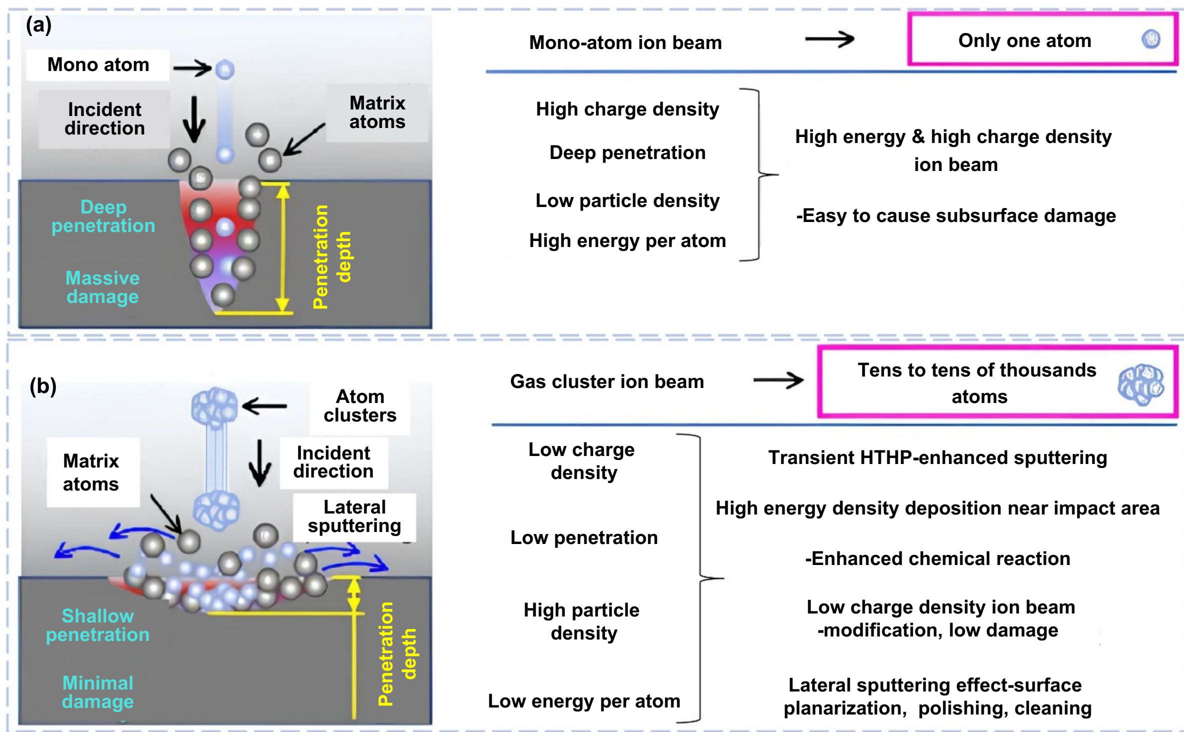

Figure 25. Comparison of (a) monatomic and (b) cluster ion beam characteristics. Reproduced from[33]. CC BY 4.0.

modified layer tend to be substituted by Ga atoms; once the fluence exceeds the threshold, carbon and Ga atoms are randomly distributed, leading to complete amorphization. Importantly, the wear resistance of ion-modified diamond tools improves significantly with increasing fluence. This enhancement is attributed to changes in surface energy, the shortening of C–C bond lengths around C–Ga bonds, the increase in surface hydrophobicity, and the strengthening of both C–Ga and adjacent C–C bond energies[41].

Furthermore, molecular dynamics simulations have elucidated the orientation-dependent mechanisms of ion-beam-induced sputtering at the atomic scale. Under identical irradiation conditions, the (110) orientation of diamond exhibits greater ion penetration depth and larger damaged areas, indicating higher sensitivity to ion-induced damage. Consequently, the (110) surface is more prone to amorphization and graphitization transitions than other orientations[86]. The ion-beam modification of diamond is governed by a combination of

defect generation, amorphization and graphitization transitions, bond structure reconfiguration, and crystallographic orientation effects. These insights provide an essential theoretical foundation for achieving high-precision, low-damage polishing and surface modification of diamond.

Plasma polishing works by introducing reactive gases such as oxygen and carbon tetrafluoride (CF_4) into the plasma torch. These gases are dissociated upon excitation, generating •OH and highly reactive oxygen/fluorine species. At high temperatures, these reactive species react with the carbon atoms on the diamond surface, forming volatile products such as CO, CO_2, or CF_4 and facilitating the efficient and selective removal of carbon atoms through chemical etching[297].

In plasma polishing, there are two modes: the etching mode and the polishing mode. Temperature is the key factor influencing the transition between these modes during plasma treatment of the diamond surface. At temperatures below 1 000 °C, plasma reactions predominantly involve random etching. These reactions primarily occur along surface defects (such as dislocations and grain boundaries) or high-activity regions, forming square etching pits (related to surface damage) or deep etching pits (related to dislocations inside the crystal). In this mode, material removal is uneven, which tends to increase surface roughness. When the temperature exceeds 1 000 °C, high temperatures increase the thermal vibrations of surface atoms, promoting reactions at high-activity sites (such as protruding atoms). In this mode, the plasma selectively removes surface protruding atoms through a “peak shaving and valley filling” mechanism, gradually exposing lower-activity atoms beneath, ultimately resulting in an atomically smooth surface[40].

The diamond surface, due to its incomplete crystal structure, forms atoms with different dangling bonds (1 to 3 dangling bonds), with atoms having three dangling bonds being the most chemically reactive. The fluorine atoms in the plasma preferentially react with and remove these highly reactive atoms (with three dangling bonds), exposing the atoms underneath. If the newly exposed atoms still have three dangling bonds, they will continue to be preferentially etched until only low-reactivity atoms (with two or one dangling bond) remain on the surface. At this point, atoms with two dangling bonds (the next most reactive) are selectively removed, leaving atoms with a single dangling bond and resulting in a surface that approaches perfect crystalline alignment. This process achieves a continuous reduction in surface roughness by selectively etching high-activity atoms, leading to an atomically smooth surface[40]. ReaxFF MD simulations also show that as C atoms are removed during the plasma etching process, C atoms with higher etching priorities (1- and 2-coordinate C atoms) dominate the tip regions of pyramid-like protrusions and are preferentially removed, leading to the flattening of PCD films[102].

The smoothing mechanism of the GCIB involves both physical and chemical contributions. When inert gases such as Ar are used, smoothing is primarily achieved through kinetic energy transfer and lateral sputtering[298]. The physical smoothing effect of GCIB is primarily attributed to three factors: (i) efficient energy transfer, (ii) surface atom dynamics, and (iii) selective material removal, which together facilitate the fabrication of ultra-smooth surfaces[29]. Among these, selective removal is considered the key mechanism. Xie et al.[33] proposed that differences in sputtering rates and atom relocation play a dominant role in this process. When clusters impact the surface at near-normal incidence, surface atoms are ejected and redeposited isotropically around the impact site. In contrast, impacts on inclined surfaces induce preferential downward displacement of atoms, thereby filling adjacent valleys. At the same time, protruding regions (hills) present higher sputtering rates than valleys do, leading to a gradual reduction of topographical height differences. Through valley filling and hill erosion, the surface is progressively leveled, ultimately enabling nanoscale or even atomic-scale planarization. In addition to physical effects, GCIB smoothing can also be dominated by chemical mechanisms when reactive gases such as O_2 or SF_6 are employed as the cluster source[107]. In this case, the bombardment process not only removes surface atoms through sputtering but also promotes chemical reactions at the impact site. The incident clusters dissociate upon collision, generating highly reactive species that interact with surface carbon atoms. These reactions increase the sputtering yield by forming volatile products, such as CO, CO_2, or CF_4, which are readily desorbed from the surface[108,109]. This chemically assisted material removal not only accelerates the etching process but also suppresses graphitization, thereby maintaining the crystallinity of the diamond surface. Consequently, reactive-gas GCIB can achieve efficient smoothing without introducing significant subsurface damage, and is particularly effective for fine polishing processes aimed at achieving nanometer- or atomic-level surface quality.

4. Conclusions and prospects

4.1. Conclusions

Diamond, the hardest known natural material, exhibits exceptional chemical stability, with negligible reactivity to acidic or alkaline reagents under ambient conditions. However, its inherent brittleness, challenges in material removal, and susceptibility to processing-induced damage significantly constrain its practical applications. The polishing technology of diamond is a core challenge in achieving atomic-level surface integrity. This paper systematically covers laser polishing (LP), mechanical polishing (MP), ion beam polishing (IBP), gas cluster ion beam polishing (GCIBP), plasma polishing, dynamic friction polishing (DFP), chemical mechanical polishing (CMP), ultraviolet-assisted polishing (UVAP), plasma-assisted polishing (PAP), laser-assisted polishing (LAP), ultrasonic-assisted polishing (UAP), and other major techniques. It reveals the inherent connections and applicability boundaries of the four major material removal mechanisms. More details with respect to the comparison of different polishing methods are concluded in Table 1.

Table 1. Comparisons of different polishing methods.

Method	Core Mechanism	Roughness	MRR	Advantages	Limitations
LP/LAP	Thermal effects, graphitization	Dozens of nanometers[49]	12.04 $\mu m^3 \cdot s^{-1}$[49]	Noncontact, high efficiency	Heat-affected zone, expensive equipment, low precision
IBP	Physical sputtering	Rms 0.1 nm[81]	300 $nm \cdot h^{-1}$[82]	Low damage, high surface quality, local shaping	Expensive equipment, low efficiency
Plasma polishing	Chemical etching	Sa 3.4 nm[102]	127 $\mu m \cdot min^{-1}$[102]	Low damage, high surface quality and efficiency	Complex equipment, low plane precision
GCIBP	Physical sputtering + Chemical etching	Ra 0.6 nm[110]	N/A	Lower damage than IBP, smooth plane	Complex equipment, low MRR
DFP	Graphitization	<5 nm[115]	1 260 $\mu m \cdot h^{-1}$[69]	High efficiency, strong adaptability	Requires precise temperature control, subsurface damage
MP	Mechanical friction	Sa 0.548 nm[128]	120.2 $\mu m \cdot h^{-1}$[136]	Simple, low cost	Low efficiency, subsurface damage
CMP	Chemical corrosion + Mechanical friction	Sa 0.079 nm[186]	881 $nm \cdot h^{-1}$[186]	Global planarization, high precision	High consumable costs
UVAP	Photochemical + Mechanical synergy	Ra 0.071 nm[208]	1 168 $nm \cdot h^{-1}$[210]	Room temperature, low damage	Dependent on photosensitive agents, expensive equipment
PAP	Plasma activation + Mechanical polishing	Sq 0.13 nm[223]	2.1 $\mu m \cdot h^{-1}$[223]	Atomic-level precision, low stress	Complex equipment

(i) Micro-fracture removal: this mechanism dominates material removal in MP and UAP, enabling rapid stripping of the material. However, it is accompanied by sub-surface damage and roughness anisotropy. It is suitable for coarse processing scenarios.

(ii) Graphitization removal: achieving through Fe/W-based polishing pads, this mechanism facilitates the diamond−graphite phase transition at high temperatures (>700 °C), with a material removal rate of up to 3.7 $\mu m \cdot min^{-1}$. However, challenges related to sub-surface micro-cleavage and delamination remain. It is also suitable for coarse processing scenarios.

(iii) Oxidation removal: this mechanism relies on chemical corrosion, photochemical reactions, and plasma activation to activate the diamond surface, forming a softer oxide layer. This oxide layer is then removed through the abrasive to obtain an atomic-level surface. Thus, it is suitable for fine processing scenarios.

(iv) Physical sputtering and chemical etching removal: this mechanism involves the use of plasma (e.g., oxygen/argon plasmas), ion beam (e.g., Ar+, Ga+) to bombard the surface, and material removal through ion sputtering or chemical reactions. When a mixed gas is used to excite high-activity particles, this technique preferentially etches the protrusions on the diamond surface with an extremely high MRR. However, owing to the difficulty in controlling these reactions and defects in crystal structure, the etching rate on the material's surface can vary significantly. As a result, it is also suitable for coarse processing scenarios.

Studies confirm that multi-energy field collaborative strategies (e.g., laser-induced graphitization + plasma fine-tuning + UV-Fenton reactive oxidation) can overcome the limitations of individual technologies, creating a new balance between processing efficiency, surface quality, and sub-surface damage. These advances lay the foundation for the application of diamond in extreme conditions, such as quantum devices and high-power laser windows.

4.2. *Prospects for diamond polishing*

The pursuit of atomic-scale surface perfection in diamond polishing represents not only a technological frontier but also a scientific imperative for extreme manufacturing fields. Given the demand for defect-free diamond surfaces with atomic-level roughness, future research must be pursued in the following directions:

1. Atomic-scale removal mechanisms
Current mechanical/chemical polishing methods lack atomic-level determinism. The convergence of artificial intelligence

(AI) and in situ transmission electron microscopy (TEM) characterization will be the direction of future pursuit. By leveraging AI to decode atomic-scale material removal mechanisms, reinforcement learning to optimize anisotropic polishing trajectories, and generative models to engineer functional lattice defects. Integrating molecular dynamic (MD) simulations with in situ TEM characterization coupled with AI-adaptive controllers can decode abrasive−diamond interactions, elucidating transitions driven by stress and interfacial chemistry to enable predictive material removal process from the perspective of atomic scale.

2. Atomic-scale processing approach
Future breakthroughs will emerge from multi-physics approaches like femtosecond laser-friction hybrid polishing, merging ultrafast ablation with mechanical shear to achieve crack-free atomic-layer removal. Machine learning-enhanced models will decode laser-plasma-mechanical interactions, enabling atomic-level control through a predictive process. Concurrently, hybrid atomic manufacturing paradigms—such as alternating mechanochemical polishing with hydrogen plasma reconstruction—will bridge macro-scale efficiency and atomic precision, realizing self-limiting material removal while aligning with extreme manufacturing principles. When coupled with AI-adaptive controllers, this achieves self-correcting polishing, while compensating tool wear—paving the way for industrial atomic manufacturing.

3. Defect detection for surface/subsurface damage
Rather than viewing surface defects, the integration of machine learning into surface and subsurface damage detection holds transformative potential for diamond polishing technologies. Future research should prioritize the development of hybrid machining learning models that synergize physics-based simulations with data-driven approaches, enabling robust defect classification even with limited labeled datasets. Deep learning architectures, such as convolutional neural networks, could be optimized for multimodal data fusion (e.g., combining ultrasonic, X-ray, and thermographic signals) to enhance the detection sensitivity for submicron-scale subsurface cracks. Additionally, generative adversarial networks may address data scarcity by synthesizing realistic defect patterns under diverse material conditions.

To sum up, the transition from micron-scale abrasion to atom-by-atom manipulation will redefine the boundaries of diamond processing. Success in this domain demands cross-disciplinary convergence, combining insights from tribochemistry, quantum materials science, and extreme-scale computational modeling. By embracing these challenges, researchers can unlock diamond's full potential as a substrate for atomic-scale devices while establishing foundational principles applicable to other ultrahard materials.

Acknowledgments

The authors would like to express thanks to the National Key R&D Program of China (No. 2023YFE0203800), National Natural Science Foundation of China (No. 52035009), Guangdong Basic and Applied Basic Research Foundation (2025A1515011366), Innovation and Technology Commission (ITC) of the Government of the HKSAR, China (MHP/151/22), and funding from the Research and Innovation Office of The Hong Kong Polytechnic University (1-W29X, 1-BECE). Appreciation extends to Peng Lyu for his efforts in revising the plasma polishing section.

Conflict of interest

The authors declare that they have no known competing financial interests or personal relationships that could have appeared to influence the work reported in this paper.

ORCID iDs

Song Yuan 0000-0002-5519-9067
Chi Fai Cheung 0000-0002-6066-7419
Fengzhou Fang 0000-0002-8716-5988
Han Huang 0000-0003-3353-2970
Chunjin Wang 0000-0001-5820-5939

References

[1] Sussmann R S. 2009. *CVD Diamond for Electronic Devices and Sensors* (John Wiley & Sons, Chichester)
[2] Zhao F Y, He Y J, Huang B, Zhang T Y and Zhu H. 2024. A review of diamond materials and applications in power semiconductor devices. *Materials* **17**, 3437.
[3] Liao M Y, Shen B and Wang Z G. 2019. *Ultra-wide Bandgap Semiconductor Materials* (Elsevier, Amsterdam)
[4] Bai Z X, Yang X Z, Chen H, Jin D, Ding J, Qi Y Y, Li S S, Yan X S, Wang Y L and Lv Z W. 2020. Research progress of high-power diamond laser technology (invited). *Infrared Laser Eng.* **49**, 20201076.
[5] Wild C. 1998. CVD diamond for optical windows. *In Low-Pressure Synthetic Diamond: Manufacturing and Applications* (eds Dischler B, Wild C) (Springer, Berlin) pp 189–206.
[6] Anoikin E, Muhr A, Bennett A, Twitchen D and de Wit H. 2015. Diamond optical components for high-power and high-energy laser applications. *Proc. SPIE* **9346**, 93460T.
[7] Sang L W. 2021. Diamond as the heat spreader for the thermal dissipation of GaN-based electronic devices. *Funct. Diamond* **1**, 174–188.
[8] Chernykh M Y et al. 2022. GaN-based heterostructures with CVD diamond heat sinks: a new fabrication approach towards efficient electronic devices. *Appl. Mater. Today* **26**, 101338.
[9] Hu X F et al. 2024. Diamond-SiC composite substrates: a novel strategy as efficient heat sinks for GaN-based devices. *Carbon* **218**, 118755.
[10] Cheng Z, Mu F W, Yates L, Suga T and Graham S. 2020. Interfacial thermal conductance across room-temperature-bonded GaN/diamond interfaces for GaN-on-diamond devices. *ACS Appl. Mater. Interfaces* **12**, 8376–8384.
[11] Uwihoreye V, Hu Y S, Cao G Y, Zhang X, Oropeza F E and Zhang K H L. 2024. Recent progress on heteroepitaxial growth of single crystal diamond films. *Electron* **2**, e70.
[12] Kamo M, Sato Y, Matsumoto S and Setaka N. 1983. Diamond synthesis from gas phase in microwave plasma. *J. Cryst. Growth* **62**, 642–644.

[13] Ren Y, Li X G, Lv W, Dong H Y, Cheng Q H, Yue F, Wöhrl N, Mendes J C, Yang X and Li Z X. 2024. Recent progress in homoepitaxial single-crystal diamond growth via MPCVD. *J. Mater. Sci., Mater. Electron.* **35**, 525.
[14] Salvatori S, Pettinato S, Piccardi A, Sedov V, Voronin A and Ralchenko V. 2020. Thin diamond film on silicon substrates for pressure sensor fabrication. *Materials* **13**, 3697.
[15] Lavrinenko V I. 2022. CVD diamonds in diamond tools: features and properties, peculiarities of processing, and application in modern diamond tools (review). *J. Superhard Mater.* **44**, 431–449.
[16] Song G H, Wang Y J and Tan D Q. 2022. A review of surface roughness impact on dielectric film properties. *IET Nanodielectr.* **5**, 1–23.
[17] Mu F W, He R and Suga T. 2018. Room temperature GaN-diamond bonding for high-power GaN-on-diamond devices. *Scr. Mater.* **150**, 148–151.
[18] Huang X R, Zhou C J, Wu B, Geng Z M and Zhang X. 2022. Wafer-scale polishing of polycrystalline MPACVD-diamond. *Surfaces* **5**, 155–164.
[19] Gao W. 2025. Editor's note: fengzhou fang's presidential address at the 73rd CIRP general assembly. *Nanomanuf. Metrol.* **8**, 10.
[20] Akbar Z, Liu H B, Zhang N, Ming P M, Zhang H G and Luo X C. 2025. Frontiers in atomic-level manufacturing: atomic-scale electrochemical deposition. *Int. J. Extrem. Manuf.* **7**, 062008.
[21] Zhang Y J, Xiao Y X, Liang J W, Zhang C and Deng H. 2024. Towards atomic-scale smooth surface manufacturing of β-Ga_2O_3 via highly efficient atmospheric plasma etching. *Int. J. Extrem. Manuf.* **7**, 015105.
[22] Fang F Z. 2023. On the three paradigms of manufacturing advancement. *Nanomanuf. Metrol.* **6**, 35.
[23] Fang F Z. 2022. The three paradigms of manufacturing advancement. *J. Manuf. Syst.* **63**, 504–505.
[24] Fang F Z. 2020. Atomic and close-to-atomic scale manufacturing: perspectives and measures. *Int. J. Extrem. Manuf.* **2**, 030201.
[25] Fang F Z, Zhang N, Guo D M, Ehmann K, Cheung B, Liu K and Yamamura K. 2019. Towards atomic and close-to-atomic scale manufacturing. *Int. J. Extrem. Manuf.* **1**, 012001.
[26] Gao J, Luo X C, Fang F Z and Sun J N. 2022. Fundamentals of atomic and close-to-atomic scale manufacturing: a review. *Int. J. Extrem. Manuf.* **4**, 012001.
[27] Wei X Y, Mitchell A, Sun R Y, Yu N and Yamamura K. 2024. A review of simulation modeling of the state evaluation and process prediction of plasma processing under atmospheric pressure. *Nanomanuf. Metrol.* **7**, 16.
[28] An H J, Wang J S and Fang F Z. 2023. Material removal on silicon towards atomic and close-to-atomic scale by infrared femtosecond laser. *Mater. Sci. Semicond. Process.* **158**, 107368.
[29] Qi H M, Wang J S, Xu Z W and Fang F Z. 2024. First-principles study of electron dynamics of MoS_2 under femtosecond laser irradiation from deep ultraviolet to near-infrared wavelengths. *J. Chem. Phys.* **161**, 224709.
[30] Mathew P T and Fang F Z. 2018. Advances in molecular electronics: a brief review. *Engineering* **4**, 760–771.
[31] An H J, Wang J S, Fang F Z and Jiang J F. 2024. Exploring ablation of GaAs at atomic and close-to-atomic scale by pulsed laser and 3D TTM–MD simulations. *Opt. Laser Technol.* **171**, 110427.
[32] An H-J, Wang J-S and Fang F-Z. 2022. Material removal at atomic and close-to-atomic scale by high-energy photon: a case study using atomistic-continuum method. *Adv. Manuf.* **10**, 59–71.
[33] Xie K G, Xie Y and Deng H. 2025. Gas cluster ion beam smoothing technique: a review. *Nanomanuf. Metrol.* **8**, 12.
[34] Zhao D W and Lu X C. 2013. Chemical mechanical polishing: theory and experiment. *Friction* **1**, 306–326.
[35] Luo H, Ajmal K M, Liu W, Yamamura K and Deng H. 2021. Atomic-scale and damage-free polishing of single crystal diamond enhanced by atmospheric pressure inductively coupled plasma. *Carbon* **182**, 175–184.
[36] Kubota A and Takita T. 2018. Novel planarization method of single-crystal diamond using 172 nm vacuum-ultraviolet light. *Precis. Eng.* **54**, 269–275.
[37] Ralchenko V G, Ashkinazi E E, Zavedeev E V, Khomich A A, Bolshakov A P, Ryzhkov S G, Sovyk D N, Shershulin V A, Yurov V Y and Rudnev V V. 2016. High-rate ultrasonic polishing of polycrystalline diamond films. *Diam. Relat. Mater.* **66**, 171–176.
[38] Yan B, Chen N, He N, Wu Y, Zhang X L and Li L. 2021. Surface modeling and component analysis of picosecond laser ablation of CVD diamond. *Diam. Relat. Mater.* **111**, 108191.
[39] Zheng Y T, Cumont A E L, Bai M J, Liang Y F, Liu J L, Wei J J, Zhang X T, Ye H T and Li C M. 2021. Smoothing of single crystal diamond by high-speed three-dimensional dynamic friction polishing: optimization and surface bonds evolution mechanism. *Int. J. Refract. Met. Hard Mater.* **96**, 105472.
[40] Liu W, Xiao Y X, Zhang Y J, He Q P and Deng H. 2024. Highly efficient and atomic-scale smoothing of single crystal diamond through plasma-based atom-selective etching. *Diam. Relat. Mater.* **143**, 110840.
[41] Du J B, Liu H Z, Yang N, Chen X Z and Zong W J. 2023. Modification of diamond tool by focused ion beam in dry single-point diamond turning. *Appl. Surf. Sci.* **637**, 157882.
[42] Lee S J et al. 2022. Characteristics of a mixed-gas cluster ion beam for time-of-flight secondary ion mass spectrometry. *Appl. Surf. Sci.* **572**, 151467.
[43] Yuan S, Guo X G, Jin Z J, Kang R K and Guo D M. 2024. A review of high-efficiency and ultra-low damage processing mechanism and technology of diamond. *J. Mech. Eng.* **60**, 337–353.
[44] Luo H, Ajmal K M, Liu W, Yamamura K and Deng H. 2021. Polishing and planarization of single crystal diamonds: state-of-the-art and perspectives. *Int. J. Extrem. Manuf.* **3**, 022003.
[45] Chao J Q, Chen F Z, Xia L, Cai Z X, Wang F J, Tian Y L and Zhang D W. 2023. Laser ablation and chemical oxidation synergistically induced micro/nano Re-entrant structures for super-oleophobic surface with cassie state. *Nanomanuf. Metrol.* **6**, 18.
[46] Wang L X, Chen X K, Wu G, Cao S Z, Xiong Y Q, Wang J X and Zhao D C. 2017. Study on site-specific polishing of polycrystalline diamond film by KrF excimer laser. *J. Laser Micro Nanoeng.* **12**, 62–66.
[47] Zhang Q L, Xu B X, Li J H, Liu J, Wu M T and Fu Y C. 2024. Experimental study of nanosecond laser ablation mechanism and polishing of CVD diamond (inner cover paper·invited). *Infrared Laser Eng.* **53**, 20240285.
[48] Takayama N and Yan J W. 2017. Mechanisms of micro-groove formation on single-crystal diamond by a nanosecond pulsed laser. *J. Mater. Process. Technol.* **243**, 299–311.
[49] Xing Y Q, Liu L, Hao X Q, Wu Z, Huang P and Wang X S. 2018. Micro-channels machining on polycrystalline diamond by nanosecond laser. *Opt. Laser Technol.* **108**, 333–345.
[50] Konov V I. 2012. Laser in micro and nanoprocessing of diamond materials. *Laser Photonics Rev.* **6**, 739–766.

[51] Wei X Y, Wen Q L, Chen J H, Lu J, Cui C C, Huang G Q and Jiang F. 2023. Research on gold film-assisted ultraviolet nanosecond laser machining of diamond microgrooves. *Opt. Laser Technol.* **158**, 108793.
[52] Chen N, Wang R K, Nagarajan B, Yan B, Wu Y, He N and Castagne S. 2022. Investigation of metal-coating-assisted IR nanosecond pulsed laser ablation of CVD diamond. *J. Mater. Res. Technol.* **18**, 4114–4129.
[53] Liu N, Sugimoto K, Yoshitaka N, Yamada H, Sun R Y, Arima K and Yamamura K. 2023. Highly efficient finishing of large-sized single crystal diamond substrates by combining nanosecond pulsed laser trimming and plasma-assisted polishing. *Ceram. Int.* **49**, 19109–19123.
[54] Liu N, Lei L, Zhu J M, Lu H, Xiao J F, Zhang J G, Chen X, Xu J F and Yamamura K. 2024. An interior damage free approach for nanosecond pulsed laser ablation of single crystal diamond via metal film induced self-maintaining graphitization. *J. Manuf. Process.* **131**, 958–972.
[55] Michael K, Greiner L, Dreizehnter P, Weixler J, Putzer M, Schudeleit T, Bambach M and Wegener K. 2023. Ultrashort pulsed laser processing of single crystalline diamonds for tooling applications. *J. Laser Appl.* **35**, 042042.
[56] Takayama N, Ishizuka J and Yan J W. 2018. Microgrooving of a single-crystal diamond tool using a picosecond pulsed laser and some cutting tests. *Precis. Eng.* **53**, 252–262.
[57] Wang H L, Wen Q L, Xu X P, Lu J, Jiang F and Cui C C. 2021. Ablation characteristics and material removal mechanisms of a single-crystal diamond processed by nanosecond or picosecond lasers. *Opt. Express* **29**, 22714–22731.
[58] Prieske M and Vollertsen F. 2021. Picosecond-laser polishing of CVD-diamond coatings without graphite formation. *Mater. Today Proc.* **40**, 1–4.
[59] Han H L, He M L, Liu H, Zhang B and Zhou C. 2024. Damage evolution and crystalline orientation effects in ultrafast laser micro/nano processing of single-crystal diamond. *Opt. Laser Technol.* **169**, 110120.
[60] Zhai J C, Zhang Q L and Zhu Y D. 2022. Picosecond laser ablation of polycrystalline CVD diamond. *Opt. Laser Technol.* **155**, 108403.
[61] Pimenov S M, Vlasov I I, Khomich A A, Neuenschwander B, Muralt M and Romano V. 2011. Picosecond-laser-induced structural modifications in the bulk of single-crystal diamond. *Appl. Phys. A* **105**, 673–677.
[62] Okamoto Y, Okada A, Kajitani A and Shinonaga T. 2019. High surface quality micro machining of monocrystalline diamond by picosecond pulsed laser. *CIRP Ann.* **68**, 197–200.
[63] Meshram T and Yan J W. 2023. Formation of laser-induced periodic surface structures on reaction-bonded silicon carbide by femtosecond pulsed laser irradiation. *Nanomanuf. Metrol.* **6**, 4.
[64] Zhou Z Q, Xu Z W, Song Y, Shi C K, Zhang K and Dong B. 2023. Silicon vacancy color centers in 6H-SiC fabricated by femtosecond laser direct writing. *Nanomanuf. Metrol.* **6**, 7.
[65] Ali B, Litvinyuk I V and Rybachuk M. 2021. Femtosecond laser micromachining of diamond: current research status, applications and challenges. *Carbon* **179**, 209–226.
[66] Han H L, Liu H, Huang J X, Qiu P, Li J, Zhang B and Xu S L. 2025. Atomic-level insight into sequential evolution of nanocomposite carbon structures in femtosecond laser processing of diamond. *Int. J. Mach. Tools Manuf.* **206**, 104247.
[67] Yin J, Chen G Y, Zhu Z C, Jin M Q and Hu B. 2021. Ablation mechanism investigation and ablation threshold prediction of single crystal diamond irradiated by femtosecond laser. *Diam. Relat. Mater.* **111**, 108173.
[68] Chu W B et al. 2025. Structural color display of polycrystalline diamond processed by femtosecond laser processing. *Diam. Relat. Mater.* **152**, 111987.
[69] Wei C, Ma Y P, Han Y, Zhang Y, Yang L and Chen X H. 2019. Study on femtosecond laser processing characteristics of nano-crystalline CVD diamond coating. *Appl. Sci.* **9**, 4273.
[70] Zou J J, Wang Q J, Shen W, Peng S, Qi Z J, Wu G, Cao Q and Liu S. 2024. Research on the fabrication of high-quality patterned diamond using femtosecond laser. *Diam. Relat. Mater.* **150**, 111755.
[71] Chen Y Q and Zhang L C. 2013. *Polishing of Diamond Materials: Mechanisms, Modeling and Implementation* (Springer, London)
[72] Malshe A P, Park B S, Brown W D and Naseem H A. 1999. A review of techniques for polishing and planarizing chemically vapor-deposited (CVD) diamond films and substrates. *Diam. Relat. Mater.* **8**, 1198–1213.
[73] Spencer E G and Schmidt P H. 1972. Ion machining of diamond. *J. Appl. Phys.* **43**, 2956–2958.
[74] Miyamoto I and Taniguchi N. 1982. Polishing and sharpening of diamond point tools by ion sputter-machining. *Precis. Eng.* **4**, 191–194.
[75] Hoffman A, Paterson P J K and Prawer S. 1990. Comparison of the effect of argon and hydrogen ion bombardment on the diamond (100) surface as studied by AES and EELS. *Nucl. Instrum. Methods Phys. Res. B* **52**, 63–67.
[76] Koslowski B, Strobel S and Ziemann P. 2000. Ion polishing of a diamond (100) surface artificially roughened on the nanoscale. *Diam. Relat. Mater.* **9**, 1159–1163.
[77] Ostrovskaya L Y, Dementiev A P, Kulakova I I and Ralchenko V G. 2005. Chemical state and wettability of ion-irradiated diamond surfaces. *Diam. Relat. Mater.* **14**, 486–490.
[78] Du J B, Liu H Z, Wang S, Wu B and Zong W J. 2023. Atomic-scale observation and prediction of gallium ion implantation induced amorphization on natural diamond surface. *Vacuum* **214**, 112226.
[79] Du J B, Liu H Z and Zong W J. 2023. Cutting performance assessment on the modified single crystal diamond tool by focused ion beam. *Diam. Relat. Mater.* **139**, 110354.
[80] Zhao T J, Grogan D F, Bovard B G and Macleod H A. 1990. Diamond film polishing with argon and oxygen ion beams. *Proc. SPIE* **1325**, 142–151.
[81] Nagase T, Kato H, Pahlovy S A and Miyamoto I. 2010. Nanosmoothing of single crystal diamond chips by 1 keV Ar^{+} ion bombardment. *J. Vac. Sci. Technol. B* **28**, 263–267.
[82] Mi S C, Toros A, Graziosi T and Quack N. 2019. Non-contact polishing of single crystal diamond by ion beam etching. *Diam. Relat. Mater.* **92**, 248–252.
[83] Jia G J et al. 2024. Study of amorphous layer on CVD diamond surface induced by Ga ion implantation in focused ion beam processing. *Diam. Relat. Mater.* **145**, 111108.
[84] Rubanov S and Suvorova A. 2011. Ion implantation in diamond using 30 keV Ga^{+} focused ion beam. *Diam. Relat. Mater.* **20**, 1160–1164.
[85] McKenzie W R, Quadir M Z, Gass M H and Munroe P R. 2011. Focused ion beam implantation of diamond. *Diam. Relat. Mater.* **20**, 1125–1128.
[86] Yang Y, Wang Q-L, Chen L, Ma C-L, Zheng X and Shi J-H. 2025. Orientation-dependent effects in single-crystal diamond during focused gallium ion beam processing. *Diam. Relat. Mater.* **158**, 112631.
[87] Tong Z and Luo X C. 2015. Investigation of focused ion beam induced damage in single crystal diamond tools. *Appl. Surf. Sci.* **347**, 727–735.
[88] Fang Z D, Zhang Y, Li R L, Liang Y N and Deng H. 2020. An efficient approach for atomic-scale polishing of single-crystal silicon via plasma-based atom-selective etching. *Int. J. Mach. Tools Manuf.* **159**, 103649.
[89] Wu B, Zhang Y, Yi R and Deng H. 2022. Tuning the plasma etching mode for the atomic-scale smoothing of single-crystal silicon. *J. Phys. Chem. Lett.* **13**, 8580–8585.

[90] Zhang Y J, Tang J, Liang S X, Zhao J L, Hua M Y, Zhang C and Deng H. 2024. Atomic-scale smoothing of semiconducting oxides via plasma-enabled atomic-scale reconstruction. *Int. J. Mach. Tools Manuf.* **196**, 104119.

[91] Zhang L F, Wu B, Zhang Y and Deng H. 2023. Highly efficient and atomic scale polishing of GaN via plasma-based atom-selective etching. *Appl. Surf. Sci.* **620**, 156786.

[92] Liang S X, Zhang L F and Deng H. 2022. Theoretical and experimental study on plasma-induced atom-migration manufacturing (PAMM) of glass. *Appl. Surf. Sci.* **599**, 153976.

[93] Sandhu G S and Chu W K. 1989. Reactive ion etching of diamond. *Appl. Phys. Lett.* **55**, 437–438.

[94] Thoms B D, Owens M S, Butler J E and Spiro C. 1994. Production and characterization of smooth, hydrogen-terminated diamond C (100). *Appl. Phys. Lett.* **65**, 2957–2959.

[95] Küttel O M, Diederich L, Schaller E, Carnal O and Schlapbach L. 1995. The preparation and characterization of low surface roughness (111) and (100) natural diamonds by hydrogen plasma. *Surf. Sci.* **337**, L812–L818.

[96] Buchkremer-Hermanns H, Long C and Weiss H. 1996. ECR plasma polishing of CVD diamond films. *Diam. Relat. Mater.* **5**, 845–849.

[97] Detrick M S, Washington G N and Subramaniam V V. 2003. Control of polishing of diamond films using microactuation and an atmospheric pressure plasma. *IEEE/ASME Trans. Mechatronics* **8**, 45–55.

[98] Lyu P, Pan J Y, Liu Z and Fang F Z. 2025. Polishing of fused silica by laser-enhanced plasma at the atomic and close-to-atomic scale. *CIRP Ann.* **74**, 281–285.

[99] Uetsuka H, Yamada T and Shikata S. 2008. ICP etching of polycrystalline diamonds: fabrication of diamond nano-tips for AFM cantilevers. *Diam. Relat. Mater.* **17**, 728–731.

[100] Zhao L, Wang X B, Jiang M X, Zhao C, Jiang N, Nishimura K, Yi J and Fang S Q. 2025. Optimization of diamond polishing process for sub-nanometer roughness using $Ar/O_2/SF_6$ plasma. *Materials* **18**, 2615.

[101] Xiao Y X, Li X Y, Zhang Y J and Deng H. 2024. Highly efficient polishing of polycrystalline CVD diamond via atmosphere inductively coupled plasma. *Diam. Abras. Eng.* **44**, 553–562.

[102] Liu N, Lei L, Jiang H L, Zhang Y J, Xiao J F, Zhang J G, Chen X, Xu J F and Yamamura K. 2024. A highly efficient semi-finishing approach for polycrystalline diamond film via plasma-based anisotropic etching. *J. Mater. Process. Technol.* **332**, 118578.

[103] Toyoda N. 2018. Surface planarization with gas cluster ion beams and application to wide-bandgap semiconductors. *Int. J. Autom. Technol.* **12**, 170–174.

[104] Yamada I, Matsuo J, Toyoda N and Kirkpatrick A. 2001. Materials processing by gas cluster ion beams. *Mater. Sci. Eng. R* **34**, 231–295.

[105] Isogai H, Toyoda E, Senda T, Izunome K, Kashima K, Toyoda N and Yamada I. 2006. Cross-sectional TEM observations of Si wafers irradiated with gas cluster ion beams. *AIP Conf. Proc.* **866**, 194–197.

[106] Nagato K, Tani H, Sakane Y, Toyoda N, Yamada I, Nakao M and Hamaguchi T. 2008. Study of gas cluster ion beam planarization for discrete track magnetic disks. *IEEE Trans. Magn.* **44**, 3476–3479.

[107] Toyoda N, Hagiwara N, Matsuo J and Yamada I. 1999. Surface treatment of diamond films with Ar and O_2 cluster ion beams. *Nucl. Instrum. Methods Phys. Res. B* **148**, 639–644.

[108] Wang J S, Yamada H, Suga T and Mokuno Y. 2023. Polishing of CVD diamond for direct bonding using Ar and SF_6-gas cluster ion beams. *In 2023 IEEE CPMT Symposium Japan (ICSJ)* (IEEE, Kyoto, Japan) pp 17–20.

[109] Wang J S and Suga T. 2024. Cathodoluminescence characterization of diamond polished by gas cluster ion beam. *In 2024 International Conference on Electronics Packaging (ICEP)* (IEEE, Toyama, Japan) pp 137–138.

[110] Wang J S, Takeuchi K, Kataoka I and Suga T. 2022. Polishing diamond substrates using gas cluster ion beam (GCIB) irradiation for the direct bonding to power devices. *In 2022 International Conference on Electronics Packaging (ICEP)* (IEEE, Sapporo, Japan) pp 57–58.

[111] Chen Y and Zhang L C. 2009. Polishing of polycrystalline diamond by the technique of dynamic friction, part 4: establishing the polishing map. *Int. J. Mach. Tools Manuf.* **49**, 309–314.

[112] Chen Y, Zhang L C and Arsecularatne J A. 2007. Polishing of polycrystalline diamond by the technique of dynamic friction. Part 2: material removal mechanism. *Int. J. Mach. Tools Manuf.* **47**, 1615–1624.

[113] Ye S, Zheng Y T, Zhao S M, Liu J L, Chen L X, Ye H T, Zhang X T, Ouyang X P, Li C M and Wei J J. 2024. Evolutionary features of subsurface defects of single crystal diamond after dynamic friction polishing. *Funct. Diam.* **4**, 2316147.

[114] Huang S T, Zhou L, Xu L F and Jiao K R. 2010. A super-high speed polishing technique for CVD diamond films. *Diam. Relat. Mater.* **19**, 1316–1323.

[115] Zheng Y T et al. 2020. Subsurface cleavage of diamond after high-speed three-dimensional dynamic friction polishing. *Diam. Relat. Mater.* **101**, 107600.

[116] Tang F Z, Chen Y Q and Zhang L C. 2012. Analysis of polished polycrystalline diamond using dual beam focused ion beam microscopy. *Phil. Mag.* **92**, 1680–1690.

[117] Liang Y F, Zheng Y T, Wei J J, Jia X, Zhu X H, An K, Liu J L, Chen L X and Li C M. 2021. Effect of grain boundary on polycrystalline diamond polishing by high-speed dynamic friction. *Diam. Relat. Mater.* **117**, 108461.

[118] Guo X G, Zhai C H, Jin Z J and Guo D M. 2015. The study of diamond graphitization under the action of iron-based catalyst. *J. Mech. Eng.* **51**, 162–168.

[119] Guo X G, Liu T, Zhai C H, Yuan Z W, JIn Z J and Guo D M. 2016. Study on the mechanism of diamond graphite with the action of transition metals. *J. Mech. Eng.* **52**, 23–29.

[120] Kubota A, Nagae S, Motoyama S and Touge M. 2015. Two-step polishing technique for single crystal diamond (100) substrate utilizing a chemical reaction with iron plate. *Diam. Relat. Mater.* **60**, 75–80.

[121] Yuan Z W, Jin Z J, Kang R K and Wen Q. 2012. Tribochemical polishing CVD diamond film with FeNiCr alloy polishing plate prepared by MA-HPS technique. *Diam. Relat. Mater.* **21**, 50–57.

[122] Jin Z J, Shi S J, Lin J Z and Jin L C. 2014. Preparation and performance of dynamic friction polishing plate for diamond film. *Mater. Manuf. Process.* **29**, 20–26.

[123] Zhou L, Huang S T and Xu L F. 2011. An efficient super-high speed polishing method for CVD diamond films. *Int. J. Refract. Met. Hard Mater.* **29**, 698–704.

[124] Cui Z P, Li G and Zong W J. 2019. A polishing method for single crystal diamond (100) plane based on nano silica and nano nickel powder. *Diam. Relat. Mater.* **95**, 141–153.

[125] Hitchiner M P, Wilks E M and Wilks J. 1984. The polishing of diamond and diamond composite materials. *Wear* **94**, 103–120.

[126] Li C, Wang K C, Piao Y, Cui H L, Zakharov O, Duan Z Y, Zhang F H, Yan Y D and Geng Y Q. 2024. Surface micro-morphology model involved in grinding of GaN crystals driven by strain-rate and abrasive coupling effects. *Int. J. Mach. Tools Manuf.* **201**, 104197.

[127] Schuelke T and Grotjohn T A. 2013. Diamond polishing. *Diam. Relat. Mater.* **32**, 17–26.

[128] Lu Y X, Wang B, Mu Q, Yang K, Li H, Rosenkranz A, Jiang N and Zhou P. 2022. Nanoscale smooth and damage-free polycrystalline diamond surface ground by coarse diamond grinding wheel. *Diam. Relat. Mater.* **125**, 108971.
[129] Saho E, Hindmarsh S, Sánchez A M, Birks F, Kermode J R, Dale M W, Fisher D and Beanland R. 2024. Microcracks in CVD diamond produced by scaife polishing. *Diam. Relat. Mater.* **144**, 111008.
[130] Kubota A, Nagae S and Motoyama S. 2020. High-precision mechanical polishing method for diamond substrate using micron-sized diamond abrasive grains. *Diam. Relat. Mater.* **101**, 107644.
[131] Lu Y X, Wang B, Wang Y Z, Nishimura K, Jiang N, Zhou P and Goel S. 2025. Novel surface characteristics observed during grinding of polycrystalline diamond. *Appl. Surf. Sci.* **684**, 161883.
[132] Tatsumi N, Harano K, Ito T and Sumiya H. 2016. Polishing mechanism and surface damage analysis of type IIa single crystal diamond processed by mechanical and chemical polishing methods. *Diam. Relat. Mater.* **63**, 80–85.
[133] Xin Y K, Lu J, Li C, Luo Q F, Li Z S, Ke C M and Xu X P. 2024. Effects of processing parameters and grinding direction on the material removal mechanism of (100) surface single crystal diamond in self-rotating mechanical grinding. *Diam. Relat. Mater.* **141**, 110685.
[134] Xu H Q, Zang J B, Yang G P, Tian P F, Wang Y H, Yu Y Q, Lu J, Xu X P and Zhang P W. 2018. An efficient titanium-containing corundum wheel for grinding CVD diamond films. *Diam. Relat. Mater.* **84**, 119–126.
[135] Xu H Q et al. 2017. High-efficiency grinding CVD diamond films by Fe-Ce containing corundum grinding wheels. *Diam. Relat. Mater.* **80**, 5–13.
[136] Xu H Q, Zang J B, Tian P F, Yuan Y G, Wang Y H, Yu Y Q, Lu J, Xu X P and Zhang P W. 2018. Surface conversion reaction and high efficient grinding of CVD diamond films by chemically mechanical polishing. *Ceram. Int.* **44**, 21641–21647.
[137] Zhou Y K, Zang J B, Su S Y, Zhang C Y, Zhao L X, Yuan Y G, Wang Y H, Lu J, Xu X P and Zhang P W. 2023. Mechanochemical grinding diamond film using titanium-coated diamond active abrasives prepared by vacuum micro-evaporation coating. *Appl. Surf. Sci.* **638**, 158094.
[138] Li C. 2023. *High Efficiency and Low Damage Process of Ultra-precision Grinding Polycrystalline Diamond Film* (Huaqiao University, Quanzhou, China)
[139] Huang C, Peng X H, Yang B, Xiang H G, Sun S, Chen X, Li Q B, Yin D Q and Fu T. 2018. Anisotropy effects in diamond under nanoindentation. *Carbon* **132**, 606–615.
[140] Hird J R and Field J E. 2005. A wear mechanism map for the diamond polishing process. *Wear* **258**, 18–25.
[141] Yang B, Liu Y M, Chen J T, Su Y, Ren Y B, Wu S, Ding X Y, Zhao L B and Hu N. 2024. Investigation on the atomic level removal mechanism of diamond with intrinsically anisotropic surface. *Tribol. Int.* **192**, 109322.
[142] Grodzinski P. 1953. *Diamond Technology: Production Methods for Diamond and Gem Stones* (N.A.G. Press, London)
[143] Tsai H Y, Ting C J and Chou C P. 2007. Evaluation research of polishing methods for large area diamond films produced by chemical vapor deposition. *Diam. Relat. Mater.* **16**, 253–261.
[144] Doronin M A, Polyakov S N, Kravchuk K S, Molchanov S P, Lomov A A, Troschiev S Y and Terentiev S A. 2018. Limits of single crystal diamond surface mechanical polishing. *Diam. Relat. Mater.* **87**, 149–155.
[145] Yang N, Zong W J, Li Z Q and Sun T. 2015. Wear process of single crystal diamond affected by sliding velocity and contact pressure in mechanical polishing. *Diam. Relat. Mater.* **58**, 46–53.
[146] Zong W J, Sun T, Li D, Cheng K and Li Z Q. 2008. Nano-precision diamond cutting tools achieved by mechanical lapping versus thermo-mechanical lapping. *Diam. Relat. Mater.* **17**, 954–961.
[147] Zong W J, Li D, Sun T, Cheng K and Liang Y C. 2007. The ultimate sharpness of single-crystal diamond cutting tools—part II: a novel efficient lapping process. *Int. J. Mach. Tools Manuf.* **47**, 864–871.
[148] Zong W J, Li D, Sun T and Cheng K. 2006. Contact accuracy and orientations affecting the lapped tool sharpness of diamond cutting tools by mechanical lapping. *Diam. Relat. Mater.* **15**, 1424–1433.
[149] Wilks J. 1973. Experiments on polishing of diamond. *Nature* **243**, 15–18.
[150] Wilks E M and Wilks J. 1972. The resistance of diamond to abrasion. *J. Phys. D: Appl. Phys.* **5**, 1902–1919.
[151] Hu X et al. 2024. Roughness control in the processing of 2-inch polycrystalline diamond films on 4H-SiC wafers. *Mater. Sci. Semicond. Process.* **184**, 108824.
[152] Mallik A K, Bhar R and Bysakh S. 2016. An effort in planarising microwave plasma CVD grown polycrystalline diamond (PCD) coated 4 in. Si wafers. *Mater. Sci. Semicond. Process.* **43**, 1–7.
[153] Qiang M, Chen S Y, Yin X M, Wu L Z, Fan Y Y, Xu X K, Wang Z and Dun A H 2024. Two-step polishing progress and mechanism for polycrystalline diamond. Optica Open. Preprint. (https://doi.org/10.1364/opticaopen.24980724.v1)
[154] Xu Y C, Zhu J H, Wang N C, Shi C Y, Zhao Y K, Shao J Y and Xu S. 2022. Analysis on the lapping uniformity of MPCVD polycrystalline diamond wafer. *Diam. Abras. Eng.* **42**, 705–712.
[155] Gaissmaier K and Weis O. 1993. Superpolishing of diamond. *Diam. Relat. Mater.* **2**, 943–948.
[156] Xiao C, Hsia F-C, Sutton-Cook A, Weber B and Franklin S. 2022. Polishing of polycrystalline diamond using synergies between chemical and mechanical inputs: a review of mechanisms and processes. *Carbon* **196**, 29–48.
[157] Sun H G, Zhang Z Y, Xue Z H, Zhou H X, Geng Z M, Cheng C S, Chen L L and Tian Y. 2025. Atomic surface of titanium alloy using novel chemical mechanical polishing with rare earth composite abrasives. *J. Manuf. Process.* **134**, 79–89.
[158] Zhang S, Wang D, Zhao F, Zhang Z Y, Zhou H X, Chen L L, Yan L J and Zhao B S. 2025. Close atomic surface of titanium alloy produced by novel photocatalytic chemical mechanical polishing using developed $SiO_2@Al_2O_3@CeO_2$ composite abrasives with high material removal rate. *Appl. Surf. Sci.* **703**, 163436.
[159] Liao L X, Zhang Z Y, Meng F N, Liu D D, Wu B, Li Y B and Xie W X. 2021. A novel slurry for chemical mechanical polishing of single crystal diamond. *Appl. Surf. Sci.* **564**, 150431.
[160] Liu D D, Zhang Z Y, Zhou H X, Deng X Q, Shi C J, Meng F N, Yu Z B and Feng J Y. 2023. Angstrom surface on copper induced by novel green chemical mechanical polishing using ceria and silica composite abrasives. *Appl. Surf. Sci.* **640**, 158382.
[161] Wang D, Xie W X, Zhang Z Y, Wang J M, Shi C J, Meng F N, Zhuang X Y, Tong D Y and Cao C. 2024. Atomic surface of silicon wafers induced by grafted silica nanoparticles and sodium carbonate. *Appl. Surf. Sci.* **664**, 160234.
[162] Zhang Z Y, Liu J, Hu W, Zhang L Z, Xie W X and Liao L X. 2021. Chemical mechanical polishing for sapphire wafers using a developed slurry. *J. Manuf. Process.* **62**, 762–771.
[163] Zhao F, Zhang Z Y, Deng X Q, Feng J Y, Zhou H X, Liu Z S, Meng F N and Shi C J. 2024. Atomic surface achieved through a novel cross-scale model from macroscale to nanoscale. *Nanoscale* **16**, 2318–2336.

[164] Dong L G, Zhang Z Y, Zhao F, Li Q Y, Zhou H X, Yang X F, Liu X Q, Guo J D and Zheng X. 2025. Atomic surface on a Ni alloy produced by novel green chemical mechanical polishing. *Tribol. Int.* **211**, 110902.
[165] Wang D, Liu L, Zhang Z Y, Peng Q B, Shi C J, Liu X Q, Liu X Y, Zhou H X and Wen W. 2024. Atomic-scale planarization surface of quartz glass induced by novel green chemical mechanical polishing using three ingredients. *Mater. Today Sustain.* **25**, 100669.
[166] Zhao F, Zhang Z Y, Zhou H X, Feng J Y, Deng X Q, Liu Z S, Meng F N and Shi C J. 2024. Novel full-scale model verified by atomic surface and developed composite microfiber and slurry polishing system. *Composites B* **283**, 111598.
[167] Zhao F, Zhang Z Y, Zhou H X, Chen L L, Hai K, Wu L W, Yu J H, Zhang Z F and Fan C. 2025. Unprecedented developed composite polishing system to achieve atomic surface integrating rough and fine polishing using a novel hyper-conjugated pad through controlling the temperature of a proposed green slurry. *Adv. Compos. Hybrid Mater.* **8**, 234.
[168] Jin Z J, Yuan Z W, Li Q and Wang K. 2011. Tribological aspects of chemical mechanical polishing diamond surfaces. *Adv. Mater. Res.* **325**, 464–469.
[169] Yuan Z W, Zheng P, Wen Q and He Y. 2018. Chemical kinetics mechanism for chemical mechanical polishing diamond and its related hard-inert materials. *Int. J. Adv. Manuf. Technol.* **95**, 1715–1727.
[170] Cheng C Y, Tsai H Y, Wu C H, Liu P Y, Hsieh C H and Chang Y Y. 2005. An oxidation enhanced mechanical polishing technique for CVD diamond films. *Diam. Relat. Mater.* **14**, 622–625.
[171] Werrell J M, Mandal S, Thomas E L H, Brousseau E B, Lewis R, Borri P, Davies P R and Williams O A. 2017. Effect of slurry composition on the chemical mechanical polishing of thin diamond films. *Sci. Technol. Adv. Mater.* **18**, 654–663.
[172] Thomas E L H, Nelson G W, Mandal S, Foord J S and Williams O A. 2014. Chemical mechanical polishing of thin film diamond. *Carbon* **68**, 473–479.
[173] Thomas E L H, Mandal S, Brousseau E B and Williams O A. 2014. Silica based polishing of {100} and {111} single crystal diamond. *Sci. Technol. Adv. Mater.* **15**, 035013.
[174] Yang N, Huang W and Lei D J. 2020. Control of nanoscale material removal in diamond polishing by using iron at low temperature. *J. Mater. Process. Technol.* **278**, 116521.
[175] Yuan Z W, Jin Z J, Zhang Y J and Wen Q. 2013. Chemical mechanical polishing slurries for chemically vapor-deposited diamond films. *J. Manuf. Sci. Eng.* **135**, 041006.
[176] Deng J Y, Pan J S, Zhang Q X, Yan Q S and Lu J B. 2020. The mechanism of Fenton reaction of hydrogen peroxide with single crystal 6H-SiC substrate. *Surf. Interfaces* **21**, 100730.
[177] Lu J B, Huang Y F, Fu Y Z, Yan Q S and Zeng S. 2021. Synergistic effect of photocatalysis and Fenton on improving the removal rate of 4H-SiC during CMP. *ECS J. Solid State Sci. Technol.* **10**, 044001.
[178] Deng J Y, Lu J B, Yan Q S and Pan J S. 2021. Basic research on chemical mechanical polishing of single-crystal SiC-electro-Fenton: reaction mechanism and modelling of hydroxyl radical generation using condition response modelling. *J. Environ. Chem. Eng.* **9**, 104954.
[179] Hu D, Lu J B, Deng J Y, Yan Q S, Long H T and Luo Y R. 2023. The polishing properties of magnetorheological-elastomer polishing pad based on the heterogeneous Fenton reaction of single-crystal SiC. *Precis. Eng.* **79**, 78–85.
[180] Xue H M, Jin Z J and Shi Z Y. 2015. Mechanical lapping and chemical-mechanical polishing process for single crystal diamond. *Nanotechnol. Precis. Eng.* **13**, 102–107.
[181] Yuan S, Guo X G, Huang J X, Lu M G, Jin Z J, Kang R K and Guo D M. 2019. Sub-nanoscale polishing of single crystal diamond (100) and the chemical behavior of nanoparticles during the polishing process. *Diam. Relat. Mater.* **100**, 107528.
[182] Yang H P, Jin Z J, Niu L, Wang H C and Niu H. 2022. Visible-light catalyzed assisted chemical mechanical polishing of single crystal diamond. *Diam. Relat. Mater.* **125**, 108982.
[183] Wang X H, Xiong Q, Lu J B, Yan Q S and Liu W T. 2022. Characterization of Fenton reaction-based material removal on single crystal diamond surface. *Diam. Relat. Mater.* **129**, 109320.
[184] Kubota A, Nagae S and Touge M. 2016. Improvement of material removal rate of single-crystal diamond by polishing using H_2O_2 solution. *Diam. Relat. Mater.* **70**, 39–45.
[185] Kubota A, Motoyama S and Touge M. 2016. Development of an ultra-finishing technique for single-crystal diamond substrate utilizing an iron tool in H_2O_2 solution. *Diam. Relat. Mater.* **64**, 177–183.
[186] Yuan S, Guo X G, Li M, Jin Z J and Guo D M. 2022. An insight into polishing slurry for high quality and efficiency polishing of diamond. *Tribol. Int.* **174**, 107789.
[187] Lin J L, Hu D, Wang X H, Lu J B and Yan Q S. 2025. The influence of Fenton reaction chemical parameters on the removal of single crystal diamond. *Diam. Relat. Mater.* **153**, 112040.
[188] Luo Z Y, Lu J B, Zeng J, Wang X H and Yan Q S. 2024. Experimental study on single crystal diamond CMP based on Fenton reaction and analysis of oxidation mechanism. *Mater. Sci. Semicond. Process.* **182**, 108739.
[189] Lin Y C, Lu J, Tong R L, Luo Q F and Xu X P. 2018. Surface damage of single-crystal diamond (100) processed based on a sol-gel polishing tool. *Diam. Relat. Mater.* **83**, 46–53.
[190] Xu X P, Liu J, Yu Y Q and Lu J. 2013. Fabrication and application of gel-bonded abrasive tools for grinding and polishing tools. *J. Mech. Eng.* **49**, 156–462.
[191] Kim Y-C and Kang S-J L. 2011. Novel CVD diamond-coated conditioner for improved performance in CMP processes. *Int. J. Mach. Tools Manuf.* **51**, 565–568.
[192] Yuan Z W, Jin Z J, Li Q and Du H Y. 2016. Study on the chemical mechanical polishing technique of CVD diamond. *J. Synth. Cryst.* **45**, 73–79.
[193] Nakata K and Fujishima A. 2012. TiO_2 photocatalysis: design and applications. *J. Photochem. Photobiol. C* **13**, 169–189.
[194] Deng J Y, Lu J B, Yan Q S and Pan J S. 2021. Enhancement mechanism of chemical mechanical polishing for single-crystal 6H-SiC based on electro-fenton reaction. *Diam. Relat. Mater.* **111**, 108147.
[195] Ni Z F, Xia M H, Chen G M, Yu J, Lu X Y, Qian S H and Bian D. 2024. Study on the mechanism of chemical mechanical polishing for 4H-SiC based on photoelectro-fenton reaction. *ECS J. Solid State Sci. Technol.* **13**, 124002.
[196] Ran B, Pan J S, Yan Q S, Wu Q Y, Zhuang R J, Zhou Y Z, Zhao Z Q and Zhang X W. 2024. Chemical-mechanical synergetic effect of single crystal SiC polishing using Fe_3O_4@ MIL-100 (Fe) magnetic photo-Fenton catalyst. *Diam. Relat. Mater.* **149**, 111545.
[197] Yu X, Zhang B G, Wang R, Kao Z, Yang S H and Wei W. 2021. Effect of photocatalysts on electrochemical properties and chemical mechanical polishing rate of GaN. *Mater. Sci. Semicond. Process.* **121**, 105387.
[198] Wang J, Wang T Q, Pan G S and Lu X C. 2016. Effects of catalyst concentration and ultraviolet intensity on chemical mechanical polishing of GaN. *Appl. Surf. Sci.* **378**, 130–135.
[199] Ou L-W, Wang Y-H, Hu H-Q, Zhang -L-L, Dong Z-G, Kang R-K, Guo D-M and Shi K. 2019. Photochemically combined mechanical polishing of N-type gallium nitride wafer in high efficiency. *Precis. Eng.* **55**, 14–21.

[200] Ren Y H, Li K X, Li W, Han X and Liu X M. 2021. Research on a UV-assisted chemical modification strategy for monocrystalline silicon. *Mech. Sci.* **12**, 133–141.

[201] Shi D, Zhou W and Zhao T C. 2023. Polishing of diamond, SiC, GaN based on the oxidation modification of hydroxyl radical: status, challenges and strategies. *Mater. Sci. Semicond. Process.* **166**, 107737.

[202] Shao J Y, Zhao Y J, Zhu J H, Yuan Z W, Du H Y and Wen Q. 2023. A new slurry for photocatalysis-assisted chemical mechanical polishing of monocrystal diamond. *Machines* **11**, 664.

[203] Xiong Q, Lu J B, Yan Q S, Liu W T, Wang X H and Zhang F L. 2024. Tribological behavior of single-crystal diamond in a UV photocatalytic-Fenton composite reaction environment. *Wear* **536-537**, 205175.

[204] Liu W T, Xiong Q, Lu J B, Wang X H and Yan Q S. 2022. Tribological behavior of single crystal diamond based on UV photocatalytic reaction. *Tribol. Int.* **175**, 107806.

[205] Cai W M, Lu J B, Xiong Q, Luo Z Y and Yan Q S. 2023. Tribological behavior of polycrystalline diamond based on photo-Fenton reaction. *Diam. Relat. Mater.* **140**, 110430.

[206] Liu W T, Lu J B, Xiong Q, Wang X H and Yan Q S. 2024. Investigation on influence of polishing disc materials in UV-catalytic polishing of single crystal diamond. *Diam. Relat. Mater.* **141**, 110678.

[207] Luo Z Y, Lu J B, Yan Q S, Cai W M and Huang W L. 2025. Experimental study of chemical mechanical polishing of polycrystalline diamond based on photo-Fenton reaction. *Mater. Sci. Semicond. Process.* **186**, 109072.

[208] Yuan S, Guo X G, Wang H and Gao S. 2023. A theoretical and experimental study on high-efficiency and ultra-low damage machining of diamond. *J. Manuf. Sci. Eng.* **145**, 071006.

[209] Li H L, Lu J B, Cai W M, Hu D and Yan Q S. 2024. Optimisation of chemically assisted mechanical polishing process parameters for polycrystalline diamond based on photo-Fenton reaction. *Diam. Relat. Mater.* **150**, 111750.

[210] Yu Z B, Zhang Z Y, Zeng Z N, Fan C, Gu Y, Shi C J, Zhou H X, Meng F N and Feng J Y. 2024. Atomic surface of diamond induced by novel green photocatalytic chemical mechanical polishing with high material removal rate. *Int. J. Extrem. Manuf.* **7**, 025102.

[211] Watanabe J, Touge M and Sakamoto T. 2013. Ultraviolet-irradiated precision polishing of diamond and its related materials. *Diam. Relat. Mater.* **39**, 14–19.

[212] Jiang X W, Wu G, Guan S Y, Mao Y H, Yang Z Y, Long X W, Zhao L S, Qi Q and Tan Z Q. 2023. A novel low-rotation-speed dynamic friction polishing of diamond. *Diam. Relat. Mater.* **136**, 109932.

[213] Touge M, Anan S, Wada S, Kubota A, Nakanishi Y and Watanabe J. 2010. Atomic-scale planarization of single crystal diamond substrates by ultraviolet rays assisted machining. *Key Eng. Mater.* **447-448**, 66–70.

[214] Wu G, Mao Y H, Guan S Y, Yang Z Y, Zhao L S, Jiang X W and Tan Z Q. 2024. Global flattening realization and kinematic analysis of UV-assisted low-speed 3D dynamic friction-polished diamonds. *Diam. Relat. Mater.* **146**, 111221.

[215] Liu N, Lei L, Lu H, Jiang H L, Zhang Y J, Xiao J F, Zhang J G, Chen X and Xu J F. 2025. C-C bond rupture initiated graphitization achieves highly efficient diamond polishing. *Int. J. Mech. Sci.* **287**, 109958.

[216] Deng H, Endo K and Yamamura K. 2017. Damage-free finishing of CVD-SiC by a combination of dry plasma etching and plasma-assisted polishing. *Int. J. Mach. Tools Manuf.* **115**, 38–46.

[217] Yamamura K, Takiguchi T, Ueda M, Deng H, Hattori A N and Zettsu N. 2011. Plasma assisted polishing of single crystal SiC for obtaining atomically flat strain-free surface. *CIRP Ann.* **60**, 571–574.

[218] Deng H and Yamamura K. 2013. Atomic-scale flattening mechanism of 4H-SiC (0 0 0 1) in plasma assisted polishing. *CIRP Ann.* **62**, 575–578.

[219] Deng H, Endo K and Yamamura K. 2015. Plasma-assisted polishing of gallium nitride to obtain a pit-free and atomically flat surface. *CIRP Ann.* **64**, 531–534.

[220] Deng H, Endo K and Yamamura K. 2015. Atomic-scale and pit-free flattening of GaN by combination of plasma pretreatment and time-controlled chemical mechanical polishing. *Appl. Phys. Lett.* **107**, 051602.

[221] Lyu P, Lai M, Liu Z and Fang F Z. 2022. Damage-free finishing of Lu_2O_3 by combining plasma-assisted etching and low-pressure polishing. *CIRP Ann.* **71**, 169–172.

[222] Lyu P, Lai M, Liu Z and Fang F Z. 2023. Atomic and close-to-atomic scale polishing of Lu_2O_3 by plasma-assisted etching. *Int. J. Mech. Sci.* **252**, 108374.

[223] Yamamura K, Emori K, Sun R, Ohkubo Y, Endo K, Yamada H, Chayahara A and Mokuno Y. 2018. Damage-free highly efficient polishing of single-crystal diamond wafer by plasma-assisted polishing. *CIRP Ann.* **67**, 353–356.

[224] Li X Y, Xiao Y X, Wang Y H, He Q P, Zhang Y J and Deng H. 2025. Microwave plasma-assisted polishing of polycrystalline diamond. *Diam. Relat. Mater.* **152**, 111907.

[225] Yuan S, Cheung C F, Shokrani A, Zhan Z J and Wang C J. 2025. Atomic-level flat polishing of polycrystalline diamond by combining plasma modification and chemical mechanical polishing. *CIRP Ann.* **74**, 441–445.

[226] Liu N, Yamada H, Yoshitaka N, Sugimoto K, Sun R Y, Kawai K, Arima K and Yamamura K. 2021. Comparison of surface and subsurface damage of mosaic single-crystal diamond substrate processed by mechanical and plasma-assisted polishing. *Diam. Relat. Mater.* **119**, 108555.

[227] Liu N, Sugawara K, Yoshitaka N, Yamada H, Takeuchi D, Akabane Y, Fujino K, Kawai K, Arima K and Yamamura K. 2020. Damage-free highly efficient plasma-assisted polishing of a 20-mm square large mosaic single crystal diamond substrate. *Sci. Rep.* **10**, 19432.

[228] Yu J R, Liu X Y, Xu R B and Yu D Q. 2025. Single crystal diamond polishing assisted by inductively coupled plasma etching. *Diam. Relat. Mater.* **152**, 111978.

[229] Lyu P, Lai M, Liu Z and Fang F Z. 2021. Ultra-smooth finishing of single-crystal lutetium oxide by plasma-assisted etching. *Precis. Eng.* **67**, 77–88.

[230] Lyu P, Lai M and Fang F-Z. 2020. Nanometric polishing of lutetium oxide by plasma-assisted etching. *Adv. Manuf.* **8**, 440–446.

[231] Yan B, He N, Chen N, Weigold M, Chen H W, Sun S C, Wu Y, Fu S Y, Li L and Abele E. 2025. Achieving precise graphenization of diamond coatings below the interfacial thermal stress threshold. *Int. J. Extrem. Manuf.* **7**, 015106.

[232] Fang F Z, Luo X C, Dai G L, Takaya Y, Gao W and Ehmann K. 2024. Atomic and close-to-atomic scale manufacturing: the fundamental technology of manufacturing III. *In CIRP Novel Topics in Production Engineering: Volume 1* (ed Tolio T) (Springer, Cham) pp 315–360.

[233] Zhang Z Y, Yan J W and Kuriyagawa T. 2019. Manufacturing technologies toward extreme precision. *Int. J. Extrem. Manuf.* **1**, 022001.

[234] Dongming G. 2024. High-performance manufacturing. *Int. J. Extrem. Manuf.* **6**, 060201.

[235] Huang N, Zhou P and Fang F Z. 2025. Effect of mechanical load on atomic-scale fabrication based on local anodic oxidation. *Nanomanuf. Metrol.* **8**, 11.

[236] Li X L, Bonilla M R, Lu M Y and Huang H. 2024. Atomistic understanding of ductile-to-brittle transition in single crystal Si and GaAs under nanoscratch. *Int. J. Mech. Sci.* **282**, 109689.

[237] Wu Y Q, Rao Q J, Qin Z Y, Tan S P, Huang G Q, Huang H, Xu X P and Huang H. 2024. A distinctive material removal

mechanism in the diamond grinding of (0001)-oriented single crystal gallium nitride and its implications in substrate manufacturing of brittle materials. *Int. J. Mach. Tools Manuf.* **203**, 104222.

[238] Yang S Y, Li X L, Zhao Y T, Al-Amin M, Grøndahl L, Lu M Y, Cheung C F and Huang H. 2023. MD simulation of chemically enhanced polishing of 6H-SiC in aqueous H_2O_2. *J. Manuf. Process.* **107**, 515–528.

[239] Wang Y Q, Zhang S Y, Xia H, Wu Y Q and Huang H. 2023. Unveiling the effect of crystal orientation on gallium nitride cutting through MD simulation. *Int. J. Mech. Sci.* **259**, 108619.

[240] van Duin A C T, Dasgupta S, Lorant F and Goddard W A. 2001. ReaxFF: a reactive force field for hydrocarbons. *J. Phys. Chem. A* **105**, 9396–9409.

[241] Li C, Hu Y X, Wei Z Z, Wu C J, Peng Y F, Zhang F H and Geng Y Q. 2024. Damage evolution and removal behaviors of GaN crystals involved in double-grits grinding. *Int. J. Extrem. Manuf.* **6**, 025103.

[242] Li C, Wang K C, Zakharov O, Cui H L, Wu M T, Zhao T C, Yan Y D and Geng Y Q. 2025. Damage evolution mechanism and low-damage grinding technology of silicon carbide ceramics. *Int. J. Extrem. Manuf.* **7**, 022015.

[243] Jeon B, Sankaranarayanan S K R S, van Duin A C T and Ramanathan S. 2012. Reactive molecular dynamics study of chloride ion interaction with copper oxide surfaces in aqueous media. *ACS Appl. Mater. Interfaces* **4**, 1225–1232.

[244] Assowe O, Politano O, Vignal V, Arnoux P, Diawara B, Verners O and van Duin A C T. 2012. Reactive molecular dynamics of the initial oxidation stages of Ni (111) in pure water: effect of an applied electric field. *J. Phys. Chem. A* **116**, 11796–11805.

[245] Raju M, Kim S-Y, van Duin A C T and Fichthorn K A. 2013. ReaxFF reactive force field study of the dissociation of water on titania surfaces. *J. Phys. Chem. C* **117**, 10558–10572.

[246] Russo M F Jr, Li R, Mench M and van Duin A C T. 2011. Molecular dynamic simulation of aluminum–water reactions using the ReaxFF reactive force field. *Int. J. Hydrog. Energy* **36**, 5828–5835.

[247] Wen J L, Ma T B, Zhang W W, van Duin A C T and Lu X C. 2017. Surface orientation and temperature effects on the interaction of silicon with water: molecular dynamics simulations using ReaxFF reactive force field. *J. Phys. Chem. A* **121**, 587–594.

[248] DorMohammadi H, Pang Q, Árnadóttir L and Isgor O B. 2018. Atomistic simulation of initial stages of iron corrosion in pure water using reactive molecular dynamics. *Comput. Mater. Sci.* **145**, 126–133.

[249] Wen J L, Ma T B, Zhang W W, van Duin A C T and Lu X C. 2017. Atomistic mechanisms of Si chemical mechanical polishing in aqueous H_2O_2: reaxFF reactive molecular dynamics simulations. *Comput. Mater. Sci.* **131**, 230–238.

[250] Wen J L, Ma T B, Zhang W W, Psofogiannakis G, van Duin A C T, Chen L, Qian L M, Hu Y Z and Lu X C. 2016. Atomic insight into tribochemical wear mechanism of silicon at the Si/SiO_2 interface in aqueous environment: molecular dynamics simulations using ReaxFF reactive force field. *Appl. Surf. Sci.* **390**, 216–223.

[251] Chen L, Wen J L, Zhang P, Yu B J, Chen C, Ma T B, Lu X C, Kim S H and Qian L M. 2018. Nanomanufacturing of silicon surface with a single atomic layer precision via mechanochemical reactions. *Nat. Commun.* **9**, 1542.

[252] Li M, Guo X G, Dai S Y, Yuan S, Ma J L, Liu F M, Zhang L M, Guo D M and Zhou P. 2022. Effect of grinding damage on cutting force and ductile machining during single grain scratching of monocrystalline silicon. *Mater. Sci. Semicond. Process.* **151**, 107019.

[253] Yuan S, Guo X G, Liu S T, Li P H, Liu F M, Zhang L M and Kang R K. 2022. Atomistic understanding of the subsurface damage mechanism of silicon (100) during the secondary nano-scratching processing. *Mater. Sci. Semicond. Process.* **144**, 106624.

[254] Guo X G, Yuan S, Gou Y J, Wang X L, Guo J, Jin Z J and Kang R K. 2020. Study on chemical effects of H_2O_2 and glycine in the copper CMP process using ReaxFF MD. *Appl. Surf. Sci.* **508**, 145262.

[255] Guo X G, Wang X L, Jin Z J and Kang R K. 2018. Atomistic mechanisms of Cu CMP in aqueous H_2O_2: molecular dynamics simulations using ReaxFF reactive force field. *Comput. Mater. Sci.* **155**, 476–482.

[256] Yue D-C, Ma T-B, Hu Y-Z, Yeon J, van Duin A C T, Wang H and Luo J B. 2015. Tribochemical mechanism of amorphous silica asperities in aqueous environment: a reactive molecular dynamics study. *Langmuir* **31**, 1429–1436.

[257] Wang M, Duan F L and Mu X J. 2019. Effect of surface silanol groups on friction and wear between amorphous silica surfaces. *Langmuir* **35**, 5463–5470.

[258] Guo X G, Yuan S, Huang J X, Chen C, Kang R K, Jin Z J and Guo D M. 2020. Effects of pressure and slurry on removal mechanism during the chemical mechanical polishing of quartz glass using ReaxFF MD. *Appl. Surf. Sci.* **505**, 144610.

[259] Zhang S H, Guo X G, Jin Z J, Kang R K, Tang W C and Gao S. 2024. Subnanoscale ion beam modification-assisted smoothing of heterostructure surfaces. *ACS Appl. Mater. Interfaces* **16**, 38744–38756.

[260] Li X W, Wang A Y and Lee K-R. 2019. Insights on low-friction mechanism of amorphous carbon films from reactive molecular dynamics study. *Tribol. Int.* **131**, 567–578.

[261] Li X W, Wang A Y and Lee K-R. 2019. Atomistic understanding on friction behavior of amorphous carbon films induced by surface hydrogenated modification. *Tribol. Int.* **136**, 446–454.

[262] Li X W, Wang A Y and Lee K-R. 2018. Mechanism of contact pressure-induced friction at the amorphous carbon/alpha olefin interface. *npj Comput. Mater.* **4**, 53.

[263] Zong W J, Li Z Q, Sun T, Cheng K, Li D and Dong S. 2010. The basic issues in design and fabrication of diamond-cutting tools for ultra-precision and nanometric machining. *Int. J. Mach. Tools Manuf.* **50**, 411–419.

[264] Tolkowsky M. 1920. *Research on the Abrading, Grinding or Polishing of Diamonds* (University of London, London, UK)

[265] Bowden F and Tabor D. 1965. *Physical Properties of Diamond* (Clarendon Press, Oxford, UK)

[266] Brezoczky B and Seki H. 1990. Triboattraction: friction under negative load. *Langmuir* **6**, 1141–1145.

[267] Couto M, van Enekevort W J P, Wichman B and Seal M. 1992. Scanning tunneling microscopy of polished diamond surfaces. *Appl. Surf. Sci.* **62**, 263–268.

[268] Couto M S, van Enckevort W J P and Seal M. 1994. On the mechanism of diamond polishing in the soft directions. *J. Hard Mater.* **5**, 31–47.

[269] Grillo S E, Field J E and van Bouwelen F M. 2000. Diamond polishing: the dependency of friction and wear on load and crystal orientation. *J. Phys. D: Appl. Phys.* **33**, 985–990.

[270] Grillo S E and Field J E. 1997. The polishing of diamond. *J. Phys. D: Appl. Phys.* **30**, 202–209.

[271] Zong W J, Li D, Cheng K, Sun T, Wang H X and Liang Y C. 2005. The material removal mechanism in mechanical lapping of diamond cutting tools. *Int. J. Mach. Tools Manuf.* **45**, 783–788.

[272] Zong W, Cheng K, Li D, Sun T and Liang Y. 2007. The ultimate sharpness of single-crystal diamond cutting tools—part I: theoretical analyses and predictions. *Int. J. Mach. Tools Manuf.* **47**, 852–863.
[273] Cheng X and Zong W J. 2018. Anisotropic evolution of damaged carbons of a mechanically polished diamond surface in low-temperature annealing. *Diam. Relat. Mater.* **90**, 7–17.
[274] Pastewka L, Moser S, Gumbsch P and Moseler M. 2011. Anisotropic mechanical amorphization drives wear in diamond. *Nat. Mater.* **10**, 34–38.
[275] Zong W J, Cheng X and Zhang J J. 2016. Atomistic origins of material removal rate anisotropy in mechanical polishing of diamond crystal. *Carbon* **99**, 186–194.
[276] Yang N, Zong W J, Li Z Q and Sun T. 2014. Amorphization anisotropy and the internal of amorphous layer in diamond nanoscale friction. *Comput. Mater. Sci.* **95**, 551–556.
[277] Liu H Z, Zong W J and Cheng X. 2020. Origins for the anisotropy of the friction force of diamond sliding on diamond. *Tribol. Int.* **148**, 106298.
[278] Wang Y, Xu J X, Ootani Y, Bai S D, Higuchi Y, Ozawa N, Adachi K, Martin J M and Kubo M. 2017. Tight-binding quantum chemical molecular dynamics study on the friction and wear processes of diamond-like carbon coatings: effect of tensile stress. *ACS Appl. Mater. Interfaces* **9**, 34396–34404.
[279] Peguiron A, Moras G, Walter M, Uetsuka H, Pastewka L and Moseler M. 2016. Activation and mechanochemical breaking of C-C bonds initiate wear of diamond (110) surfaces in contact with silica. *Carbon* **98**, 474–483.
[280] Cadot G B J, Billingham J and Axinte D A. 2017. A study of surface swelling caused by graphitisation during pulsed laser ablation of carbon allotrope with high content of sp^3 bounds. *J. Phys. D: Appl. Phys.* **50**, 245301.
[281] Shi S J, Jin Z J, Zhong X H, Lin J Z and Yin B. 2015. Processing and mechanism of dynamic friction polishing diamond using manganese-based alloy. *Mater. Manuf. Process.* **30**, 654–660.
[282] Shi S J, Lin J Z, Jin Z J, Guo X G, Zhou P and Kang R K. 2014. Study of grinding wheel for polishing diamond by dynamic friction polishing. *Adv. Mater. Res.* **1017**, 304–309.
[283] Wang C H, An R L, Shi S J and Guo D M. 2017. Dynamic friction dressing of the diamond abrasive brick by W-Mo-Cr alloy. *Diam. Abras. Eng.* **37**, 51–55.
[284] Mandal S, Thomas E L H, Gines L, Morgan D, Green J, Brousseau E B and Williams O A. 2018. Redox agent enhanced chemical mechanical polishing of thin film diamond. *Carbon* **130**, 25–30.
[285] Yu Z B, Jia Z H, Liu W, Zhang Z Y, Zhao F, Fan C, Zhang H S, Lyv Y and Liu D D. 2025. Facet-dependent oxidative fabrication of diamond determined by operando scanning electron microscopy. *Nano Lett.* **25**, 5391–5397.
[286] Zhu J H, Zhao Y J, Yuan Z W, Du H Y and Xu Y C. 2025. Mechanism of photocatalysis-assisted chemical mechanical polishing of CVD single crystal diamond. *Funct. Diamond* **5**, 2433955.
[287] Yuan S, Guo X G, Li P H, Mao Q, Lu M G, Jin Z J, Kang R K and Guo D M. 2021. Insights into the surface oxidation modification mechanism of nano-diamond: an atomistic understanding from ReaxFF simulations. *Appl. Surf. Sci.* **540**, 148321.
[288] Yuan S, Guo X G, Lu M G, Jin Z J, Kang R K and Guo D M. 2019. Diamond nanoscale surface processing and tribochemical wear mechanism. *Diam. Relat. Mater.* **94**, 8–13.
[289] Shi Z Y, Jin Z J, Guo X G, Yuan S and Guo J. 2019. Insights into the atomistic behavior in diamond chemical mechanical polishing with radical ·OH environment using ReaxFF molecular dynamics simulation. *Comput. Mater. Sci.* **166**, 136–142.
[290] He Y, Zhou G X, Tang M L, Fan L, Gao X J and Sun J T. 2025. Investigation on mechanism of mechanical activation and chemical reactions in CMP of diamond assisted by hydroxyl free radicals. *Appl. Surf. Sci.* **681**, 161527.
[291] Yuan S, Guo X G, Huang J X, Gou Y, Jin Z J, Kang R K and Guo D M. 2020. Insight into the mechanism of low friction and wear during the chemical mechanical polishing process of diamond: a reactive molecular dynamics simulation. *Tribol. Int.* **148**, 106308.
[292] Yuan S, Guo X G, Mao Q, Guo J, van Duin A C T, Jin Z J, Kang R K and Guo D M. 2021. Effects of pressure and velocity on the interface friction behavior of diamond utilizing ReaxFF simulations. *Int. J. Mech. Sci.* **191**, 106096.
[293] Yuan S, Guo X G, Wang H, Kang R K and Gao S. 2024. Atomistic understanding of rough surface on the interfacial friction behavior during the chemical mechanical polishing process of diamond. *Friction* **12**, 1119–1132.
[294] Yuan S, Guo X G, Zhang S H, Zhang C Y, Li P H, Jin Z J, Kang R K and Guo D M. 2021. Influence mechanism of defects on the subsurface damage and structural evolution of diamond in CMP process. *Appl. Surf. Sci.* **566**, 150638.
[295] Liu N, Jiang H L, Xiao J F, Zhang J G, Chen X, Zhu J M, Xu J F and Yamamura K. 2024. Insights into the atomic-scale removal mechanism of single crystal diamond in plasma-assisted polishing with quartz glass. *Tribol. Int.* **194**, 109507.
[296] Bundy F P. 1980. The *P, T* phase and reaction diagram for elemental carbon, 1979. *J. Geophys. Res.* **85**, 6930–6936.
[297] Li Z, Jiang F, Jiang Z Y, Tian Z G, Qiu T, Zhang T, Wen Q L, Lu X Z, Lu J and Huang H. 2024. Energy beam-based direct and assisted polishing techniques for diamond: a review. *Int. J. Extrem. Manuf.* **6**, 012004.
[298] Yoshida A, Deguchi M, Kitabatake M, Hirao T, Matsuo J, Toyoda N and Yamada I. 1996. Atomic level smoothing of CVD diamond films by gas cluster ion beam etching. *Nucl. Instrum. Methods Phys. Res. B* **112**, 248–251.